ANALYSIS AND EXPERIMENTAL VALIDATION OF TEMPERATURE COMPENSATING HYDRAULIC DASHPOT FOR SHUT-OFF ROD DRIVE MECHANISM

By

NARENDRA KUMAR SINGH

ENGG01200904039

Bhabha Atomic Research Centre, Mumbai

A thesis submitted to the

Board of Studies in Engineering Sciences

In partial fulfillment of requirements

for the Degree of

DOCTOR OF PHILOSOPHY

of

HOMI BHABHA NATIONAL INSTITUTE

May, 2018

Homi Bhabha National Institute

Recommendations of the Viva Voce Comittee

As members of the Viva Voce Committee, we certify that we have read the dissertation prepared by **Narendra Kumar Singh** entitled **"Analysis and Experimental Validation of Temperature Compensating Hydraulic Dashpot for Shut-Off Rod Drive Mechanism"** and recommend that it may be accepted as fulfilling the thesis requirement for the award of Degree of Doctor of Philosophy.

BK Dutta	14-5-18
Chairman – Prof. B. K. Dutta	Date:
Badodkar	14.05.2018
Guide / Convener – Prof. D. N. Badodkar	Date:
PS Gandhi	14/05/18
Examiner – Prof. P. S. Gandhi	Date:
J. Chattopadhyay	14/5/18
Member 1 – Prof. J. Chattopadhyay	Date:
Dwarakanath	14/05/18
Member 2 – Prof. T. A. Dwarakanath	Date:
Member 3 – Prof. R. Balasubramaniam	Date: 14/5/18

Final approval and acceptance of thesis is contingent upon the candidate's submission of the final copies of the thesis to HBNI.

I/~~We~~ hereby certify that I/~~We~~ have read this thesis prepared under my/~~our~~ direction and recommend that it may be accepted as fulfilling the thesis requirement.

Date: 14.05.2018

Place: Mumbai

Badodkar

Dr. D. N. Badodkar
Guide

STATEMENT BY AUTHOR

This dessertation has been submitted in partial fulfillment of requirement for an advanced degree at Homi Bhabha National Institute (HBNI) and is deposited in the Libraray to be made available to borrowers under rules of the HBNI.

Brief quotations from this dessertation are allowable without special permission, provided that accurate acknowledgement of source is made. Requests for permission for extended quotation from or reproduction of this manuscript in whole or in part may be granted by the Competent Authority of HBNI when in his or her judgement the proposed use of the material is in the interests of scholarship. In all other instances, however, permission must be obtained from the author.

Narendra Kumar Singh

DECLERATION

I, hereby declare that the investigation presented in the thesis has been carried out by me. The work is original and has not been submitted earlier as a whole or in part for a degree / diploma at this or any other Institution / University.

Narendra Kumar Singh

List of Publications

International Journal: 03

1. Narendra K. Singh, Deepak N. Badodkar, Manjit Singh. "*Numerical and experimental study of hydraulic dashpot used in the shut-off rod drive mechanism of a nuclear reactor*" 'Nuclear Engineering and Design' 273 (2014) 469-482.
2. Narendra K. Singh, Deepak N. Badodkar. *"Passive temperature compensation in hydraulic dashpot used for the shut-off rod drive mechanism of a nuclear reactor"*. 'Nuclear Engineering and Design' 293 (2015) 510-524.
3. Narendra K. Singh, Deepak N. Badodkar. *"Modeling and analysis of hydraulic dashpot for impact free operation in a shut-off rod drive mechanism"*. 'Engineering Science and Technology an International Journal' 19 (2016) 1514-1525.

International Conference: 02

1. N. K. Singh, D. N. Badodkar, Manjit Singh *"Development and qualification of rotary shaft seals for reactivity control mechanisms of Indian nuclear research and power reactors"* Paper presented during 17th International Sealing Conference held at Stuttgart, Germany, on Sept 13-14, 2012, VDMA Fluidtechnik publisher P153-168.
2. N. K. Singh, D. N. Badodkar, Manjit Singh *"Friction based comparison of mechanical shaft seal and dynamic 'O' ring module developed for rudders and fins of Autonomous Underwater Vehicle"* Paper presented during 8th International Conference on Industrial Tribology held at Pune, India on Dec 7-9, 2012.

Narendra Kumar Singh

Dedicated

to

My Family & Friends

ACKNOWLEDGEMENTS

I wish to express heartfelt gratitude to Dr. D. N. Badodkar, Director, RD&DG, BARC for his patient guidance and encouragement throughout the course of this research. I am indebted to him for giving proper direction and adequate time for this endeavour. I also wish to express my deepest appreciation to Mr. Manjit Singh, Ex. Director, DM&AG, BARC for his inspirational support and valuable suggestions for this research work.

I would like to express my special gratitude and thanks to Prof. B. K. Dutta (Chairman, Doctoral Committee), Prof. V. K. Suri (Ex. Chairman, Doctoral Committee) and all doctoral committee members; Prof. J. Chattopadhyay, Prof. T. A. Dwarakanath, Prof. R. Balasubramaniam, Prof. R.K. Singh, Prof. P. Chellapandi, Prof. R. Reddy, Prof. P. V. Varde for their valuable suggestions and support throughout the duration of my work. My special thanks to them for their valuable time attending my periodical doctoral committee meetings.

I also would like to thank my colleagues, Mr. N. S. Dalal, Mr. A. K. Ratha, Mr. Firoz Alam and others in Control Mechanism Section, DRHR for providing helping hands at hard times and obtaining experimental data. My special thanks to Mr. Karimulla Shaik of MDD, Dr. Naveen Kumar of RED and Dr. Gaurav Bhutani of DRHR, to whom, I had interacted regularly. With their inputs and comments this research work has seen a light of the day. My thanks are also due to the staff of drawing office and the workshop, which always extended their full co-operation.

Finally, I wish to thank my wife, Jyoti and son, Hardik, whose patience and sacrifice made this endeavour successful.

Narendra Kumar Singh

Nomenclature

A	total vane area
b	length of vane
c	clearance thickness
C	elasticity tensor
C_p	specific heat capacity of fluid at constant pressure
c_θ	damping coefficient
cc	cubic centimeter
cst	centistokes
det	determinant
E_d	Energy absorbed in the dashpot
Eq	Equation
F	volume force vector in Eq. 3.4 and 5.4
F	deformation gradient tensor in Eqs. 5.1b and 5.1d
Fig.	figure
F_d	total dashpot force
F_p	force due to differential pressure
F_s	force due to skin friction
F_v	body force per unit volume
I	identity matrix
ID	inner diameter
I_e	effective moment of inertia at the joint
I_{dest}	destination moment of inertia
I_{src}	source moment of inertia
J	jacobian matrix

k	coefficient of thermal conductivity
k_θ	spring constant
k_o	orifice coefficient
kg.	kilogram
L	depth of clearance
L_C	length of clearance
m	meter
mm	millimeter
M	the damping moment
Ma	Mach number
N	Newton
No.	number
OD	outer diameter
p	pressure
Δp	differential pressure across clearance
Pa	Pascal
p_u	penalty factor
Q	heat sources
r_v	outer radius of moving vane
r_s	radius of vane shaft
R	torque arm
RPM	rotation per minute
R_{dest}	rotation matrices describing the rotation of destination attachments
R_{src}	rotation matrices describing the rotation of source attachments
S	stress tensor
S_0	initial stress value

sec	second
T	absolute temperature in Eqs. 4.4 and 5.2b
T	transpose at rest of places
t	time
T_d	torque on the dashpot shaft
T_q	torque
T_{ref}	reference absolute temperature
U	moving vane velocity
u	displacement field (u, v, w)
u_2	velocity field (u_2,v_2,w_2)
$u_{c.dest}$	displacement vectors for destination attachments
$u_{c.src}$	displacement vectors for source attachments
u_{dest}	displacements at the centroid of the destination attachments
u_{src}	displacements at the centroid of the source attachments
u_{sw}	velocity of sliding wall
u_w	velocity of moving wall
w.r.t.	with respect to
X_c	joint center
$X_{c.src}$	positions of centroids for source attachments
$X_{c.dest}$	positions of centroids for destination attachments
1-D	one dimensional
2-D	two dimensional
3-D	three dimensional

Greek symbols

ξ	coefficient of hydraulic resistance
ρ	density of fluid

∇	divergence
μ	dynamic viscosity
η	kinematic viscosity
ϵ	strain tensor
ϵ_0	initial strain value
α	coefficient of thermal expansion
σ	stress
Φ_{dest}	rotation about the axis for destination attachments
Φ_{src}	rotation about the axis for source attachments
ω	angular velocity
θ	relative rotation
θ_0	pre-deformation

Abbreviation

AHWR	Advanced Heavy Water Reactor
BWR	Boiling Water Reactor
ALE	Arbitrary Lagrangian Eulerian
CFD	Computational Fluid Dynamics
EM	Electro-Magnetic
FEM	Finite Element Method
FSI	Fluid Structure Interaction
LWR	Light Water Reactor
MWe	Megawatt Electric
PHWR	Pressurized Heavy Water Reactor
PWR	Pressurized Water Reactor
SOR	Shut-off Rod
SRDM	Shut-off Rod Drive Mechanism

CONTENTS

Synopsis

Shut-off rods are used to shut down a nuclear reactor, thus forming a safety critical system. These rods are moved using Shut-off Rod Drive Mechanisms (SRDM). At the time of reactor start-up, rods are withdrawn at a given speed and are held in position during the reactor operation. On actuation of a reactor trip, shut-off rods fall freely into the reactor core. However, at the end of the rod travel, the rod velocity is smoothly brought to zero using a passive device called 'Hydraulic Dashpot'. In this rotary hydraulic dashpot, fluid (typically silicone oil) is allowed to flow from one chamber to the other through narrow clearances, giving damping action. After dashpot engagement, the oil pressure increases to the peak value in the high-pressure chamber and thereafter reduces at the end of travel as oil passes to the low-pressure chamber.

In a shut-off rod drive mechanism, the motor sub-assembly is connected to a worm gear and an electromagnetic (EM) clutch sub-assembly, which is further connected to a sheave (deep groove pulley) through a set of spur gears. An absorber element (shut-off rod) is mounted on the sheave through a wire rope. The EM clutch is energized to raise the rod through the motor. As soon as the rod reaches the top position, the motor is cut-off and the rod remain at that position, due to irreversibility of worm gear design. During reactor scram, the EM clutch is de-energized and the rod falls freely due to gravity. A set of pick-up rings are used, which lapse one over the other bringing hydraulic dashpot into action precisely at the desired position (typically 90% of the rod drop). A spiral spring is used for resetting the hydraulic dashpot during the rod withdrawal.

Shut-off rod drive mechanisms are to be qualified at the room temperature during the reactor start-up as well as at elevated temperature during the reactor operation, where heat is exchanged with the environment. The hydraulic dashpot designs are finalized with an optimum combination of the dashpot clearances and the oil viscosity. If a hydraulic dashpot with fixed clearances utilizes less viscous oil, then it works well at the room temperature, but we see impact at elevated temperatures as the viscosity decreases and the dashpot becomes under damped. Otherwise if we go for high viscous oil with the same clearances, then we don't see the impact at elevated temperatures, but we get higher rod drop times at the room temperature as the dashpot becomes highly over damped and we don't meet the drop time criterion. These calls for a hydraulic dashpot design that can passively compensate for the viscosity change and the dashpot can be used for a wide range of temperature variation.

Primarily in the literature the dashpot fluid flow and the pressure calculations are done by solving the continuity equation only with utilization of the coefficient of hydraulic resistance. To study more precisely parameters affecting the dashpot performance a Computational Fluid Dynamics (CFD) study of the hydraulic dashpot is required. To make hydraulic dashpot temperature compensating, the fluid-structure analysis is required. Conventionally Fluid Structure Interaction (FSI) problems are studied in which effects of the fluid flow on the structure are studied. Not much literature is available on effects of structural changes on the fluid flow for damper applications. Recently, a lot of research work has been done on smart fluid dampers, but these are active devices which are not suitable for the shut-off rod drive mechanism applications, where we need a passive temperature compensating hydraulic dashpot. The present research is focused on these gap areas.

The scope and motivation of the present research are; (i) Study and analysis of change in dashpot clearances and oil properties with the change in the environment temperature. (ii) Suggestion for incorporating temperature compensating parts and their geometries in the hydraulic dashpot to reduce clearances at the elevated temperatures. This can be achieved by using a combination of materials with different coefficients of thermal expansion. (iii) Experimental validation of the temperature compensating hydraulic dashpot for desired rod drop velocity profile using full-scale test facility.

Present work consists of:

(i) CFD analysis of a hydraulic dashpot with experimental validation to investigate effects of dashpot clearances and the damping oil viscosity on dashpot performance. Performance of the hydraulic dashpot is studied in terms of the dashpot pressure and the dashpot force.

(ii) Multi-body dynamics modeling, simulation and experimental validation. The study is focused on obtaining the dashpot responses in terms of the relative rotation, the relative angular velocity and the relative angular acceleration at various environmental temperatures and with variation in different mechanical parameters like increase in the moment of inertia, reduction in the constraint angle and increase in the constant applied moment.

(iii) Fluid-structure analysis (CFD) of the hydraulic dashpot to propose a novel passive temperature compensating hydraulic dashpot. The study is focused on reducing the clearances of the hydraulic dashpot at elevated temperature which in turn compensates for the reduction in the viscosity of the damping oil and the dashpot gives uniform performance for a wide range of temperatures. The temperature compensation effects are mainly due to the difference in the thermal expansion of materials. Different combinations of materials are used to reduce the dashpot clearances at elevated temperature. The fluid-structure analysis has been carried-out to study the thermal expansion and the pressure generated in the hydraulic dashpot.

The analysis of the dashpot parameters gives that the force generated due to the differential pressure is a main contributor to the total dashpot force. The dashpot pressure is highly dependent on its clearance thickness. Multi-body dynamics model of the hydraulic dashpot has resulted in a handy tool to analyze effects of various parameters on the dashpot performance. With an increase in the moment of inertia, a reduction in constraint angle and an increase in the constant applied moment, an over damped dashpot system can become under damped without change in the damping and the spring coefficients. The fluid structure analysis for passive temperature compensation gives that the clearances in the dashpot can be reduced at elevated temperature to compensate for the reduction in the oil viscosity. It is concluded that a temperature compensating hydraulic dashpot design utilizing bimetallic strips is possible. Thus, the objective of presenting a novel temperature compensating hydraulic dashpot is achieved.

List of Figures

List of Tables

Chapter I

INTRODUCTION

1.1 Nuclear Reactor Safety and Shut-off Rod Drive Mechanism

In the 1950s attention turned to harnessing the power of the atom in a controlled way, as demonstrated in Chicago in 1942 and subsequently for military research, and applying the steady heat yield to generate electricity. This naturally gave rise to concerns about accidents and their possible effects. However, nuclear reactor safety depends on intelligent planning, proper design with conservative margins and back-up systems, high-quality components and a well-developed safety culture in operations. The fundamental safety functions that are required to be performed for the safe operation of a reactor are as follows:

(i) Reactor shut down for a prolong period of time.

(ii) Heat removal from the core.

(iii) Confinement of the radioactive material to limit its release to the environment.

Shut-off rods are used to shut down a nuclear reactor, thus forming a safety critical system. These rods are moved using Shut-off Rod Drive Mechanisms (SRDM). At the time of the reactor start-up, rods are withdrawn at a given speed and are held in position during the reactor operation. On actuation of a reactor trip, shut-off rods fall freely into the core. These rods are inserted into the reactor core as rapidly as possible. This is generally referred to as 'scram'. However, at the end of the rod travel, the rod velocity is smoothly brought to zero using a passive device called as 'Hydraulic Dashpot'. In this, a fluid (typically silicone oil) is allowed to flow from one chamber to the other through narrow clearances, giving damping action. After the dashpot engagement, the oil pressure increases to the peak value in the high-pressure chamber and thereafter reduces at the end of travel as the oil passes to the low-pressure chamber. The hydraulic dashpot vane rotates typically by 120° in one rod drop cycle. Fig. 1.1 gives the general arrangement of a typical shut-off rod drive mechanism along with the guide tube components. The drive mechanism components are given in Fig. 1.2 while Fig. 1.3 gives the hydraulic dashpot construction.

In a shut-off rod drive mechanism, the motor sub-assembly is connected to a worm gear sub-assembly and an electromagnetic (EM) clutch sub-assembly, which is further connected to a sheave (deep groove pulley) through a set of spur gears. An absorber element (shut-off rod) is mounted on the sheave through a wire rope. The EM clutch is energized to raise the rod through the motor. As soon as the rod reaches the top position, the motor is cut-off and the rod remain at that position, due to the irreversibility of the worm gear design. During reactor scram, the EM clutch is de-energized and the rod falls freely due to gravity. A set of pick-up rings are used, which lapse one over the other bringing the hydraulic dashpot into action precisely at the desired position (typically 90% of the rod drop). A spiral spring is used for resetting the hydraulic dashpot during the rod withdrawal.

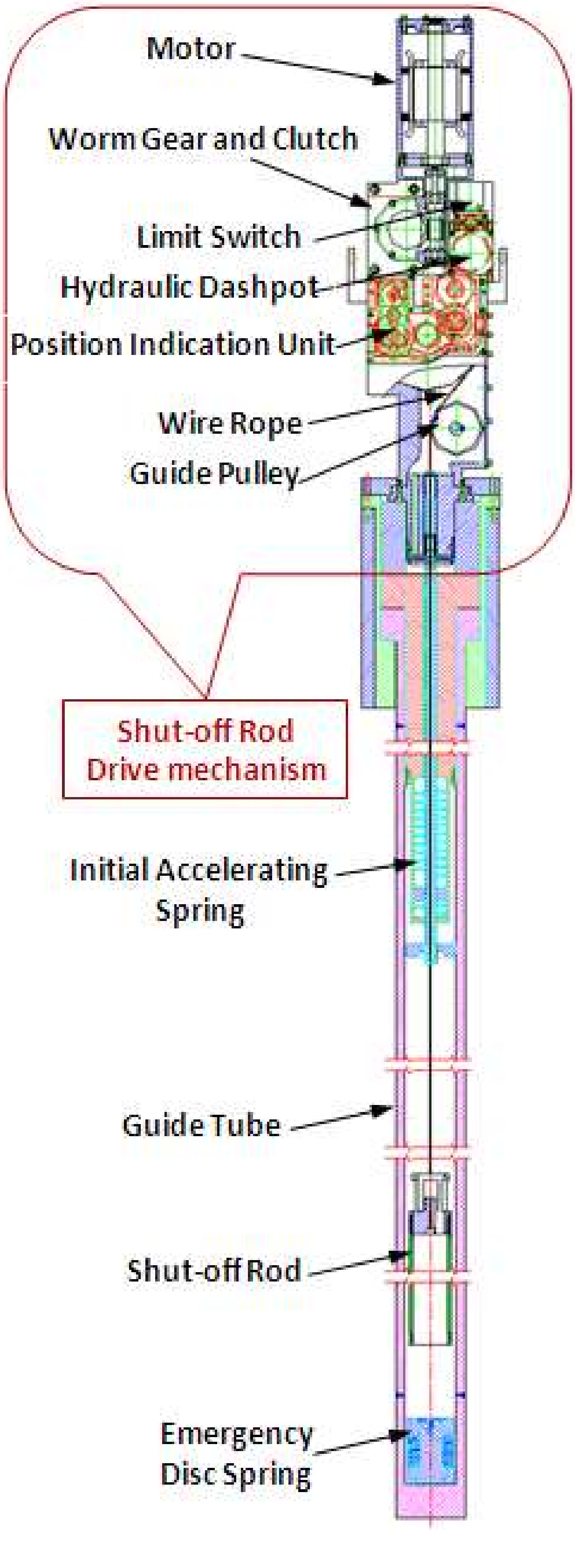

Fig. 1.1 General arrangement of a shut-off rod drive mechanism

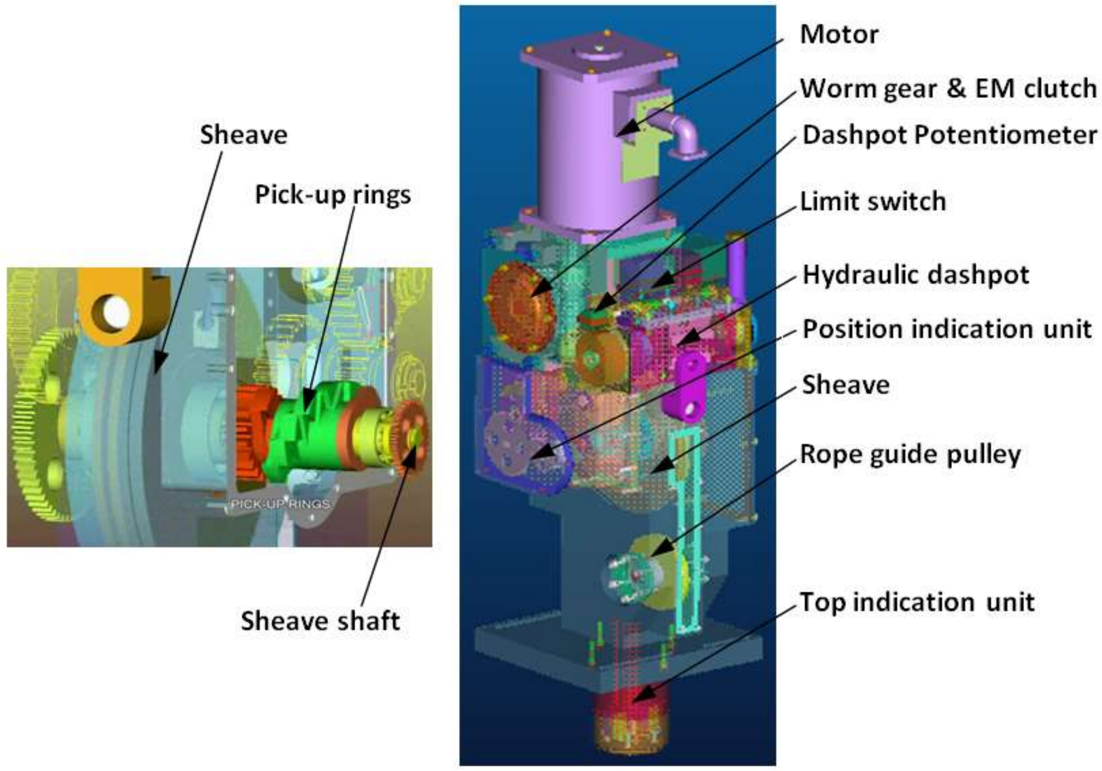

Fig. 1.2 Shut-off rod drive mechanism components

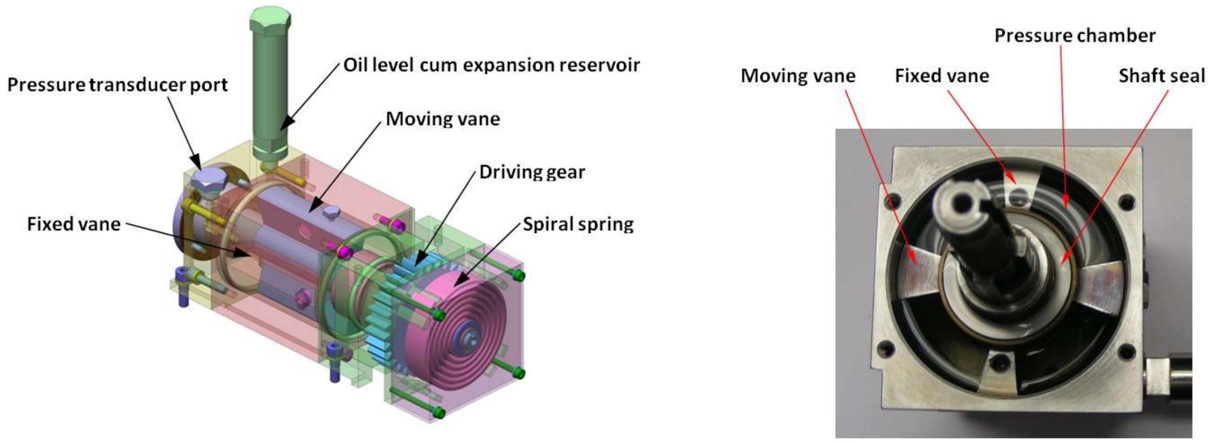

Fig. 1.3 Hydraulic dashpot construction

1.2 Design of Shut-off Rod Drive Mechanism

Designs of shut-off rod/control rod drive mechanisms vary with the type of the reactor. The Light Water Reactors, i.e., the Pressurized Water Reactors (PWRs) and the Boiling Water Reactors (BWRs) which operate at a high pressure are provided with mechanisms which can have a hermetically sealed enclosure for the primary system. The mechanisms used in PWRs are generally either a magnetic jack or a roller nut type mechanism. Hydraulic jack type mechanisms are generally used in BWRs. Rack and pinion type mechanisms are more suitable for pool type research reactors. Fast breeder reactors utilize screw nut type mechanisms.

Pressurized Heavy Water Reactors (PHWRs); Bajaj and Gore [1] have a high pressure primary system and a low-pressure moderator system. Shut-off rods are inserted in the low-pressure moderator system. The cable winch (pulley or sheave) type mechanisms are more suitable for PHWRs. These mechanisms are compact and don't require much head room. Cable winch type mechanisms are also used in research reactors where sufficient head room is not available. Cable winch type mechanisms in very compact tubular form are designed for some research reactors and upcoming Advanced Heavy Water Reactor (AHWR); Sinha and Kakodkar [2].

In general, for PWRs, the same rods are used to control and shut down the reactor and the rods are called control rods. In PHWRs the rods used to control the reactor are called control rods and the rods used to shut down the reactor are called as shut-off rods. Fig. 1.4 gives the mounting of a shut-off rod drive mechanisms on a PHWR and Fig. 1.5 gives the actual photograph of the mechanism on the reactor.

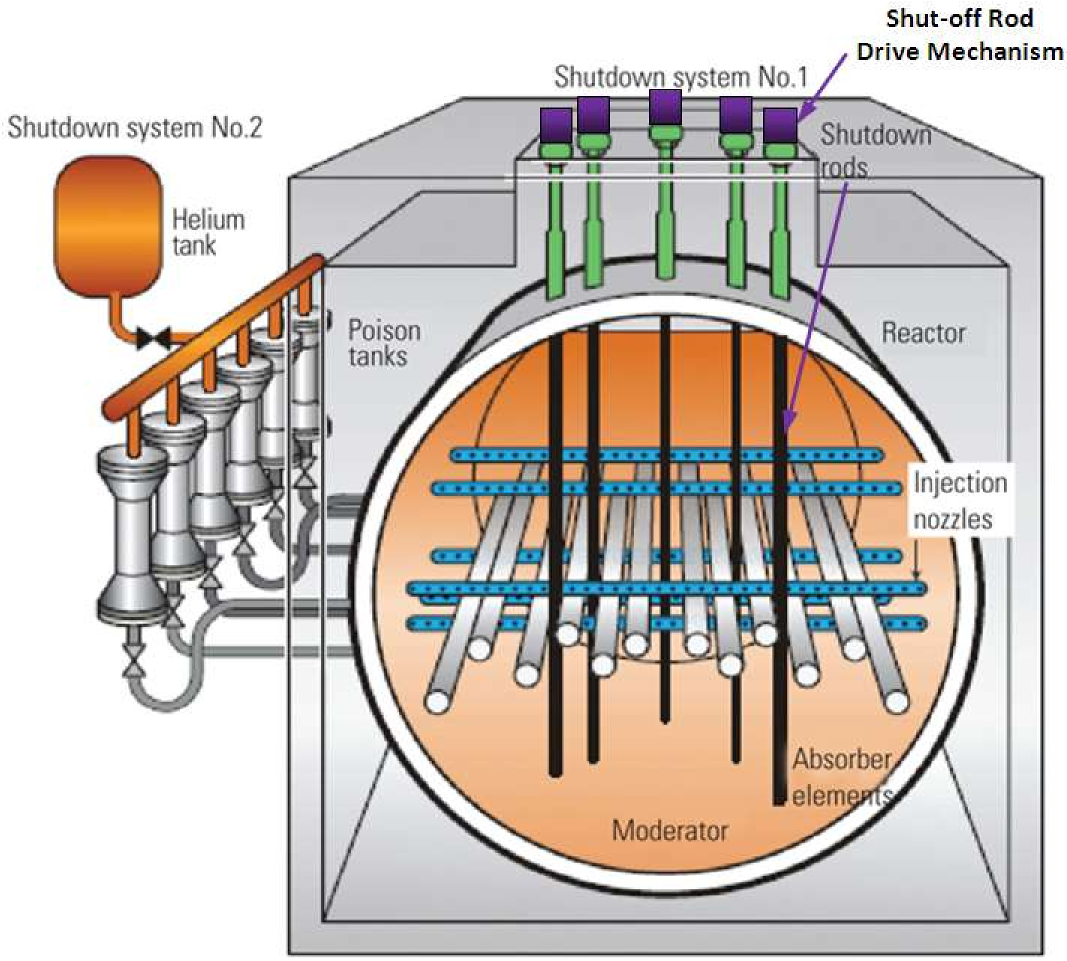

Fig. 1.4 Shut-off rod drive mechanisms on a PHWR
(Image: www.powermag.com)

Fig. 1.5 Actual photograph of the shut-off rod drive mechanisms on a PHWR (Image: NPCIL)

1.3 Forces Acting on a Falling Shut-off Rod

Fig. 1.6 shows the forces acting on a falling shut-off rod. These forces can be categorized into two groups; accelerating forces and retarding forces.

1.3.1 Accelerating Forces

These forces accelerate the rod in the direction of rod fall. These forces can be further categorized as:

a) Self-Weight of Shut-off Rod (absorber element) Assembly (F_w)

Total weight of shut-off rod assembly includes; weight of absorber element with top and bottom attachment and effective weight of wire rope.

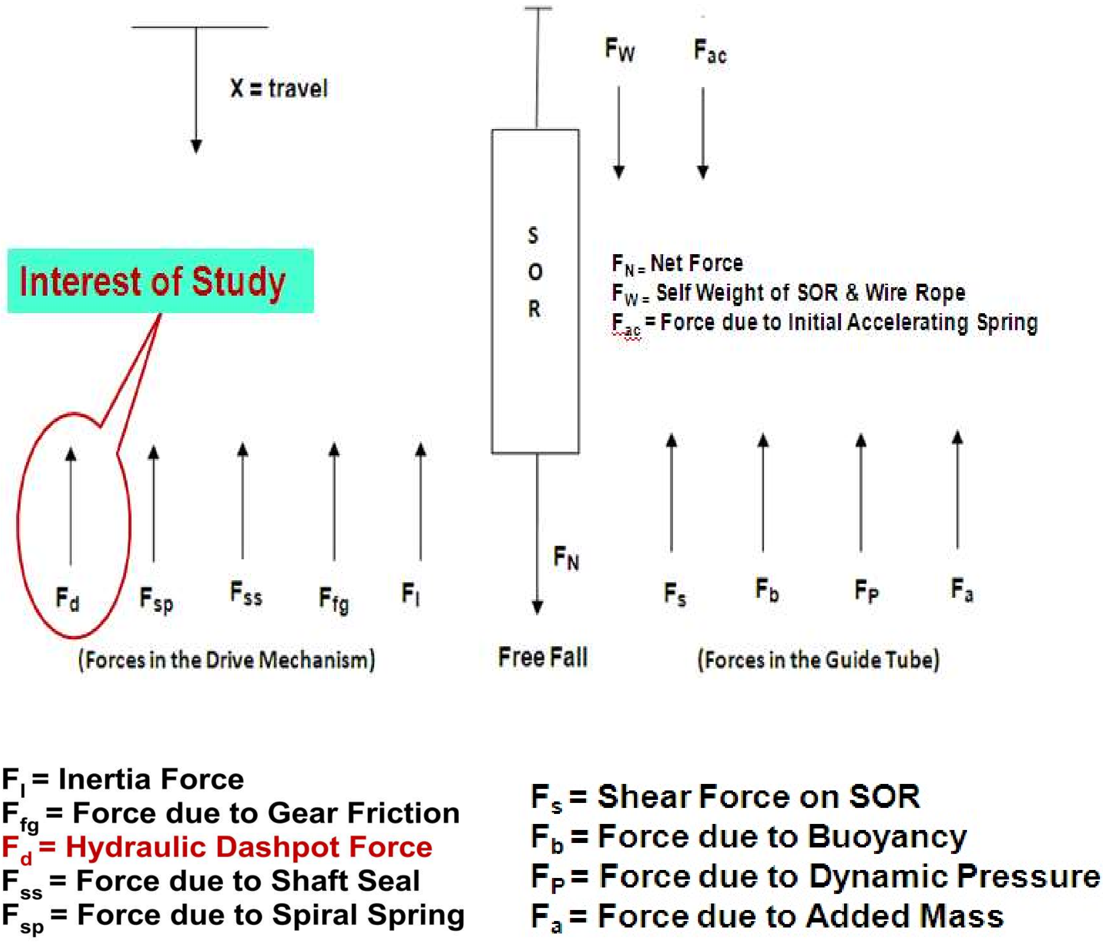

Fig. 1.6 Forces acting on a falling shut-off rod

b) Force due to Initial Accelerating Spring (F_{ac})

These mechanisms are provided with an initial acceleration spring. The spring remains compressed when the rod is in the parked-up position. It gives initial thrust to the shut-off rod when the clutch is released. The stroke of the spring is limited to the initial travel of the rod.

1.3.2 Retarding Forces

These forces decelerate the rod during free fall. Some of these forces act inside the drive mechanism and others act inside the guide tube in the reactor core. So, these can be categorized into two groups; retarding forces in the drive mechanism and the guide tube. In some of the reactors, the shut-off rod falls in the air as there is no water inside the guide tube. In this case no retarding forces are present in the guide tube.

a) Retarding Forces in the Drive Mechanism

The forces acting inside the drive mechanism are:

(i) Inertial force due to angular acceleration of the wire rope sheave, shafts, gears and other rotating components during free fall. (F_I)

(ii) Frictional force in the gear teeth. (F_{fg})

(iii) Frictional force in the mechanical shaft seals. (F_{ss})

(iv) Hydraulic dashpot force. (F_d)

(v) Force due to the spiral spring in the hydraulic dashpot. (F_{sp})

- The sum of all these forces is equal to tension in the wire rope.

b) Retarding Forces in the Guide Tube

The retarding forces in the guide tube are:

(i) Shear force which depends upon the drag coefficient. (F_s)

(ii) Force due to Buoyancy. (F_b)

(iii) Force due to dynamic pressure (Fp). This is the retarding force seen by the rod due to the instantaneous pressure generated in the perforated guide tube.

(iv) Force due to the added mass (F_a). When the rod is accelerated in a fluid, some volume of surrounding fluid is attached with the rod that also gets accelerated. The mass of the attached fluid is called the added mass. Hence the rod feels some retarding force. This force depends upon the mass density of fluid and the geometry of falling rod.

1.4 Qualification of the Shut-off Rod Drive Mechanism

Being a safety critical system, the design of the shut-off rod drive mechanism is qualified through prototyping and life-cycle testing on a full-scale test set-up by simulating the actual reactor conditions. These mechanisms are to operate at the room temperature during the reactor start-up and at an elevated temperature during the reactor operation, where heat is exchanged with the environment. Hence, the shut-off rod drive mechanisms are to be qualified at the room temperature as well as at the elevated temperature. The hydraulic dashpot in the drive mechanism utilizes damping oil and the viscosity of the oil changes with the temperature; hence we get variation in the damping. In the Indian standardized PHWRs, these drive mechanisms are placed in the boiler room, where environment temperature remains at about 65°C. While in upcoming AHWRs these mechanisms are to be placed in tail pipe vault area, where environment temperature remains at about 285°C. Although cooling jackets are provided around these drive mechanisms, but in the event of cooling failure, these mechanisms are required to operate at a high temperature.

The hydraulic dashpot designs are to be finalized with an optimum combination of the dashpot clearances and the oil viscosity. If a hydraulic dashpot with fixed clearances utilizes less viscous oil, then it works well at the room temperature, but we see impact at an elevated temperature as the viscosity decreases and dashpot becomes under damped. Otherwise if we go for high viscous oil with the same clearances, then we don't see the impact at the elevated temperature, but we get higher rod drop times at the room temperature as the dashpot becomes highly over damped and we don't meet the drop time criterion. These calls for a hydraulic dashpot design that can passively compensate for the viscosity change and the dashpot can be used for a wide range of temperature variations.

Chapter II

LITERATURE SURVEY

2.1 Review of Previous Research

A study of a passive temperature compensating hydraulic dashpot needs the modeling of the hydraulic dashpot and the fluid-structure interaction analysis. This chapter underscores historical practices and literature review of the previous research in this field. Modeling of the rod drop dynamics and the fluid flow in a hydraulic dashpot by various researchers is presented. The literature on fluid flow between parallel plates, damper dynamics, and active as well as passive temperature compensation is also given. Previous studies related to the thermal expansion of assemblies and the fluid structure interaction is also presented in this chapter. Gap areas, the scope of the present work and problem formulation are elaborated upon.

2.1.1 Rod Drop Dynamics

The literature survey reveals that various researchers have developed models for a shut-off rod/control rod drop dynamics. In 1972 Donis and Goller [3] developed a mathematical model of a control rod drop for a PWR. The rod drop time computed by using the model is compared with the available experimental data for a rack and pinion control system. This study was mainly focused on effects of the guide tube holes on the pressure drop across the control drop and its effects on the acceleration of rod during scram. Choi et al. [4] developed a computer program for the drop time and the impact velocity of the rod cluster control assembly. The rod drops and the pressure profiles were generated. The dashpot is formed in the lower part of the guide tube and effects of dashpot are also studied. Taliyan et al. [5] presented the dynamics of a shut-off rod drop in a PHWR. A theoretical model of the shut-off rod drop with the experimental validation on a full-scale test station is presented. An empirical formula for the friction factor of the dashpot used in the prototype assembly is developed. Ren and Stabel [6] have done the analytical modeling of the control rod behavior in a PWR. A coupled structure-dynamic and a hydraulic analytical model is developed for evaluation of the Rod Control Cluster Assembly (RCCA) drop behavior down to the dashpot. In the hydraulic models the hydraulic resistance on the RCCA is evaluated by well-known laws of hydraulic resistance as given by Idelchik [7]. Hofmann et al. [8] have done the Computational Fluid Dynamics (CFD) analysis of a guide tube in a PWR, where a numerical study of the influence of the pressure forces applied to control rods and due to flow circulation is conducted. Wang et al. [9] have developed a mathematical model and a numerical simulation tool for a damping mechanism of a TRR-II reactor. The results of the code prediction were compared to the experimental results. The geometries of the damping plug located on the lower end of the control rod and damping cap with flow holes receiving the damping plug were analyzed for attaining the required damping force.

2.1.2 Fluid Flow and Modeling of Hydraulic Dashpot

In the literature the dashpot analysis is mostly focused on linear dampers which are largely in industrial use; very limited literature is available on rotary dampers. Researchers have used various approaches to analyze hydraulic dashpots. Wenzler [10] has computed the dashpot pressure by modeling all the clearances in the dashpot as an orifice. The differential pressure across the vane is calculated from the published data of the orifice coefficient (k_o) by Lenkei and Andrew [11] for narrow clearance orifices. This method is not very accurate, because at very low c/L ratio, (where c is the thickness and L is the depth of the clearance) the value of the orifice coefficient changes sharply (as in our case). Taliyan et al. [5] also calculated the dashpot force for a rotary vane type dashpot by modeling the clearance as an orifice. The differential pressure across the vane is calculated by finding the coefficient of the hydraulic resistance (ξ) given by Idelchik [7]. Hou [12] studied the fluid dynamics behavior of a linear viscous damper. For calculating the damper force, the damper is modeled as flow between two parallel plates and the momentum equations are solved to get a relation for the pressure drop across the piston. The non-Newtonian fluid behavior of a damper fluid (silicone oil) is also considered. In this type of dampers, the shear rate is very high, so the fluid shows non-Newtonian behavior beyond a shear rate. Wang et al. [13] studied a damper with damping orifice in the piston and a pressure drop equation was derived. Jia and Hua [14] have done test verification of a design method for a viscous fluid damper. The damping force equations for a large amplitude motion damper have been derived. Black and Makris [15] studied the phenomenon of viscous heating of fluid dampers under small and large amplitude motions. Various rotary hydraulic dashpot designs have been patented by researchers [16-18] for different applications.

2.1.3 Flow Between Parallel Plates

Literature on fluid flow between parallel plates is presented in this section. Fluid flow modeling in a hydraulic dashpot is given by Modi and Seth [19]. Here flow through narrow clearances is considered as laminar flow between parallel plates. Equations are derived for the pressure and the dashpot force in a linear dashpot. Erdogan and Imrak [20] studied unsteady flows generated between two parallel plates by impulsive motion of a boundary. Expressions are derived for the flow velocity, the flux and the skin friction. Erdogan [21, 22] also studied the unsteady unidirectional flows generated by the sudden application of a pressure gradient. Some exact solutions of the Navier-Stokes equations are discussed for Stoke's first problem, unsteady Couette flow, unsteady flow between two parallel plates which are suddenly moved in the same or in the opposite direction, unsteady Poiseuille flow and unsteady generalized Couette flow. Atta [23] studied the influence of temperature-dependent viscosity on the MHD Couette flow of a dusty fluid with heat transfer. The viscosity was assumed to vary exponentially with temperature and the Joule and the viscous dissipation were taken into consideration. Muzychka and Yovanovich [24] examined the unsteady viscous flows and Stoke's first problem. The relationship between three fundamental unsteady flow problems (unsteady Couette flow, unsteady Poiseuille flow and unsteady boundary layer flow) and Stoke's first problem is illustrated and their links are established by means of scaling and asymptotic analysis. Thermodynamic lubrication analysis of step bearings is presented by Ogata [25]. Finite difference equation is derived of the Reynold's equation that is consistent on the entire bearing surface including steps by defining virtual clearance and its gradient in order to satisfy the flow continuity at steps that cause discontinuous clearance. The results are compared with the solution from a commercial CFD code.

2.1.4 Damper Dynamics

Wenzer [10] has done the analysis of dashpot performance for rotating control drums of a lithium cooled fast reactor, where with manual calculation the available torque was calculated at every time step and the dashpot rotational velocity vs time curves were generated. With advancement in computational techniques various researchers have developed damper models for use in multi-body dynamic simulations. Allen et al. [26] have developed a damper model for use in multi-body dynamic simulations. In this study a warrior armoured personnel carrier rotary damper is modeled. They also studied the responses of a damper at different flow regimes. Lion and Loose [27] have given a thermo-mechanically coupled model for an automotive shock absorber. Zhong et al. [28] have done multi-body dynamic simulation of a flapping wing. In this study, the inertial force and the inertial moment between the wing and the body are reflected in the simulation model and the multi-body dynamic equation of the model is presented. Shabana [29] has done the viscoelastic analysis of multi-body systems using the Finite Element Method (FEM). In his study constraints between components are formulated. Na and Kim [30] analyzed a multi-link beam structure undergoing locking. Modeling of the system dynamic forces are assumed to be torques and restoring forces due to a torsion spring at each joint. Cheng and Wang [31] have given a simple model of an impact damper using a spring mass and a viscous damper.

2.1.5 Active Temperature Compensation: Smart Fluid Dampers

Literature survey reveals various temperature compensating techniques utilized by different researchers. Predominantly, these techniques are based on the idea of modifying the viscosity as per requirements. The most common technique is based on utilization of smart fluids, Passlack [32]. Smart fluids can change their viscosities quickly as and when required. The two common types of smart fluids are Electro-Rheological (ER) and Magneto-Rheological (MR) fluids. Both fluids consist of a dielectric carrier liquid, but differ in the type of suspended particles and the applied field necessary to trigger thickening. The thickening phenomenon for MR fluids as given by Olabi and Grunwald [33] is similar to that experienced by the ER fluid. MR fluids are a class of smart materials whose rheological properties (e.g.; viscosity) may be rapidly varied by applying a magnetic field. Under the influence of a magnetic field the suspended magnetic particles interact to form a structure that resists shear deformation or flow. This change in the material appears as a rapid increase in the apparent viscosity. Wereley et al. [34] have given the biviscous damping behavior in ER shock absorbers. Stanway [35] has given the current and the future developments of smart fluid-based devices. Shiao and Haung [36] have given the design of a novel damping-controllable damper for suspension. Carmignani et al. [37] have given the design of a novel magneto-rheological squeeze film damper. Jennifer [38] has also given applications of smart fluid dampers in real life. Zhu et al. [39] have done modeling and analysis of a MR fluid damper under impact load. The rheology of Shear Thickening fluids (STF) and the dynamic performance of an STF filled damper are studied by Zhang et al. [40]. Song and Zeng [41] designed a MR damper/lock for use in a model adaptive fan nozzle system actuated by shape memory alloy wires. The MR damper will lock the opening size of the fan nozzle and provides damping when the system vibrates. The force-displacement relationship and the force-velocity relationship of a MR damper/lock are obtained.

2.1.6 Passive Temperature Compensation in Dampers

Samantaray [42] developed mathematical models for passive liquid spring shock absorbers, which are suitable for heavy load military applications. Pan and Chongdu [43] have done the investigation of a shape memory alloy micro-damper for MEMS applications. NiTi memory alloy is used for passive damping applications in which energy may be dissipated by conversion from mechanical to thermal energy. Series of tension tests for damping behavior of NiTi wires subjected to different temperatures, strain rates and strain amplitudes were conducted. The experimental results show the energy dissipation of the wires is almost independent of temperature, but strongly depend on strain rate in the experimental conditions. Nash [44] patented the design of a rotary damper which has an inner member located within an outer member and an annular seal between the members enclosing a fluid-filled space bounded in a part by mutually adjustable faces of the members. A viscous damping force is thereby generated by the relative rotation of the members. Another patented design of a temperature compensated adjustable damper unit was presented by Hlipala and Arnold [45]. In this design the damping is provided by a magnetic restraint on a drag cup driven through the magnetic field of a permanent magnet by a planetary gear. D'Anna and Anthony [46] and Mclean [47] presented patented designs with temperature compensating elements with higher coefficient of thermal expansion.

2.1.7 Thermal Expansion of Assemblies

Rao et al. [48] have done FE analysis of a bimetallic beam under thermal loading and proposed an empirical formula which predicts the deflection of a bimetallic beam for a given temperature rise. Zahariea [49] has done detailed structural analysis of a helical bimetallic strip thermostat using the FEM. Haba and Oancca [50] have done the thermal expansion analysis of the complex body assemblies using the FEM. In this analysis the assembly is loaded with a uniformly distributed thermal field and the thermal expansion of internal sections of an engine block is determined. Boisseau et al. [51] studied a bimetal-based heat engine for thermal energy harvesting. In this device a curved bimetallic strip turns the thermal gradient into a mechanical movement. Plesca [52] has done the thermal analysis of overload protection relays using FEM and a three-dimensional thermal model of the bimetal releaser has been given. Mechanical thermal expansion correction design for an ultrasonic flow meter is given by Martinson and Delsing [53]. When an ultrasonic flow meter using the transit time technique is subjected to an increasing ambient or fluid temperature, the materials in the meter will expand due to thermal expansion and give error in measurement. By the insertion of a compensation body behind the transducers the thermal expansion of this body will work to compensate for errors due to the expansion in the materials that the flow meter is made of. It was shown by simulations that the influence from thermal expansions can theoretically be reduced to a negligible level. Kim et al. [54] has done a study on the shrink fits and internal clearance variation for a ball bearing made for a machine tool using the FEM. They have done FE analysis for clearances in the bearing using ANSYS. The influence of heat generation and the revolution of spindle upon the preload for the bearing are established. Thermal analysis of disc brake using COMSOL is done by Singh and Shergill [55]. Disc brakes with different materials have been analyzed for the heat produced and dissipated. Antoni [56] designed a novel composite piston for a diesel engine. Changes of the thermal expansion coefficient have been studied at different temperatures for different materials to get favorable effects of low hysteresis in the coefficient of thermal expansion.

2.1.8 Fluid-Structure Analysis

A large amount of literature is available on Fluid Structure Interaction (FSI) problems, where primarily the effect of fluid flow on a structure is studied. Some of the problems have both way coupling, where the effect of structure on fluid flow is also studied. Arbitrary Lagrangian Eularian (ALE) finite element methods have become popular for their capability to control mesh geometry independently from the material geometry. Souli et al. [57] apply the ALE concept to FSI problems. The control rod drop analysis by the FEM using FSI for a PWR plant was done by Yoon et al. [58]. In this analysis the fluid structure interaction between the control rod and the fluid was simulated by using a fluid structure coupled algorithm under the core conditions at the operating temperature. Kuehne et al. [59] used COMSOL Multiphysics FSI application mode to investigate the impact of the surrounding air on the damping behavior of a MEMS cantilever energy harvester. A fully coupled FSI analysis was performed where viscous forces and the fluid pressure impose forces on the surface of the solid causing mechanical deformation. In turn, the mechanical deformations influence the fluid flow characteristics.

Czop et al. [60] have developed a method for optimizing the design of a disc spring valve system by reducing the aeration and the cavitation effect which negatively influence the performance of a shock absorber. A FSI model is used in order to modify the geometry of the valve interior and, in turn, to achieve better performance of the shock absorber. Simulation of FSI in the reflow soldering process is done by Lau and Abdullah [61]. The infrared-convection reflow oven is modeled using a CFD software while the structural heating simulation is done using a FE software. Both software applications are coupled using the Multi-physics code coupling interface. Braescu and George [62] have implemented the ALE method for coupled Navier-Stokes and convection-diffusion equations with moving boundaries for a melting-solidification process using COMSOL. Bathe and Ledezma [63] presented solutions of some benchmark problems for incompressible fluid flows with structural interactions. Basic problems are considered for testing of FSI solution schemes in this paper.

2.2 Gap Areas

The literature review reveals the gap areas where more research is required. Primarily in the literature the dashpot fluid flow and the pressure calculations are done by solving the continuity equation only with utilization of the coefficient hydraulic resistance. To study more precisely the parameters affecting the dashpot performance the CFD study of a hydraulic dashpot is required. The CFD study of linear dashpots is available in the literature to some extent, but not much is available for rotary dashpots. To make a hydraulic dashpot temperature compensating, the fluid-structure analysis is required. Conventionally FSI problems are studied by various researchers, where mainly the effect of fluid flow on the structure is studied. Not much literature is available on effects of structural changes on the fluid flow in dampers. Recently a lot of research work has been done on smart fluid dampers, but these are active devices which are not suitable for shut-off rod drive mechanism applications, where we need a passive temperature compensating hydraulic dashpot. Research is focused on these gap areas.

2.3 Scope and Motivation for Present Work

Based on the literature review and the identified gap areas the scope of the current work is outlined below:

(i) Study and analysis of change in the dashpot clearances and oil properties with changes in the environmental temperature.

(ii) Suggestion for incorporating temperature compensating parts and their geometries in the hydraulic dashpot to reduce the clearances at elevated temperatures. This can be achieved by using a combination of materials with different coefficients of thermal expansion.

(iii) Design of a temperature compensating hydraulic dashpot which can be used for a wide range of temperatures without much variation in damping characteristics.

(iv) Experimental validation of the temperature compensating hydraulic dashpot for desired rod drop velocity profile using a full-scale test facility.

2.4 Present Work Profile

The objective of the present research is to achieve passive temperature compensation in a hydraulic dashpot. The study is focused on reducing the clearances of the hydraulic dashpot at elevated temperature which in turn compensate for the reduction in the viscosity of the damping oil and the dashpot gives uniform performance for a wide range of temperature variation. Temperature compensation effects are mainly due to differences in the thermal expansions of materials. Different combinations of materials are used to reduce the dashpot clearances at the elevated temperatures. The present work profile consists of:

(i) CFD analysis of hydraulic dashpot with experimental validation to investigate the effects of dashpot clearances and the damping oil viscosity on the dashpot performance.

(ii) Multi-body dynamics modeling, simulation and experimental validation.

(iii) Fluid-structure analysis (CFD/FEM) of the hydraulic dashpot to make it passive temperature compensating.

(iv) A novel passive temperature compensating design of a hydraulic dashpot using different metals for shut-off rod drive mechanism applications.

Chapter III

ANALYSIS OF DASHPOT PARAMETERS WITH EXPERIMENTAL VALIDATION

This chapter presents a detailed study of dashpot parameters like, dashpot clearances, damping oil viscosity, environmental temperature and their effects on the dashpot performance. The hydraulic dashpot performance is studied in terms of the dashpot pressure and the dashpot force using CFD techniques.

3.1 Introduction

The kinetic energy acquired by the rod at the end of free fall has to be absorbed in the hydraulic dashpot. For a shut-off rod application, the hydraulic dashpot design needs to be optimized, i.e., it should be a slightly over-damped system. If the dashpot design is highly over-damped, then the dashpot will absorb the entire energy much before its full rotation and the dashpot full rotation will take longer time which will not meet the 100% drop time criterion of the reactor. On the other hand, if the dashpot design is under-damped, then it will not absorb the whole energy even after its full rotation and the dashpot vane will hit the mechanical stopper, which results in impact loading on the drive mechanism components. Fig. 3.17 (d) and Fig. 3.19 (d) show the typical under-damped and over-damped rod drop profiles, respectively.

Dashpot force (F_d) can be described as:

$$F_d = F_p + F_s \tag{3.1}$$

where F_p is the dashpot force due to differential pressure and F_s is the dashpot force due to skin friction (shear force). Practically, the dashpot force due to skin friction is found to be negligible as compared to the dashpot force due to differential pressure, so the pressure in the dashpot chamber plays an important role. Also, the energy absorbed in the dashpot (E_d) can be described as:

$$E_d = T_d \times \theta \tag{3.2}$$

Where T_d is the torque on the dashpot shaft and θ is the angle of rotation. T_d is independent of θ.

The torque (T_d), at any instant can be described as: T_d = p x moment of vane area about its axis of rotation, where p is the dashpot pressure which is uniform on the vane area. Hence, we can say, for a particular amount of energy to be absorbed in the dashpot, an optimized value of pressure has to be generated in the hydraulic dashpot. The dashpot pressure can be optimized by a proper combination of the dashpot oil viscosity and the dashpot clearances. These parameters are studied in detail in this chapter.

3.2 Set-up Description and Working

In order to study the dashpot parameters in depth, the study was conducted on two different test set-ups; i.e., on the drive mechanisms of an AHWR and of a 540 MWe PHWR. Though the overall working of drive mechanisms and dashpots are the same, but the layout of components is different in the two set-ups. Both shut-off rods fall into water so the retarding forces in the guide tube are present. A shut-off rod drive mechanism along with the absorber assembly for an AHWR is given in Fig. 3.1 while its typical rod drop profile is given in Fig. 3.2. AHWR's SRDM is mounted inside a tube, so the whole construction of drive mechanism is in tubular form. The SRDM assembly comprises of following sub-assemblies; Motor Sub-Assembly, Worm Gear and Electromagnetic Clutch Sub-Assembly, Reduction Unit-I Sub-Assembly, Mechanism Housing Sub-Assembly, Sheave Shaft Sub-Assembly, Reduction Unit-II Sub-Assembly, Hydraulic Dashpot Sub-Assembly, Position Indication Unit Sub-Assembly, Reed Switch Sub-Assembly, Push Tube Sub-Assembly and Absorber Sub-Assembly.

Internally in a shut-off rod drive mechanism, the motor sub-assembly is connected to a worm gear and an electromagnetic (EM) clutch sub-assembly, which is further connected to a sheave (deep groove pulley) through a set of spur gears. Absorber sub-assembly (shut-off rod) is mounted on the sheave through a wire rope. The EM clutch is energized to raise the rod through the motor. As soon as the rod reaches the top position, which is sensed by reed switches, the motor is cut-off and the rod remains at that position, due to irreversibility of the worm gear design. During reactor scram, the EM clutch is de-energized and the rod falls freely due to gravity. A set of pick-up rings are used, which lapse one over the other bringing the hydraulic dashpot into action precisely at the 90% of rod drop. A spiral spring is used for resetting the hydraulic dashpot during the rod withdrawal. As soon as the rod reaches at the park up position, it also compresses a spring in the push tube assembly. This spring gives initial acceleration to the rod during the free fall.

Detailed construction of the hydraulic dashpot showing computational domains used in SRDMs for AHWR and 540 MWe PHWR is given in Figs. 3.3 and 3.4, respectively. Both hydraulic dashpots comprise of two moving vanes and two fixed vanes. As the moving vanes rotate, there is a formation of two high pressure and two low pressure chambers. Oil passes from the high-pressure chamber to the low-pressure chamber through narrow clearances. Both dashpots have clearances at the ID of the fixed vanes, OD of moving vanes and the side of the moving vanes. In AHWR dashpot there is a mechanical shaft seal on one side of the dashpot chamber and there is a passage through the shaft seal. The hydraulic dashpot of the 540 MWe PHWR SRDM comprises of two mechanical shaft seals and the passage is through the ID of the shaft.

One high pressure oil chamber is considered as the computational domain, Fig. 3.3 also shows the boundary conditions at different walls of computational domain. Table 3.1 gives the different parameters of the two cases under study.

Table 3.1: Set-up parameters for study

Parameter	**Case-1 (540 MWe PHWR)**	**Case-2 (AHWR)**
Drive mechanism overall size (mm)	350x350x1500	dia. 154x1270
Rod travel (mm)	6600	3900
Rod weight (kg)	50	40
Free fall (mm)	5940	3510
Hydraulic dashpot size (mm)	59 ID x 116 OD x 117 Length	48 ID x 115 OD x 22 Length
Hydraulic dashpot rotation (degree)	120	120
Mechanical shaft seal	on both sides	on one side
No. of dashpot vanes	two moving vanes/two fixed vanes	two moving vanes/two fixed vanes

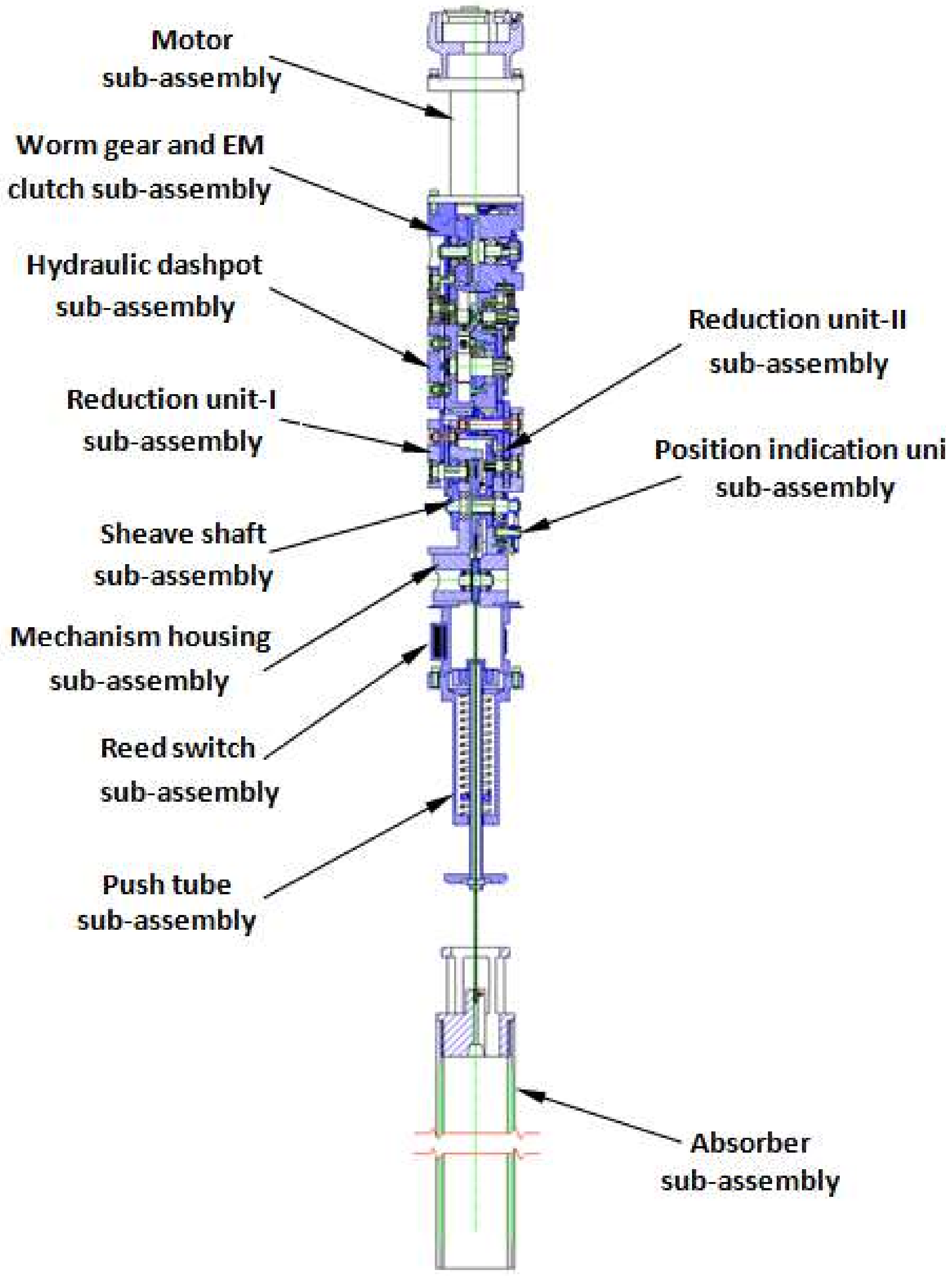

Fig. 3.1 Shut-off rod's drive mechanism for an AHWR

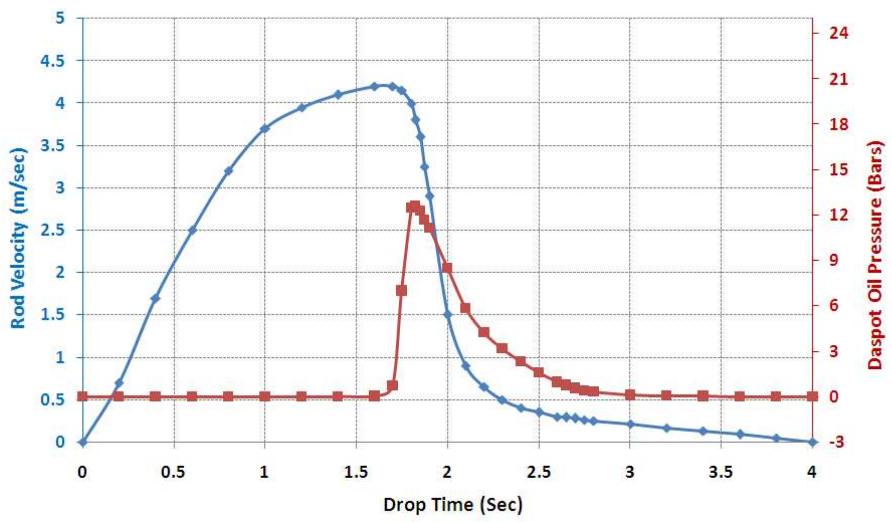

Fig. 3.2 A typical rod drop profile of a shut-off rod

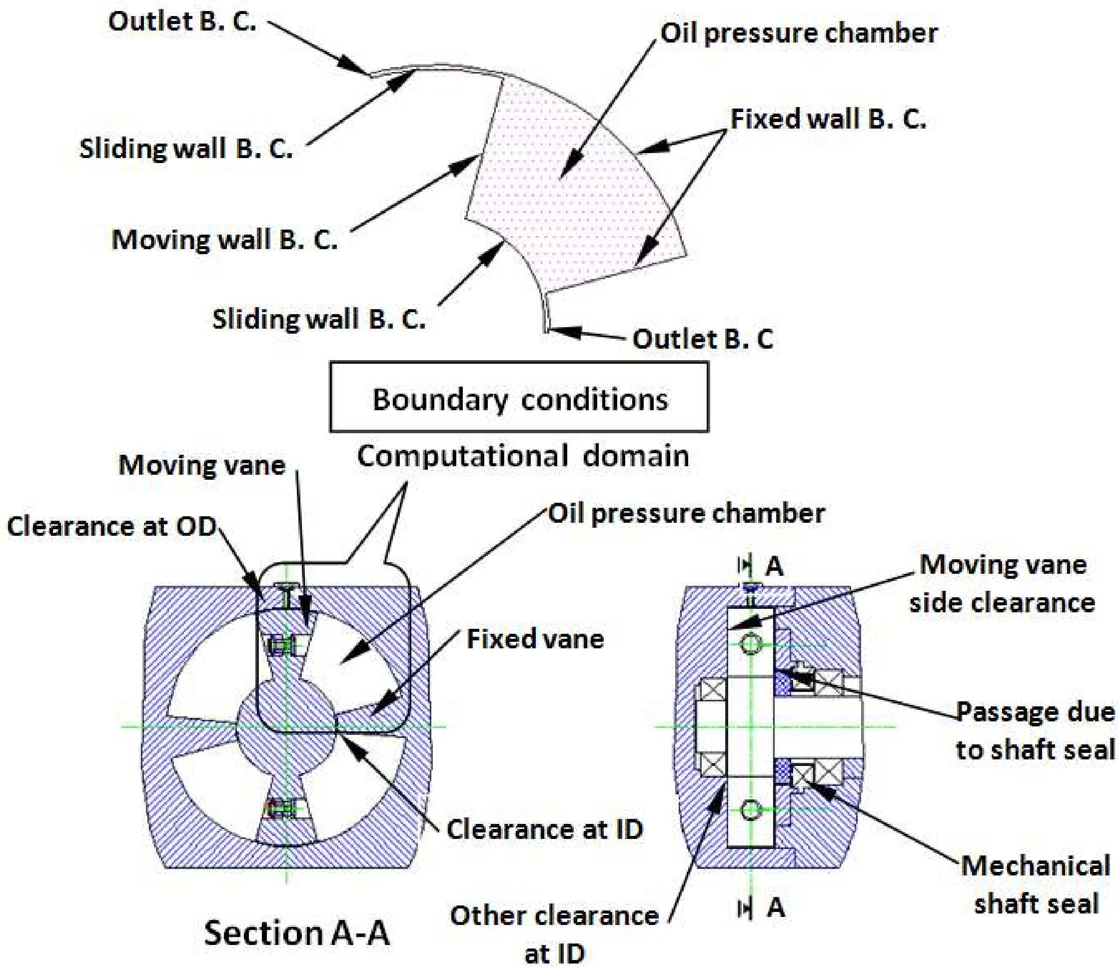

Fig. 3.3 Hydraulic dashpot construction of AHWR's SRDM showing computational domain and boundary conditions.

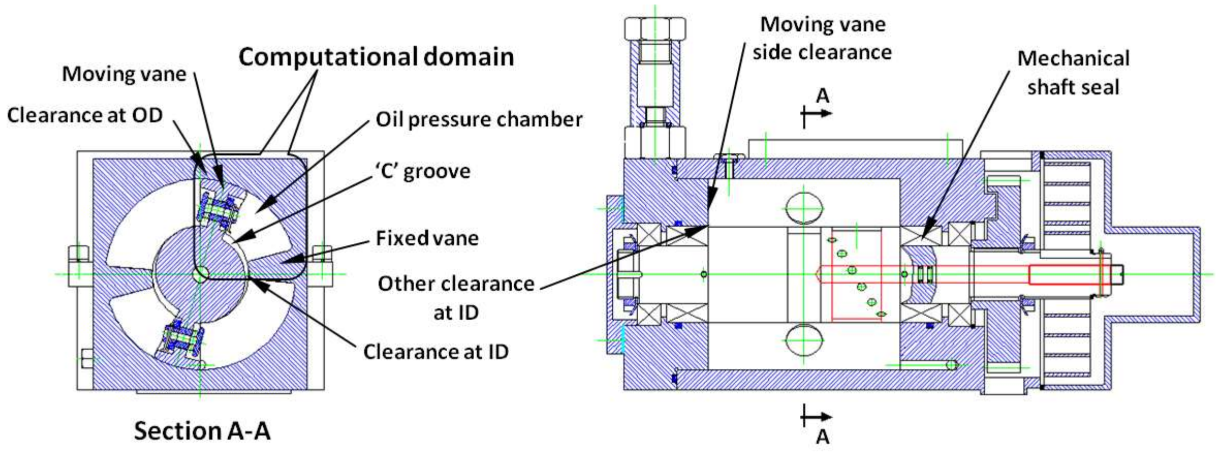

Fig. 3.4 Hydraulic dashpot construction of 540 MWe PHWRs SRDM.

3.3 Numerical Procedure

3.3.1 Governing Equations

The FEM based commercial code COMSOL Multiphysics 5.1 is used to solve the governing equations. The fluid flow in the fluid damper is described by the incompressible Navier-Stokes equations, solving for the velocity field $u_2 = (u_2,v_2,w_2)$ and the pressure. COMSOL 5.1 Documentation [64], COMSOL tutorial: Fluid damper [65].

The hydraulic dashpot operation is a transient phenomenon; hence flow variables and the computational domain change with time. The present study has been carried-out in 3-D geometry, as it is not possible to resolve the geometry in 2-D. Because of 3-D geometry and fast dashpot action, it is difficult to solve the transient equations with present computational set-up. So, alternatively the whole transient phenomenon has been divided into small time steps and the stationary equations are solved at different time steps. The computational domain (geometry) is also changed to that time step (by rotating the vane) after every time step. Further the equations are solved at the next time-step with the changed geometry and the boundary conditions. The initial condition at every time step is the wall velocity associated to the moving vane. This wall velocity is taken from the experimental measurements and given as the moving wall boundary condition. (Although a time dependent study of the dashpot dynamics is done in chapter 4 using multi-body dynamics tools) As frequency of operation is very low in these types of dashpots, the effect of viscous heating can be neglected as presented by He and Zheng, [66], hence energy equation is not solved in this study. 3-D continuity and momentum equations for incompressible flow solved in COMSOL Multiphysics for stationary conditions are:

$$\nabla . u_2 = 0 \tag{3.3}$$

$$\rho(u_2 . \nabla)\, u_2 = \nabla . [-pI + \mu\, (\nabla\, u_2 + (\nabla\, u_2)^T)] + F \tag{3.4}$$

Where, ∇ is the divergence operator, ρ is density of the fluid (kg m^{-3}), u_2 is the velocity field (u_2,v_2,w_2) (m sec^{-1}), p is the pressure (Pa), μ is the dynamic viscosity (Pa sec), I is the identity matrix, T indicates the transpose and F is the volume force vector (N m^{-3}). Equations have been discretized and solved in COMSOL.

3.3.2 Parallel Plate Model of Hydraulic Dashpot (Closed Form Solutions)

Flow through narrow clearances in the dashpot can be considered as laminar flow through parallel plates as shown in Fig. 3.5, Modi and Seth, [19]. As the vane moves rightwards, the pressure in the oil will be generated between the moving vane and the fixed vane. The oil will start moving through narrow clearances. The flow through narrow clearances is analyzed. The governing equations 3.3 and 3.4 are solved for the pressure and the velocity. In COMSOL Multiphysics, numerical solutions are achieved by solving the equations in three dimensions and we get a complete solution of the Navier-Stokes Equations. Further, if some assumptions are made in solving these equations, we get a closed form solution for the pressure in the dashpot. These assumptions are:

(i) The flow is laminar and viscous.

(ii) The flow is steady, incompressible and fluid properties are constant.

(iii) The flow in the narrow passage is 1-D (the fluid velocity components in cross flow directions are zero)

(iv) There is no body force.

(v) The pressure drop is linear through the depth of clearance.

(vi) The clearance thickness (c) in the dashpot is very small as compared to the depth of clearance (L), so the curvatures of the vane clearances are neglected.

(vii) During one dashpot operation all moving vanes, the fixed vanes, the dashpot oil and other components are at uniform temperature.

(viii) There is no internal heat generation and viscous heating is neglected.

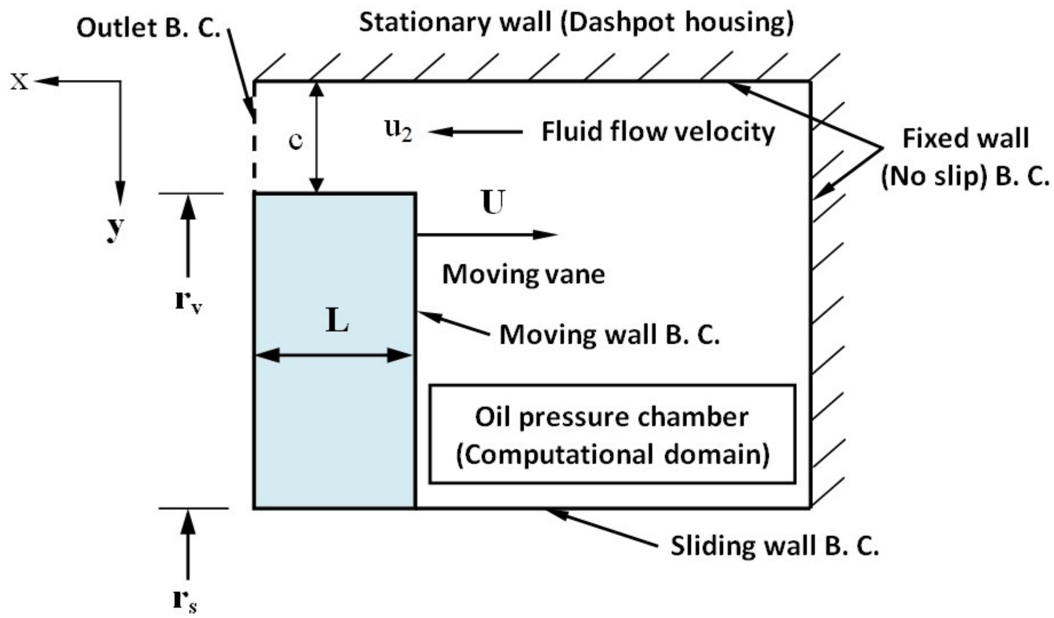

Fig. 3.5 Parallel plate model of hydraulic dashpot and COMSOL verification boundary conditions

Continuity Equation:

$$\frac{\partial u_2}{\partial x} + \frac{\partial v_2}{\partial y} = 0 \qquad (3.3')$$

Momentum Equation:

$$\rho\left[u_2\frac{\partial u_2}{\partial x} + v_2\frac{\partial u_2}{\partial y}\right] = -\frac{\partial p}{\partial x} + \mu\left[\frac{\partial^2 u_2}{\partial x^2} + \frac{\partial^2 u_2}{\partial y^2}\right] \qquad (3.4'a)$$

$$\rho\left[u_2\frac{\partial v_2}{\partial x} + v_2\frac{\partial v_2}{\partial y}\right] = -\frac{\partial p}{\partial y} + \mu\left[\frac{\partial^2 v_2}{\partial x^2} + \frac{\partial^2 v_2}{\partial y^2}\right] \qquad (3.4'b)$$

Boundary Conditions:

(i) At $y = 0$, $u_2 = 0$, $v_2 = 0$

(ii) At $y = c$, $u_2 = -U$, $v_2 = 0$

After applying the assumptions in above equations, we get

Continuity Equation:

$$\frac{\partial u_2}{\partial x} = 0 \qquad (3.3'a)$$

Momentum Equation:

$$\mu\frac{\partial^2 u_2}{\partial y^2} = \frac{\partial p}{\partial x} \qquad (3.4'c)$$

Integrating the equation (3.4'c) twice, we get

$$u_2 = \frac{y^2}{2\mu}\left(\frac{\partial p}{\partial x}\right) + C_1 y + C_2 \qquad (3.4'd)$$

where C_1 and C_2 are constants.

Applying boundary conditions in the equation (3.4'd), we get

$C_2 = 0$

$$-U = \frac{c^2}{2\mu}\left(\frac{\partial p}{\partial x}\right) + C_1 c$$

Hence,

$$C_1 = \frac{-U}{c} - \frac{c}{2\mu}\left(\frac{\partial p}{\partial x}\right)$$

Putting the values of C_1 and C_2 in equation (3.4'd), we get

$$u_2 = \frac{1}{2\mu}\left(\frac{\partial p}{\partial x}\right)(y^2 - cy) - \frac{Uy}{c} \qquad (3.4'e)$$

The fluid discharge (Q) through narrow clearance can be described as;

Discharge = Flow velocity x Flow area

Flow area = Length of clearance (L_c) x Thickness of clearance (c)

Hence,

$dQ = u_2 L_c\, dy$

$$dQ = L_c\left[\frac{1}{2\mu}\left(\frac{\partial p}{\partial x}\right)(y^2 - cy) - \frac{Uy}{c}\right]dy$$

$$Q = L_c \int_0^c \left[\frac{1}{2\mu}\left(\frac{\partial p}{\partial x}\right)(y^2 - cy) - \frac{Uy}{c}\right] dy$$

$$Q = L_c\left[\frac{-c^3}{12\mu}\left(\frac{\partial p}{\partial x}\right) - \frac{Uc}{2}\right] \qquad (3.4'f)$$

The equation (3.4'f) is the rate of flow of oil through the clearance space, which must be exactly equal to the rate at which oil is being displaced by the dashpot vane.

Oil displaced by the dashpot vane = Vane area x vane velocity

Hence,

$$(r_v - r_s)\, b\, U = L_c\left[\frac{-c^3}{12\mu}\left(\frac{\partial p}{\partial x}\right) - \frac{Uc}{2}\right] \qquad (3.4'g)$$

Assuming linear pressure drop in the x-direction, then we have;

$$\left(\frac{\partial p}{\partial x}\right) = -\frac{\Delta p}{L}$$

Further solving equation (3.4'g), we get the pressure equation for a rotary vane type dashpot as;

$$\Delta p = \frac{12\mu L U}{c^3}\left[(r_v - r_s)\frac{b}{L_c} + \frac{c}{2}\right] \qquad (3.5)$$

Where Δp is differential pressure (Pa) across the depth of clearance, μ is dynamic viscosity (Pa sec), L is depth of clearance (m), U is moving vane velocity (m sec^{-1}), c is clearance thickness or simply clearance (m), b is length of vane (m) in z-direction, L_C is length of clearance (m) in z-direction, r_v is outer radius of moving vane (m) and r_s is radius of vane shaft (m). Eq. 3.5 is used as a verification tool for the COMSOL Multiphysics. In order to verify the code, dashpot pressure has been calculated at different values of clearance thickness (c) by keeping other design parameters unchanged.

Boundary conditions (as shown in Fig. 3.5) for the COMSOL verification are as listed below:

(i) ***Initial values:*** Velocity field (u_2); $u_2 = 0$, $v_2 = 0$

(ii) ***Fixed Wall (No Slip) Boundary Conditions:*** Velocity field (u_2); $u_2 = 0$, $v_2 = 0$

(iii) ***Moving Wall Boundary Conditions:***

Velocity of moving wall (u_w); $(u_w)_x = -U$, $(u_w)_y = 0$

(iv) ***Sliding Wall Boundary Conditions:***

Velocity of sliding wall (u_{sw}); $(u_{sw})_x = -U$, $(u_{sw})_y = 0$

(v) ***Outlet Boundary Conditions:*** Pressure (p) = 0

Design data used for pressure calculations is given in Table 3.2 and the comparison of pressure results obtained from Eq. 3.5 and COMSOL Multiphysics are given in Table 3.3.

Table 3.2: Design data for COMSOL verification.

Design parameter	**Numerical value**
Dynamic viscosity (μ) Pa-s	1.96
Depth of clearance (L) m	0.031
Moving vane velocity (U) m s^{-1}	0.489
Clearance thickness (c) mm	Varied from 0.1 to 0.5
Length of vane (b) m	0.022
Length of clearance (L_C) m	0.022
Radius of moving vane (r_v) m	0.0575
Radius of vane shaft (r_s) m	0.024

Table 3.3: Comparison of pressure results obtained from Eq. 3.5 and COMSOL Multiphysics.

Clearance thickness (mm)	**Pressure obtained from Eq. 3.5 (Pa)**	**Pressure obtained from COMSOL Multiphysics (Pa)**
0.1	1.196×10^{10}	1.194×10^{10}
0.2	1.497×10^{9}	1.496×10^{9}
0.3	4.443×10^{8}	4.444×10^{8}
0.4	1.877×10^{8}	1.879×10^{8}
0.5	9.625×10^{7}	9.642×10^{7}

As shown in Table 3.3, pressure values hand calculated from Eq. 3.5 give a very good agreement with the numerical solution achieved from COMSOL Multiphysics. This validates the applicability of the code for this application. Also, in the literature, equations similar to (3.5) have been given by Hou [12], Jia and Hua [14], He and Zheng [66] for linear dashpots.

3.3.3 Boundary Conditions

In all the simulations, the wall normal to the moving vane is set as the moving wall and the adjoining faces are set as the sliding walls. The faces which are sliding with dashpot shaft are also set as the sliding walls. As COMSOL Multiphysics solves the momentum and continuity equations in Cartesian co-ordinates (x,y,z), so the whole geometry is made in the Cartesian co-ordinate system. The dashpot vane rotates in the theta direction, so all the boundary conditions are resolved accordingly. COMSOL tutorial: Tilted pad bearing [67]. The equations are solved as stationary at a particular time step. For that time step required volume in the chamber is generated. Moving vane and sliding vane boundary conditions are defined as variables in the definitions. These variables are generated as a function of the coordinates in the radial direction. All the openings of clearances in the low-pressure chamber are set as outlet boundary conditions. Remaining faces are set as no slip boundary condition. The pressure transducer and oil level indication holes don't play any role in the computation, so it is removed from the computational domain. The whole domain is meshed with structured hexahedral mesh as shown in the Fig. 3.6.

(i) Initial values:

Velocity field (u_2); $u_2 = 0$, $v_2 = 0$, $w_2 = 0$

(ii) Fixed Wall (No Slip) Boundary Conditions:

Velocity field (u_2); $u_2 = 0$, $v_2 = 0$, $w_2 = 0$

(iii) Moving Wall Boundary Conditions:

Velocity of moving wall (u_w);

$(u_w)_x = 0$ (as, x is the axis of dashpot)

$(u_w)_y = 0$ (as, wall movement is perpendicular to y direction)

$(u_w)_z$ = moving wall velocity in z direction

(iv) Sliding Wall Boundary Conditions:

Velocity of sliding wall (u_{sw});

$(u_{sw})_x = 0$ (as, x is the axis of dashpot)

$(u_{sw})_y$ = sliding wall velocity in y direction

$(u_{sw})_z$ = sliding wall velocity in z direction

(v) Outlet Boundary Conditions:

Pressure (p) = 0

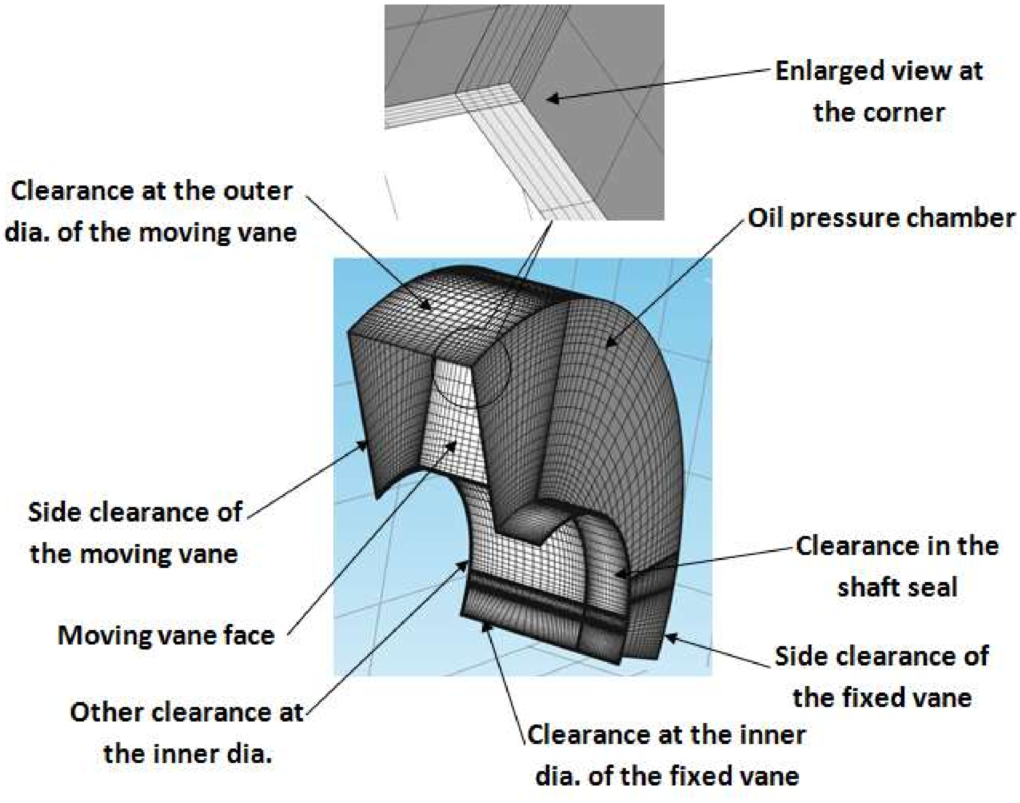

Fig. 3.6 Structured hexahedral mesh for AHWR's hydraulic dashpot.

3.3.4 Meshing and Grid Independence

A grid independence study was performed to find the mesh size that was sufficiently fine so that solution does not change by further refining the mesh. Pressure generated in the oil pressure chamber i.e. dashpot pressure was evaluated using

COMSOL Multiphysics at a particular time-step. At this time-step keeping other parameters unchanged, numbers of elements in the mesh were increased. Fig. 3.7 shows the dashpot pressure variation against the total number of elements in the mesh. No appreciable change has been found beyond 102500 numbers of elements. So, this is considered as the optimized mesh size for this geometry. In this mesh size, there are minimum 5 elements across the thickness of the clearance as shown in the Fig. 3.6.

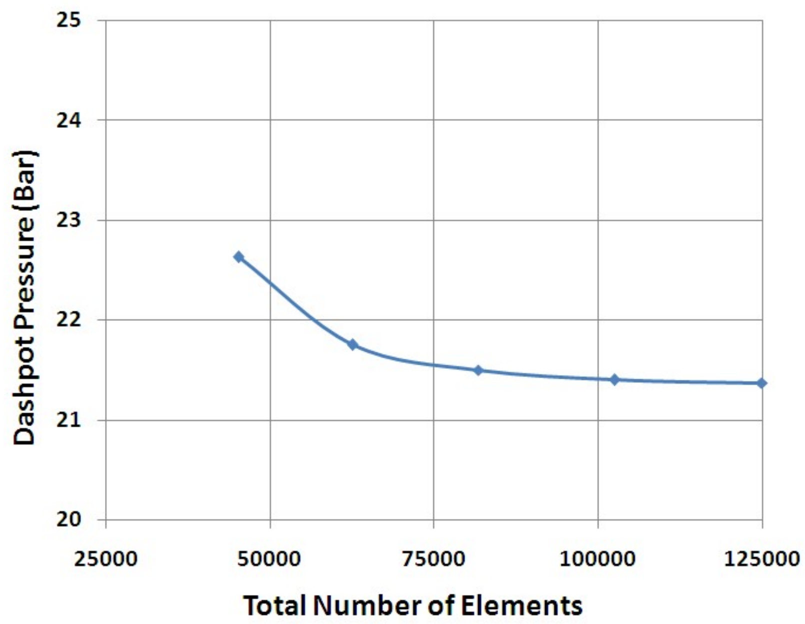

Fig. 3.7 Effect of grid size on dashpot pressure at a fixed time-step.

3.3.5 Convergence Methods

Equations are solved by using direct solvers with fully coupled approach. Nonlinear method used is automatic Newton. All the solutions were considered to be fully converged when the sum of absolute value of residuals was below 10^{-5}. Convergence is achieved on a work station with system descriptions as: Processor; 3.40 GHz, 64-bit operating system and 64.0 GB RAM and the CPU time is 5 minutes.

3.4 Experimental Studies

Shut-off rod drive mechanisms are safety critical systems of a nuclear reactor; thus, the design is qualified through prototype testing on a full-scale test station by simulating the actual reactor conditions, Singh [68]. Failure probability of the system should be less than 10^{-3} year/year as given by Singh et al. [69]. Prototype testing is done to finalize the rod drop parameters, component replacement frequency and maintenance schedule. Fig. 3.8 and 3.9 show the full-scale test-stations of 540 MWe PHWR's SRDM and AHWR's SRDM respectively. Fig. 3.10 gives the detail of hydraulic dashpot assembly of AHWR's SRDM. As discussed in section 3.2, during rod free fall the dashpot is loaded through a set of pick-up rings which lapse one over the other bringing dashpot into action precisely at the 90% of rod drop. A tacho-generator (Make: Servo-tek, Accuracy: 0.571%) is mounted on the mechanism to measure the sheave shaft speed, which in turn gives the dashpot shaft speed. A pressure transducer (Make: Schaevitz, Accuracy: 0.059%) is mounted on the hydraulic dashpot to measure the pressure inside the oil chamber. A servo-mount potentiometer (Linearity: 0.15%) is mounted on the sheave shaft to measure the rod position at any time. A test console is used to operate the SRDM. Thermal array-recorder (Make: Graphtec) is used to plot the output voltage of tacho-generator, potentiometer and pressure transducer against time. The output voltages are converted into the sheave shaft speed / hydraulic dashpot speed, rod position and hydraulic dashpot pressure. Hydraulic dashpot designs have been finalized after detailed numerical and experimental analysis of various combinations of dashpot clearance and oil viscosity.

Elevated Temperature viscosity of silicone oil is taken from the Eq. 3.6 as given by ShinEtsu [70]

$$\log \eta^{t} = \frac{763.1}{273+} - 2.559 + \log \eta^{25} \tag{3.6}$$

where, η^t = kinematic viscosity (mm^2/s) at t°C

η^{25} = kinematic viscosity (mm^2/s) at 25°C

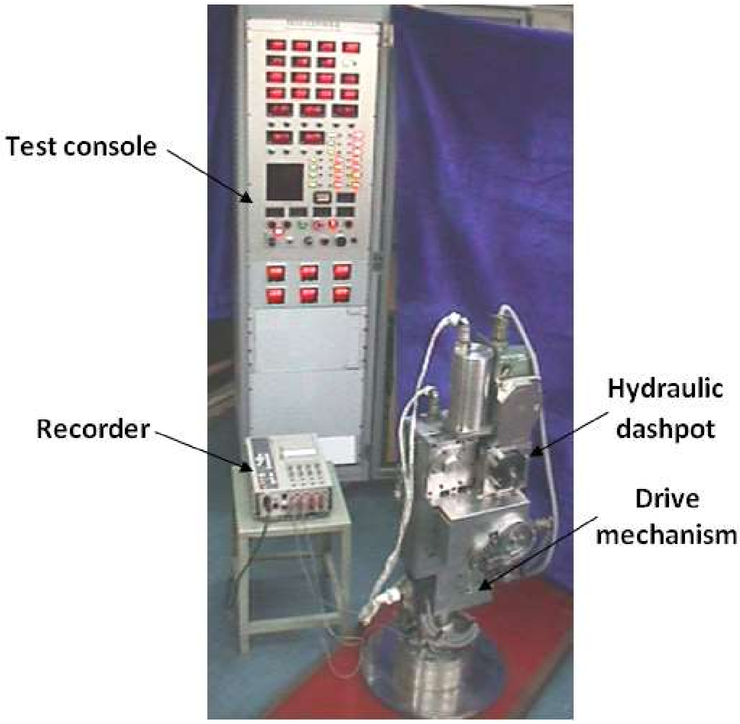

Fig. 3.8 Test set-up for 540 MWe PHWR's SRDM

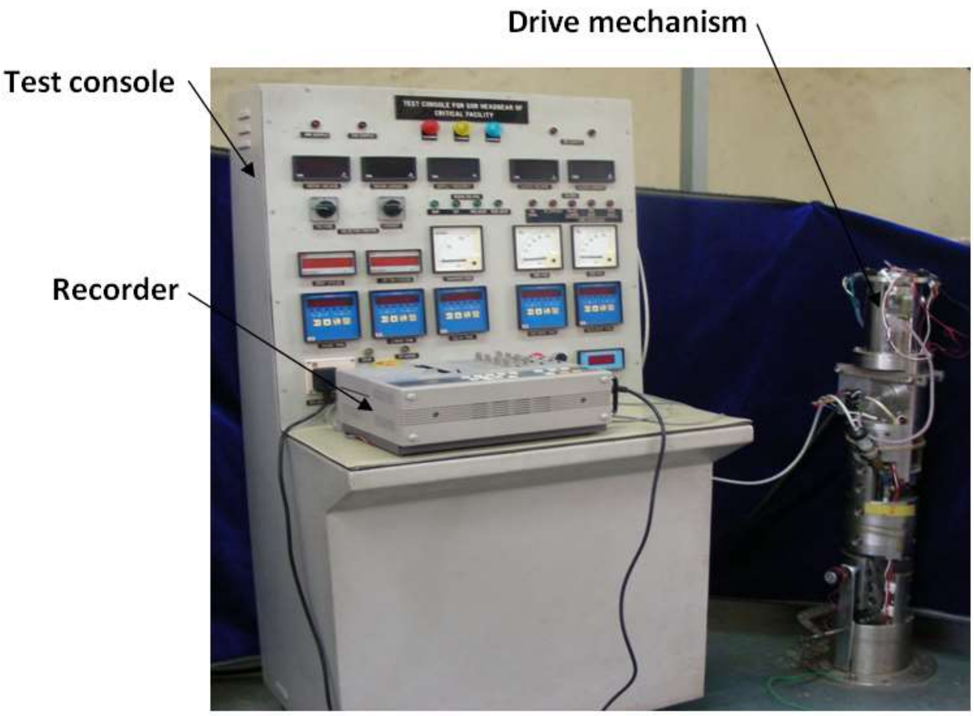

Fig. 3.9 Test set-up for AHWR's SRDM

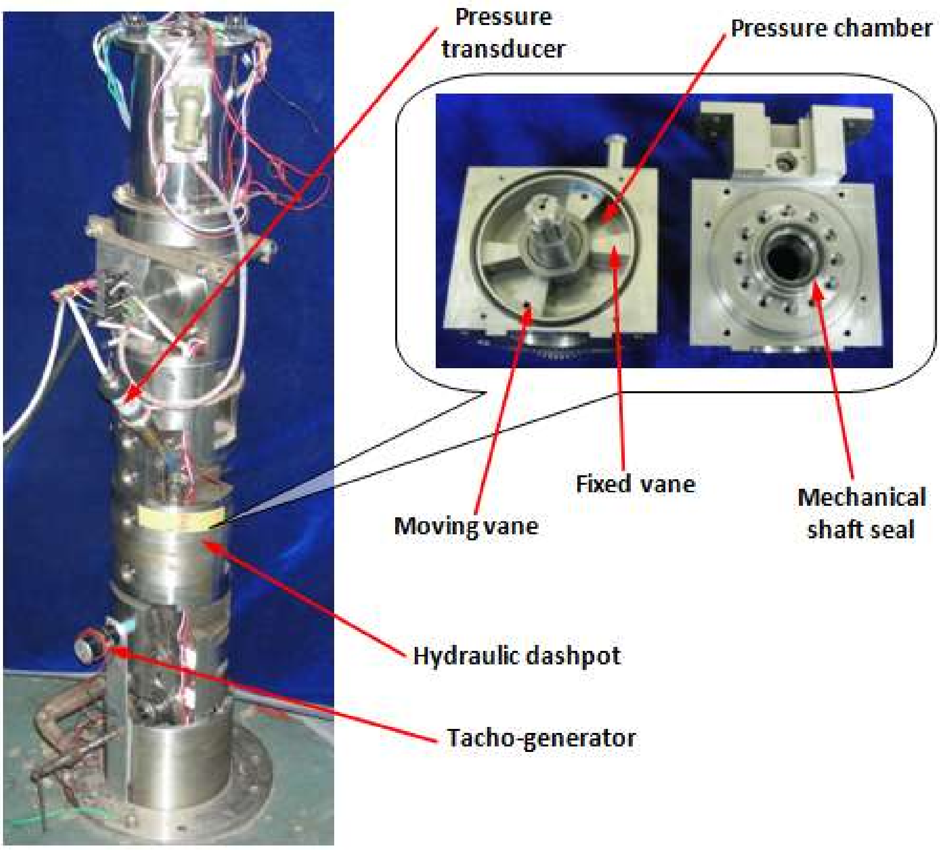

Fig. 3.10 Hydraulic dashpot details of AHWR's SRDM

3.4.1 Experimental Validation

Numerical results are compared with experimental results in order to validate the model. Figs. 3.11 and 3.12 give a comparison of numerical and experimental values of pressure developed in the oil pressure chamber of AHWR's SRDM at room temperature (35°C) and elevated temperature (75°C) respectively. Numerical results show very good agreement with the experimental results. If we compare the results of room temperature and elevated temperature, the viscosity of oil reduces to less than half at the elevated temperature, but pressure doesn't reduce in the same proportion (experimental value 19.5 bars at room temperature and 17 bars at elevated temperature). At high temperature the energy is absorbed in the dashpot towards the end of its operation, as viscosity reduces, oil passes quickly to low pressure chamber and the vane moves fast, hence less volume in the chamber results in comparatively higher pressure. Numerical values are slightly higher as compared to the experimental value, because of some pressure loss in the measurement. Both experimental and numerical curves follow the similar trend. Also, at the initial stage of Figs. 3.11 and 3.12, the experimental graphs show lesser slopes in comparison with the numerical ones. This is due to the measurement inaccuracies at the beginning, when the dashpot movement is very fast.

Figs. 3.13 and 3.14 give comparison of force due to pressure (both experimental and numerical) and total dashpot force at room temperature (35°C) and elevated temperature (75°C) respectively. Force due to pressure is calculated by multiplying the pressure to the total vane area. Total dashpot force is calculated from the experimental values of deceleration in the rod fall due to dashpot action. Total dashpot force comprises of force due to pressure drop, force due to skin friction and spiral spring force. Spiral spring force is almost constant (14.9 Kg. approx.) for both at room temperature as well as elevated temperature. This shows that the force due to skin friction is very less. If we compare the Figs. 3.13 and 3.14, we can say that, at elevated temperature the more dashpot force is generated towards the end of dashpot action. At room temperature the force is generated over a wide range of dashpot action.

Figs. 3.15 and 3.16 show the pressure distributions in computational domain of hydraulic dashpot of AHWR's SRDM and 540 MWe PHWR's SRDM respectively at the room temperature. The peak pressure for the hydraulic dashpot of AHWR's SRDM is numerically found to be 21.4 bar and that of 540 MWe PHWR's SRDM is 9.74 bar which have a very good agreement with the experimental results (19.5 bar and 8.5 bar respectively) shown in Figs. 3.21(a) and Fig. 3.20(a). It can also be seen from Figs.

3.15 and Fig. 3.16 that the pressure distribution in the whole pressure chamber is uniform. Pressure drop across all clearances is visible in Figs. 3.15 and Fig. 3.16. The pressure drop across the extra clearance in mechanical shaft seal is seen in the Fig. 3.15 and the effect of ‘C’ groove is seen in the Fig. 3.16.

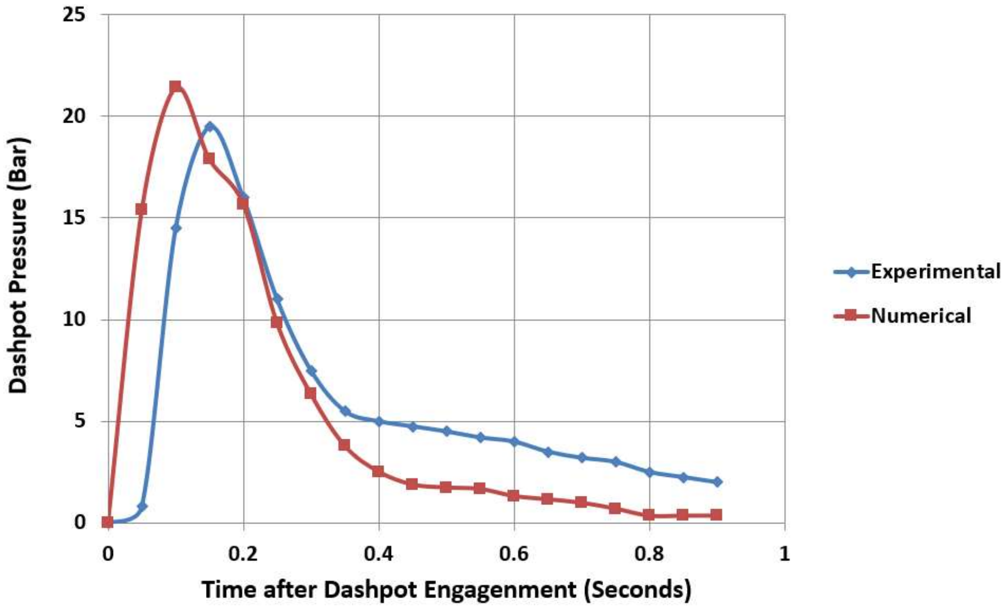

Fig. 3.11 Comparison of numerical and experimental dashpot pressure profiles of AHWR’s SRDM at room temperature (35°C).

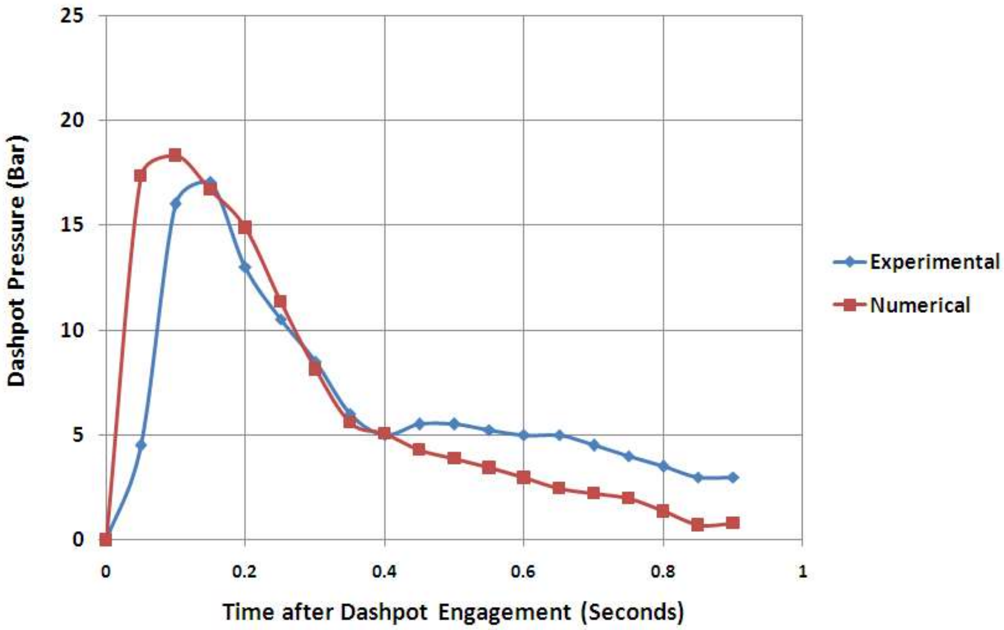

Fig. 3.12 Comparison of numerical and experimental dashpot pressure profiles of AHWR’s SRDM at elevated temperature (75°C).

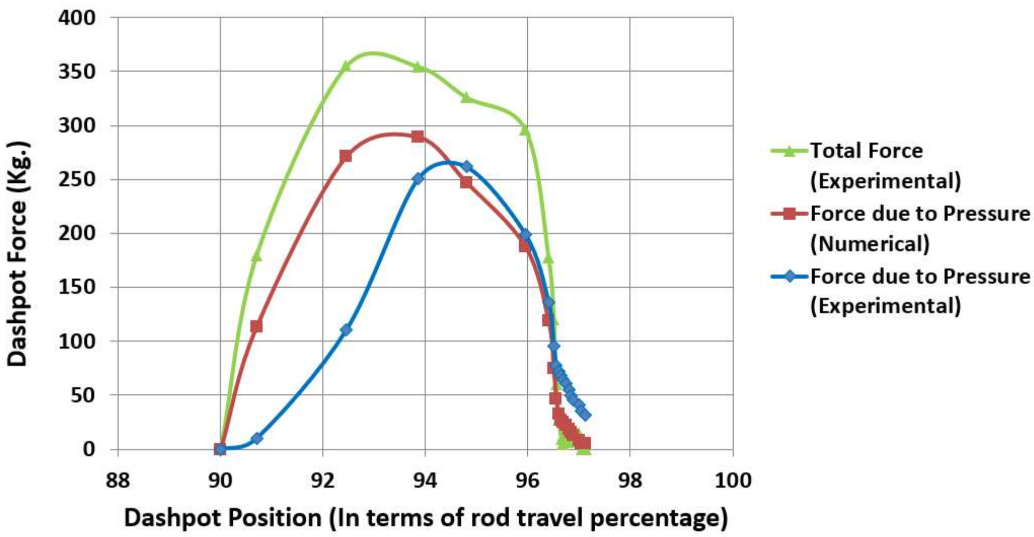

Fig. 3.13 Comparison of numerical and experimental dashpot force profiles of AHWR's SRDM at room temperature (35°C).

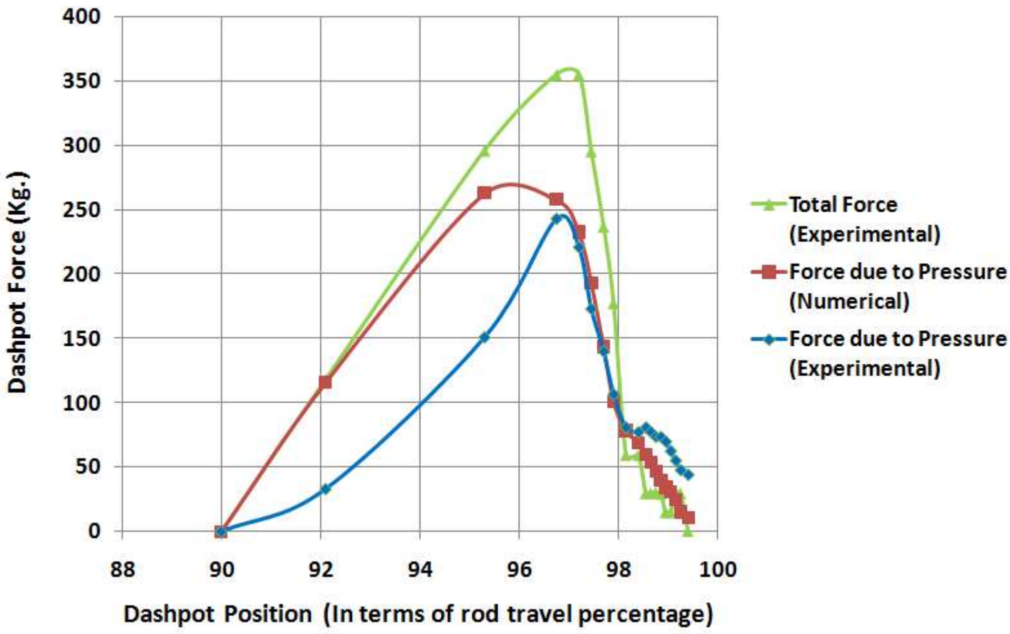

Fig. 3.14 Comparison of numerical and experimental dashpot force profiles of AHWR's SRDM at elevated temperature (75°C)

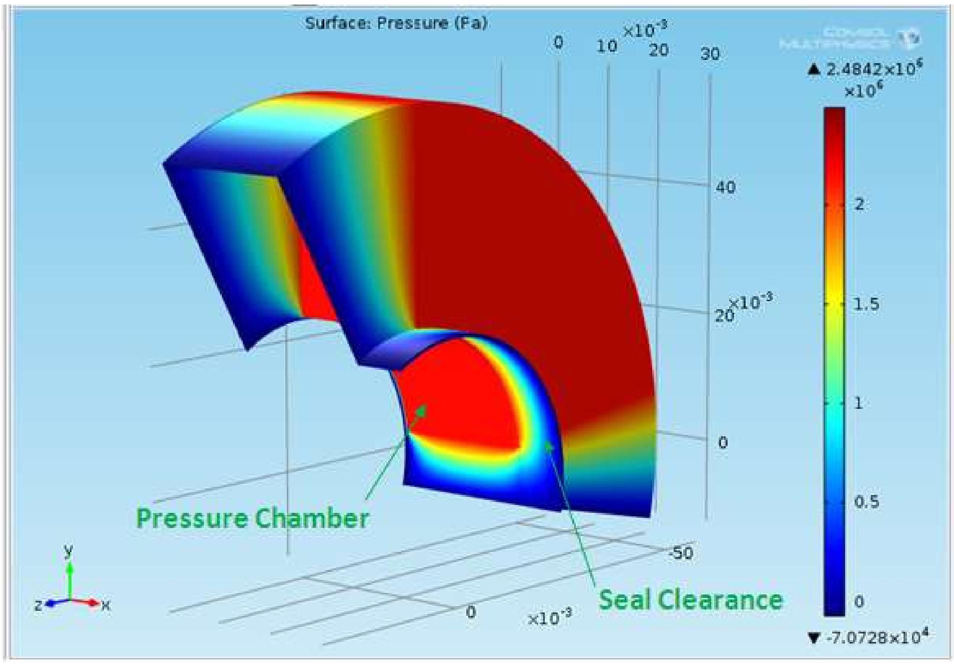

Fig. 3.15 Pressure distribution in the computational domain of hydraulic dashpot of AHWR's SRDM (COMSOL Multiphysics results)

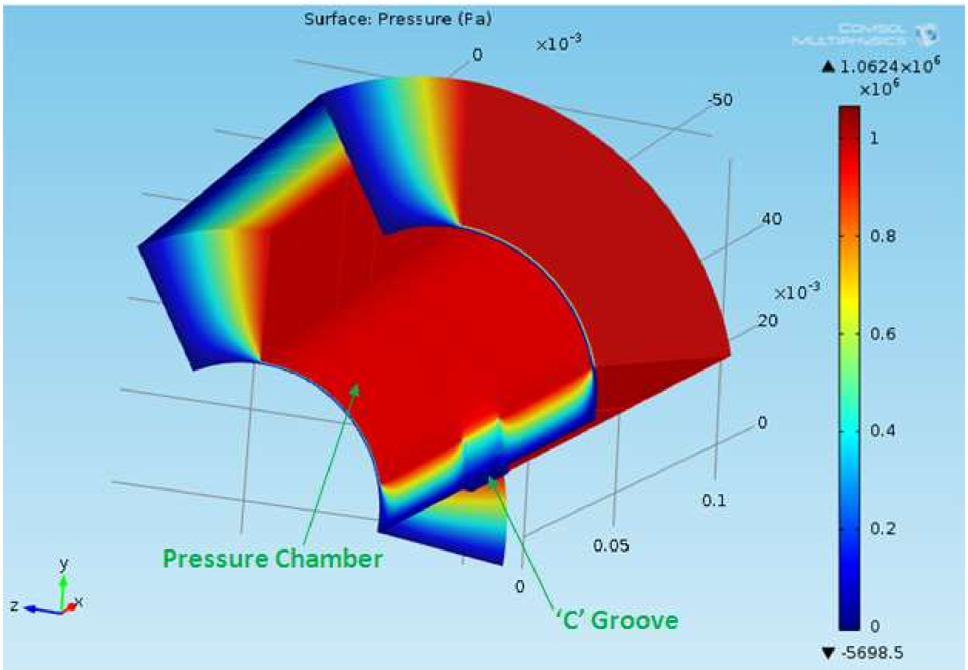

Fig. 3.16 Pressure distribution in the computational domain of hydraulic dashpot of 540 MWe PHWR's SRDM (COMSOL Multiphysics results)

3.4.2 Experimental Results

Experimental study was done in depth to draw more experimental results. Some of useful results are given in Table 3.4 and actual rod drop profiles are given in Figs.3.17-3.22 with different conditions.

Table 3.4: Parameters and results of actual drop profiles.

Plot No. (Temp.)	**Test set-up**	**X-Axis parameter**	**Y-Axis parameter**	**Oil kin. viscosity (at 25°C)**	**ID clea-rance (mm)**	**OD clea-rance (mm)**	**Side clea-rance (mm)**	**Shaft seal passage (mm)**	**'C' groove (mm)**	**Remark**
3.17 (a) (35°C)	540 MWe PHWR	Time (Seconds)	Dashpot pressure (Bar)	2000 cst	0.4	0.3	0.4	-	-	Peak pressure = 6.75 bars
3.17 (b) (35°C)	540 MWe PHWR	Time (Seconds)	Sheeve speed (rpm)	2000 cst	0.4	0.3	0.4	-	-	Total drop time = 3.6 Sec
3.17 (c) (65°C)	540 MWe PHWR	Time (Seconds)	Rod position (%)	2000 cst	0.4	0.3	0.4	-	-	-
3.17 (d) (65°C)	540 MWe PHWR	Time (Seconds)	Sheeve speed (rpm)	2000 cst	0.4	0.3	0.4	-	-	Total drop time = 2.1 Sec
3.18 (a) 35°C)	540 MWe PHWR	Time (Seconds)	Dashpot pressure (Bar)	3000 cst	0.4	0.3	0.4	-	-	Peak pressure = 6.9 bars
3.18 (b) 35°C)	540 MWe PHWR	Time (Seconds)	Sheeve speed (rpm)	3000 cst	0.4	0.3	0.4	-	-	Total drop time = 4.0 Sec
3.18 (c) (65°C)	540 MWe PHWR	Time (Seconds)	Dashpot pressure (Bar)	3000 cst	0.4	0.3	0.4	-	-	Peak pressure = 4.5 bars
3.18 (d) (65°C)	540 MWe PHWR	Time (Seconds)	Sheeve speed (rpm)	3000 cst	0.4	0.3	0.4	-	-	Total drop time = 2.2 Sec
3.19 (a) 35°C)	540 MWe PHWR	Time (Seconds)	Dashpot pressure (Bar)	7000 cst	0.4	0.3	0.4	-	-	Peak pressure = 11.0 bars
3.19 (b) 35°C)	540 MWe PHWR	Time (Seconds)	Sheeve speed (rpm)	7000 cst	0.4	0.3	0.4	-	-	Total drop time = 4.9 Sec

Plot No. (Temp.)	Test set-up	X-Axis parameter	Y-Axis parameter	Oil kin. viscosity (at 25°C)	ID clea-rance (mm)	OD clea-rance (mm)	Side clea-rance (mm)	Shaft seal passage (mm)	'C' groove (mm)	Remark
3.19 (c) (65°C)	540 MWe PHWR	Time (Seconds)	Dashpot pressure (Bar)	7000 cst	0.4	0.3	0.4	-	-	Peak pressure = 7.0 bars
3.19 (d) (65°C)	540 MWe PHWR	Time (Seconds)	Sheeve speed (rpm)	7000 cst	0.4	0.3	0.4	-	-	Total drop time = 2.6 Sec
3.20 (a) 35°C)	540 MWe PHWR	Time (Seconds)	Dashpot pressure (Bar)	2000 cst	0.15	0.15	0.3	-	2	Peak pressure = 8.5 bars
3.20 (b) 35°C)	540 MWe PHWR	Time (Seconds)	Sheeve speed (rpm)	2000 cst	0.15	0.15	0.3	-	2	Total drop time = 5.2 Sec
3.20 (c) (65°C)	540 MWe PHWR	Time (Seconds)	Dashpot pressure (Bar)	2000 cst	0.15	0.15	0.3	-	2	Peak pressure = 11 bars
3.20 (d) (65°C)	540 MWe PHWR	Time (Seconds)	Sheeve speed (rpm)	2000 cst	0.15	0.15	0.3	-	2	Total drop time = 2.7 Sec
3.21 (a) 35°C)	AHWR	Time (Seconds)	Dashpot pressure (Bar)	2000 cst	0.1	0.1	0.25	0.5	-	Peak pressure = 19.5 bars
3.21 (b) 35°C)	AHWR	Time (Seconds)	Sheeve speed (rpm)	2000 cst	0.1	0.1	0.25	0.5	-	Total drop time = 4.6 Sec
3.21 (c) 35°C)	AHWR	Time (Seconds)	Rod position (%)	2000 cst	0.1	0.1	0.25	0.5	-	-
3.21 (d) 35°C)	AHWR	Time (Seconds)	Sheeve speed (rpm)	2000 cst	0.1	0.1	0.25	0.5	-	Total drop time = 4.6 Sec
3.22 (a) (75°C)	AHWR	Time (Seconds)	Dashpot pressure (Bar)	2000 cst	0.1	0.1	0.25	0.5	-	Peak pressure = 17.0 bars
3.22 (b) (75°C)	AHWR	Time (Seconds)	Sheeve speed (rpm)	2000 cst	0.1	0.1	0.25	0.5	-	Total drop time = 3.05 Sec
3.22 (c) (75°C)	AHWR	Time (Seconds)	Rod position (%)	2000 cst	0.1	0.1	0.25	0.5	-	-
3.22 (d) (75°C)	AHWR	Time (Seconds)	Sheeve speed (rpm)	2000 cst	0.1	0.1	0.25	0.5	-	Total drop time = 3.05 Sec

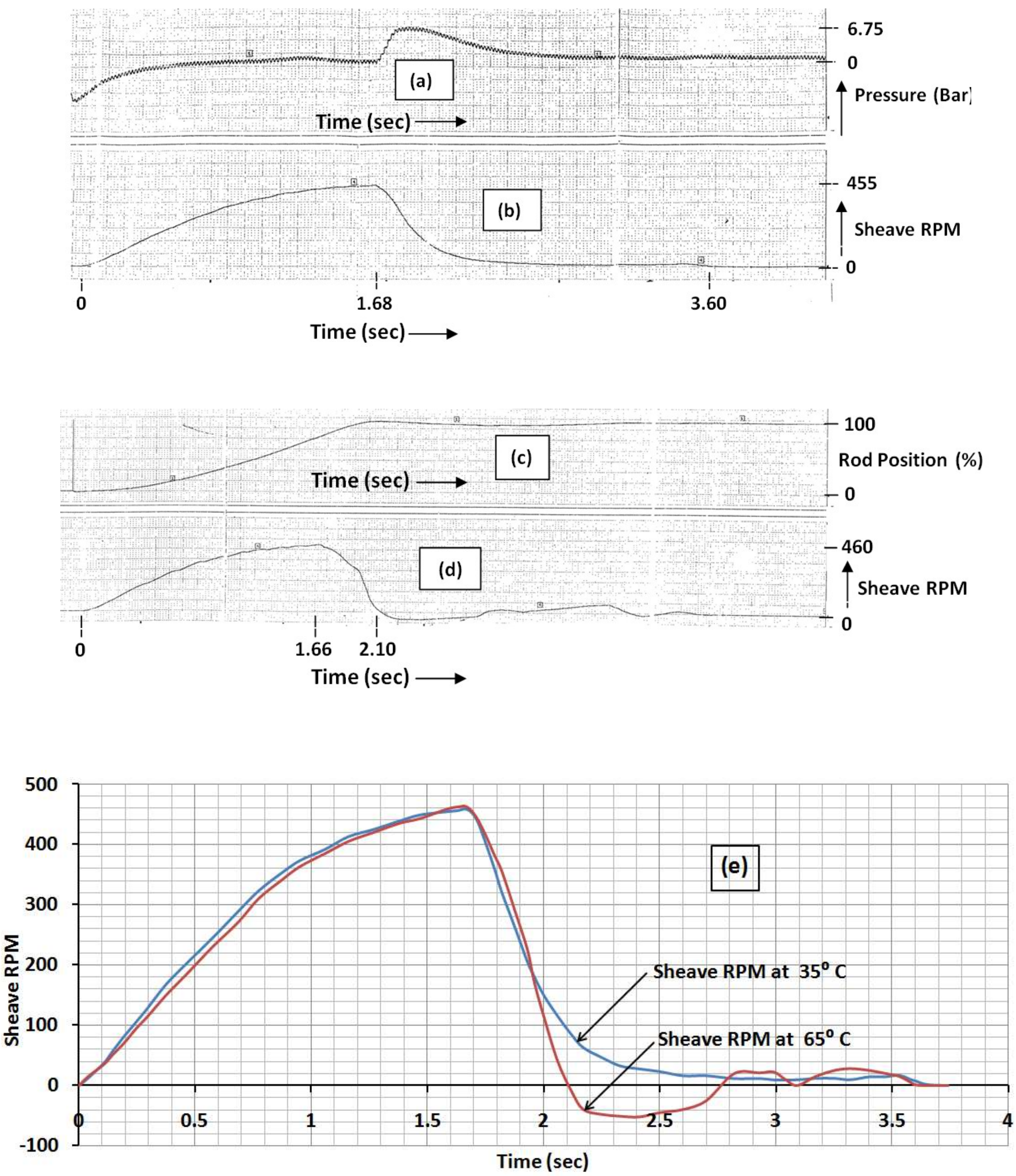

Fig. 3.17 Actual drop profiles of shut-off rod drop for 540 Mwe PHWR's SRDM with 2000 cst silicone oil in the dashpot

(a) Dashpot Pressure vs Time at 35°C
(b) Sheave Speed vs Time at 35°C
(c) Rod Position vs Time at 65°C
(d) Sheave Speed vs Time at 65°C
(e) Comparison of drop profiles at 35°C and 65°C (Data obtained by image processing)

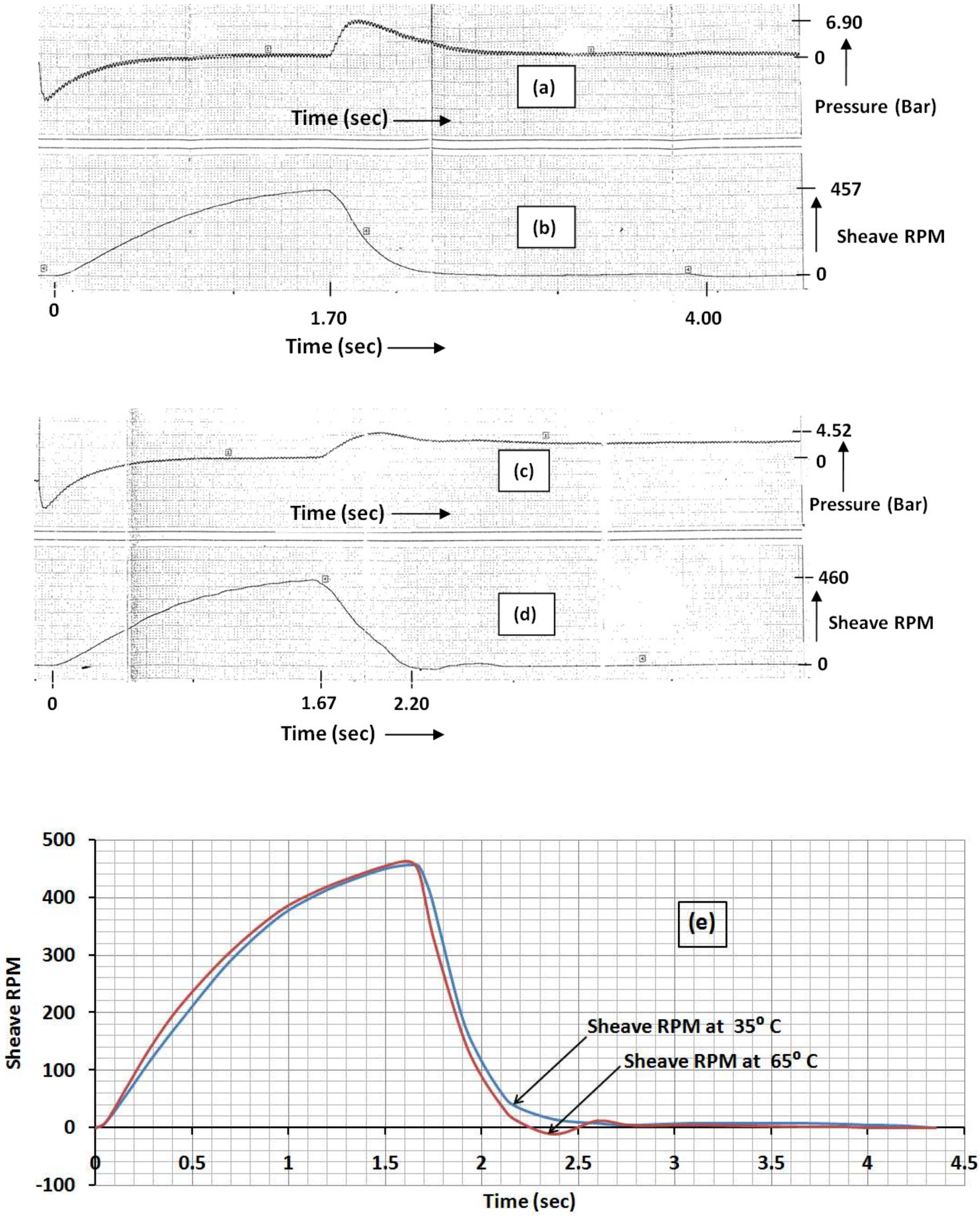

Fig. 3.18 Actual drop profiles of shut-off rod drop for 540 Mwe PHWR's SRDM with 3000 cst silicone oil in the dashpot

(a) Dashpot Pressure vs Time at 35°C
(b) Sheave Speed vs Time at 35°C
(c) Dashpot Pressure vs Time at 65°C
(d) Sheave Speed vs Time at 65°C
(e) Comparison of drop profiles at 35°C and 65°C
(Data obtained by image processing)

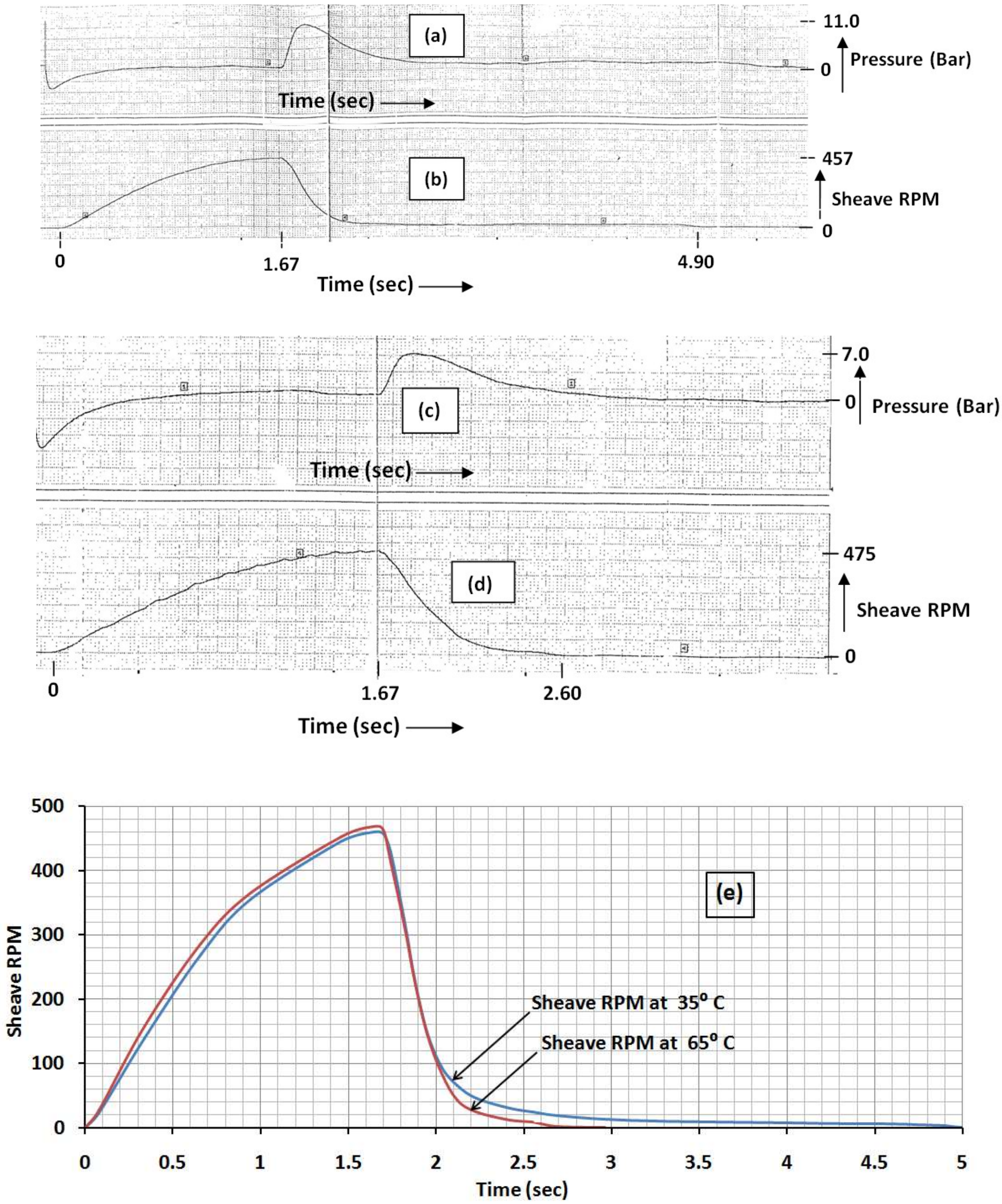

Fig. 3.19 Actual drop profiles of shut-off rod drop for 540 Mwe PHWR's SRDM with 7000 cst silicone oil in the dashpot

(a) Dashpot Pressure vs Time at 35°C
(b) Sheave Speed vs Time at 35°C
(c) Dashpot Pressure vs Time at 65°C
(d) Sheave Speed vs Time at 65°C
(e) Comparison of drop profiles at 35°C and 65°C
(Data obtained by image processing)

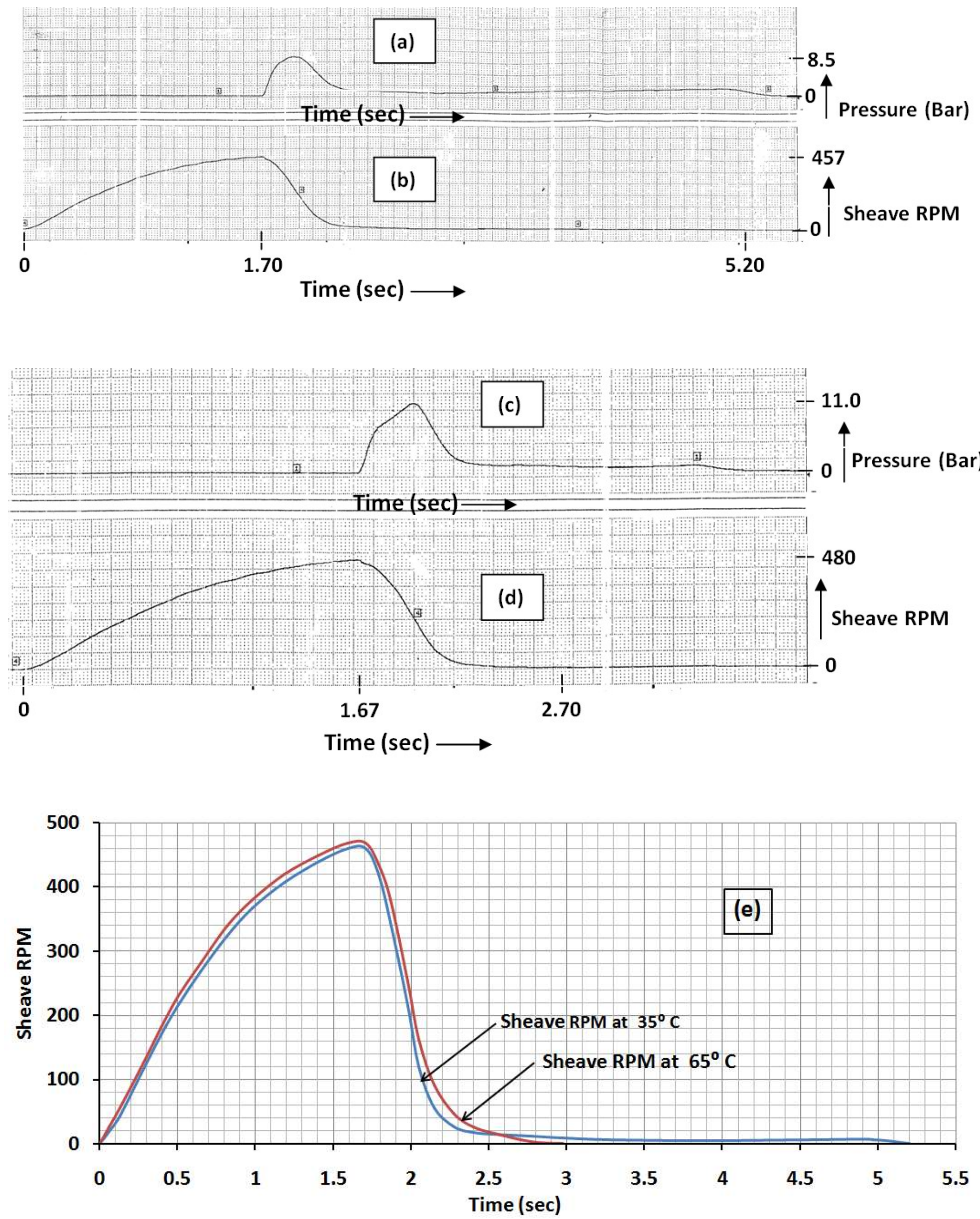

Fig. 3.20 Actual drop profiles of shut-off rod drop for 540 Mwe PHWR's SRDM with 2000 cst silicone oil (reduced clearances)

(a) Dashpot Pressure vs Time at 35°C
(b) Sheave Speed vs Time at 35°C
(c) Dashpot Pressure vs Time at 65°C
(d) Sheave Speed vs Time at 65°C
(e) Comparison of drop profiles at 35°C and 65°C
(Data obtained by image processing)

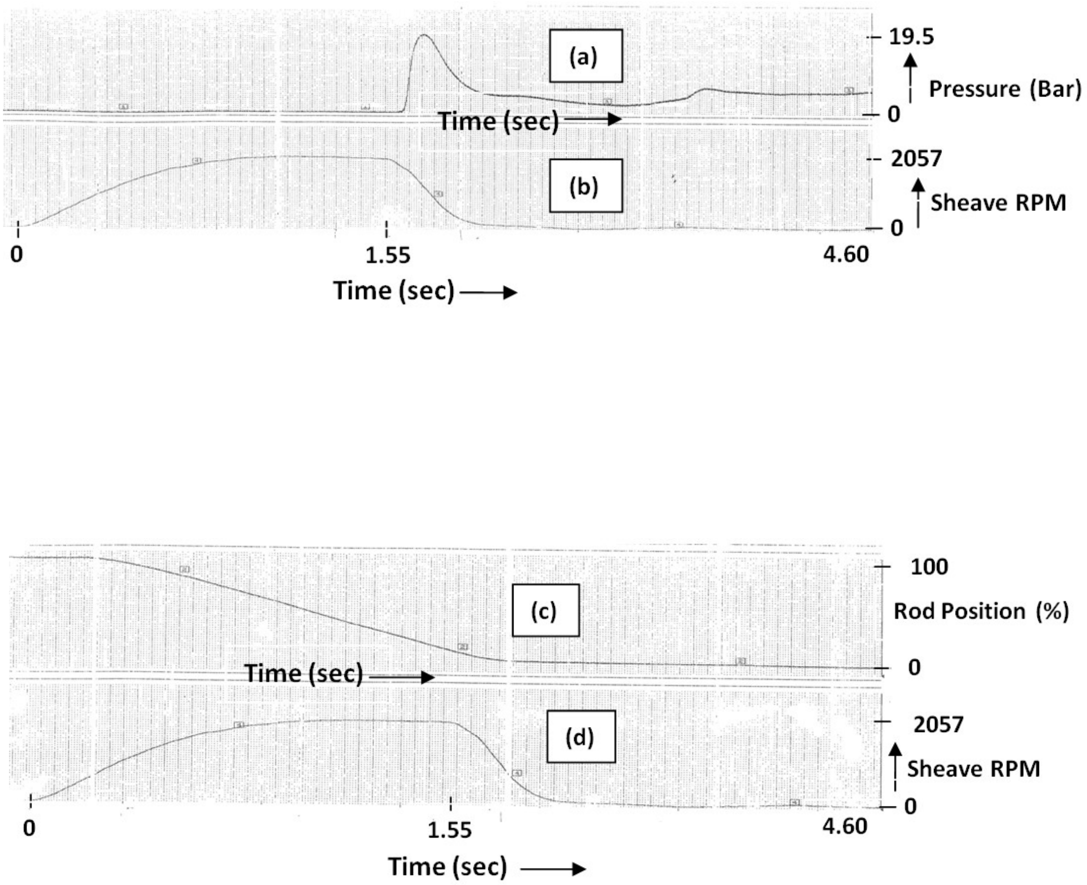

Fig. 3.21 Actual drop profiles of shut-off rod drop for AHWR's SRDM with 2000 cst silicone oil at room temperature (35°C)

(a) Dashpot Pressure vs Time
(b) Sheave Speed vs Time
(c) Rod Position vs Time
(d) Sheave Speed vs Time

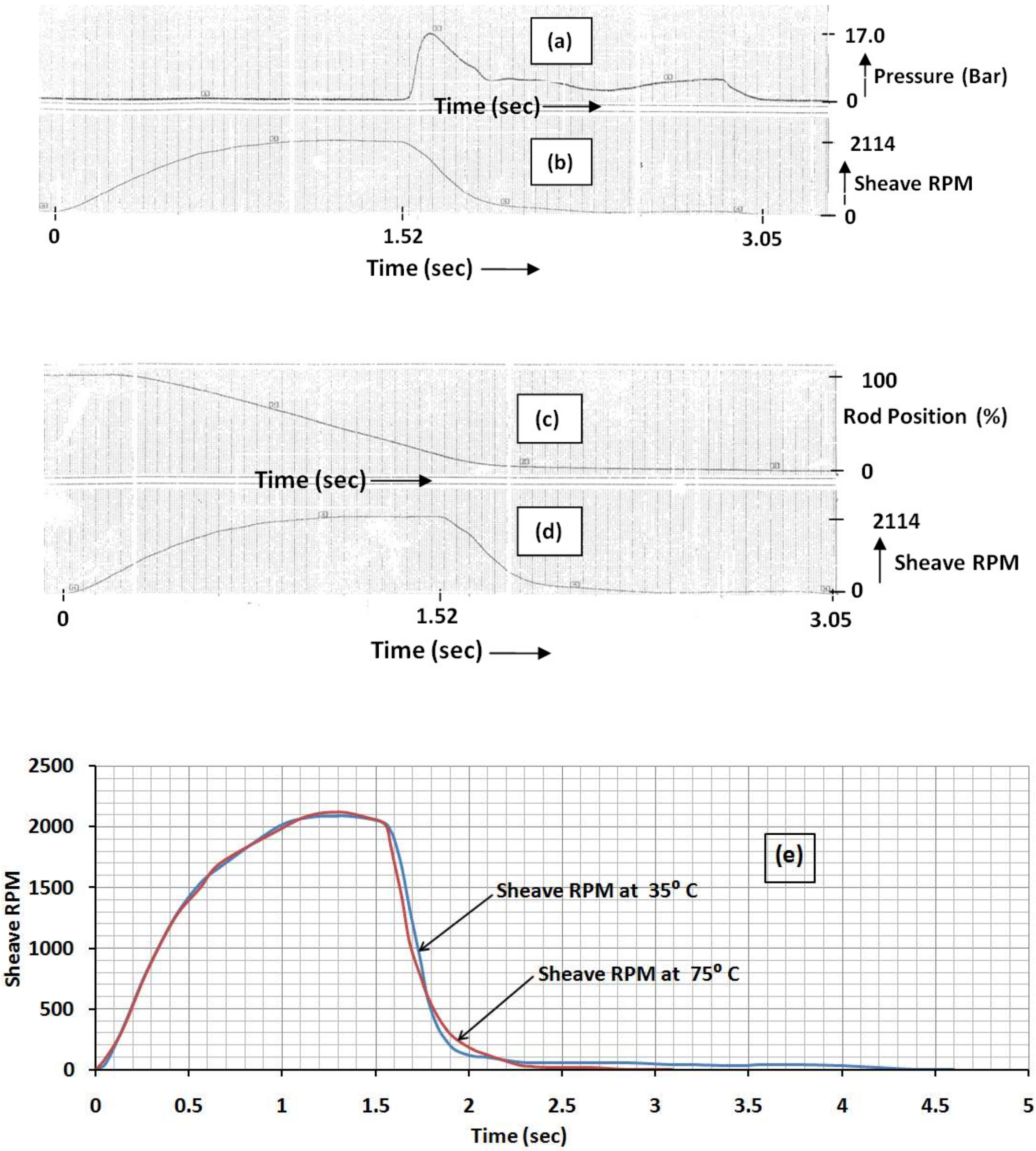

Fig. 3.22 Actual drop profiles of shut-off rod drop for AHWR's SRDM with 2000 cst silicone oil at elevated temperature (75°C).

(a) Dashpot Pressure vs Time
(b) Sheave Speed vs Time
(c) Rod Position vs Time
(d) Sheave Speed vs Time
(e) Comparison of drop profiles at 35°C and 75°C
(Data obtained by image processing)

3.5 Results and Discussion

3.5.1 Effectiveness of hydraulic dashpot on rod acceleration/deceleration

Fig. 3.23 gives a typical rod drop acceleration/deceleration profile of AHWR's SRDM. As the rod starts falling, it is assisted by initial accelerating spring for some travel, which increases the rod acceleration quickly. Thereafter the opposing forces on the falling rod (water drag, buoyancy force etc.) start building-up and rod acceleration reduces. Further, top orifices in the rod become more effective and the rod starts decelerating. As soon as dashpot comes into action (at about 90% of free-fall), the rod deceleration shoots-up (dashpot engagement point shown in Fig. 3.23) and reaches a peak value. By this time, the maximum kinetic energy of rod free-fall is absorbed, thus deceleration reduces and reaches smoothly to zero value at the end of travel.

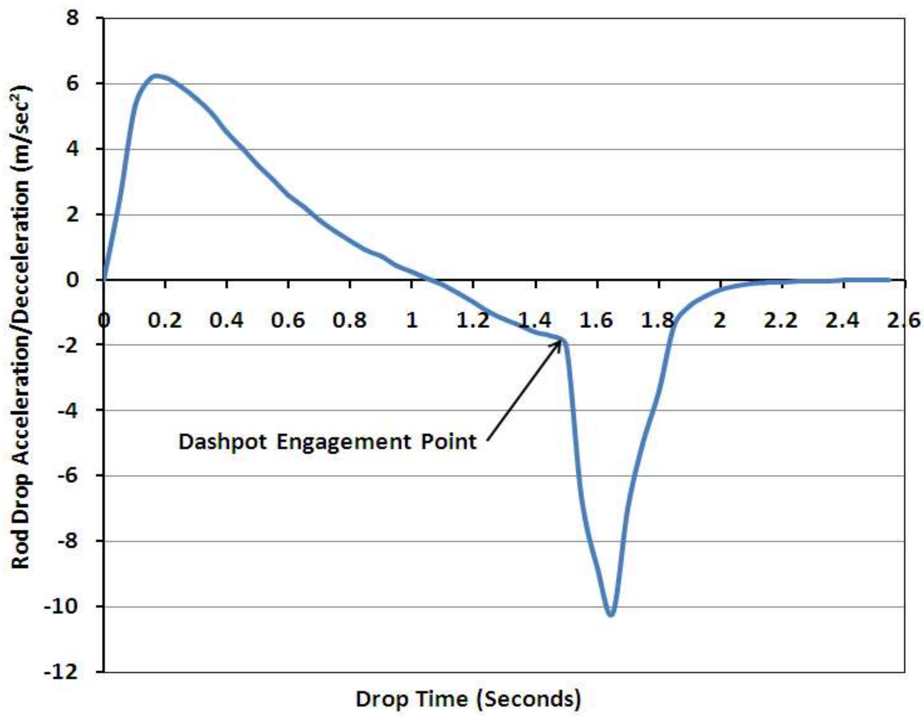

Fig. 3.23 A typical rod drop acceleration/deceleration profile of AHWR's SRDM at 35°C

3.5.2 Effect of clearance and oil viscosity on dashpot performance

Figs.3.17 to 3.22 give the actual drop profiles of shut-off rod drop and Table 3.4 gives the parameters and results of actual drop profiles. Fig. 3.17 (a,b,c,d,e) gives the drop profiles of 540 MWe PHWRs SRDM with 2000 cst silicone oil and clearances (ID 0.4 mm, OD 0.3 mm and side 0.4). Plot 3.17 (a) gives dashpot pressure variation against drop time and plot 3.17 (b) gives sheave shaft speed variation against drop time at room temperature (35°C). In this case, at the end of travel, sheave speed goes smoothly to zero without any impact (or vibration) as the dashpot system is slightly over-damped and absorbs whole energy before the end of travel. Plot 3.17 (c) gives rod position against drop time and plot 3.17 (d) gives sheave shaft speed against drop time at elevated temperature (65°C). It can be seen clearly that plot 3.17 (d) is not smooth at the end of travel. As the viscosity of dashpot oil reduces, the dashpot is not able to absorb the whole energy of rod fall, and hence we see an impact (vibration) on the dashpot stopper. The system becomes under-damped. Plot 3.17 (e) gives the comparison of drop profiles at 35°C and 65°C.

In Fig. 3.18 (a,b,c,d,e), the clearances are the same as above, but the oil viscosity is increased to 3000 cst. Here we see higher pressure in the dashpot. Dashpot is absorbing the whole energy at room temperature but still not able to absorb the energy at elevated temperature (65°C), but vibration at the stopper is less as shown in Plots 3.18 (d,e). Further the viscosity is increased to 7000 cst and drop profiles are shown in Fig. 3.19 (a,b,c,d,e). In this case the dashpot is absorbing whole energy (over-damped) at both room temperature (Plot 3.19 b) as well as at elevated temperature (Plot 3.19 d). Disadvantage in this case is that, we are getting higher 100% drop time at room temperature. Further the design was improved by reducing the clearances as shown in Fig. 3.20 (a,b,c,d,e), where the clearances at ID and OD are 0.15 mm and side clearances are 0.3 mm. Apart from these clearances, one ‘C’ groove is also made in the hydraulic dashpot shaft. ‘C’ groove is made in such a way that it provides higher clearances at the start of the dashpot operation and reduces gradually at the end. Oil viscosity used in this case was 2000 cst. This design works well at both conditions (room temperature as well as at elevated temperature). As clearances are more in initial stage, we get a flat pressure profile at room temperature and energy is absorbed over a wide range of operation. At elevated temperature, initially the clearances are high and viscosity is low, so the vane moves very fast and very less volume is left in the dashpot towards the end of operation. These results in a higher-pressure peak (more compared to room temperature) and pressure profile is not flat. This phenomenon was not there in dashpot without ‘C’ groove.

Similarly the hydraulic dashpot for AHWR’s SRDM was also studied and results are plotted in Figs. 3.21 (a,b,c,d) and 3.22 (a,b,c,d,e) at room temperature (35°C) and at elevated temperature (75°C) respectively for 2000 cst silicone oil. Plot 3.22 (e) gives the comparison of drop profiles at 35°C and75°C.

3.5.3 Application of the model in dashpot design

Numerical and experimental study of hydraulic dashpot provides the application of this model in dashpot design calculations beyond the current experimental conditions. Various design curves have been plotted to study the influence of key parameters like oil temperature (affects the oil viscosity) and structural clearances. The parameters of AHWR’s hydraulic dashpot as per Table 3.4 are used to generate the Figs. 3.24-3.28.

Fig. 3.24 gives the effect of oil temperature on the dashpot pressure. As temperature increases, the oil viscosity reduces. The oil viscosity values corresponding to different temperatures are taken from silicone oil test results Shin-Etsu [70]. Though the dashpot pressure varies linearly with viscosity (Eq. 3.5), but the variation of viscosity with temperature is non-linear, hence dashpot pressure plot against oil temperature is non-linear.

Figs. 3.25-3.28 give the dashpot pressure variation with respect to dashpot structural clearances. Dashpot pressure drops sharply when we increase the thickness of dashpot clearances (Eq. 3.5). Effect of dashpot side clearances is shown in Fig. 3.25, fixed vane ID clearances in Fig. 3.26 and moving vane OD clearances in Fig. 3.27. Dashpot fixed vane ID clearance is more effective as compared to moving vane OD clearance, because at fixed vane ID, the depth of clearance (L) is less (Eq. 3.5). This can be seen while comparing Figs. 3.26 and 3.27. Combined effect of fixed vane ID and moving vane OD clearances is shown in Fig. 3.28.

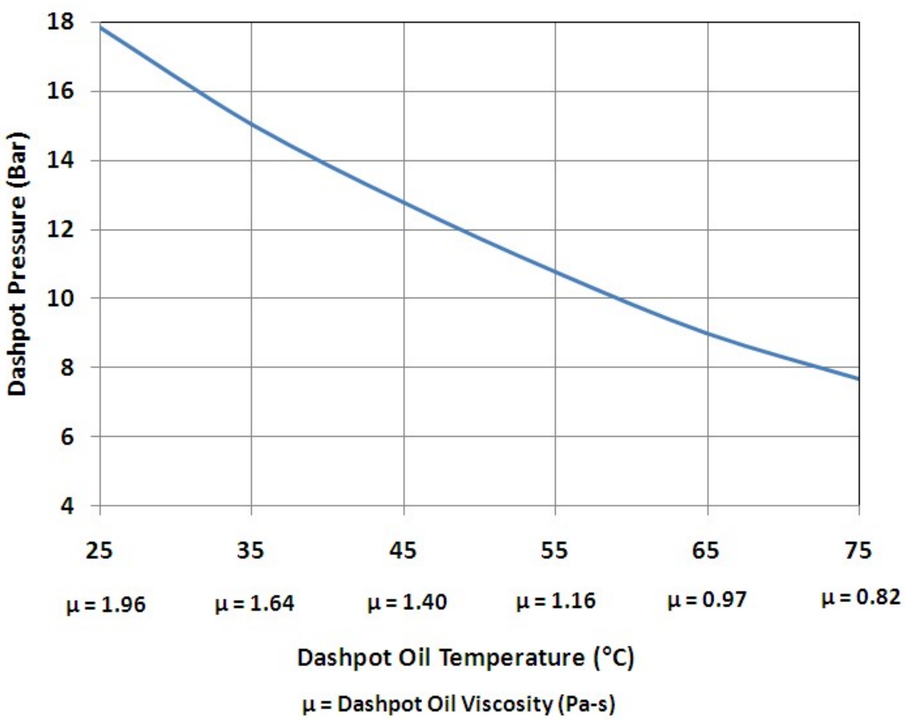

Fig. 3.24 Effect of dashpot oil temperature (viscosity) on dashpot pressure

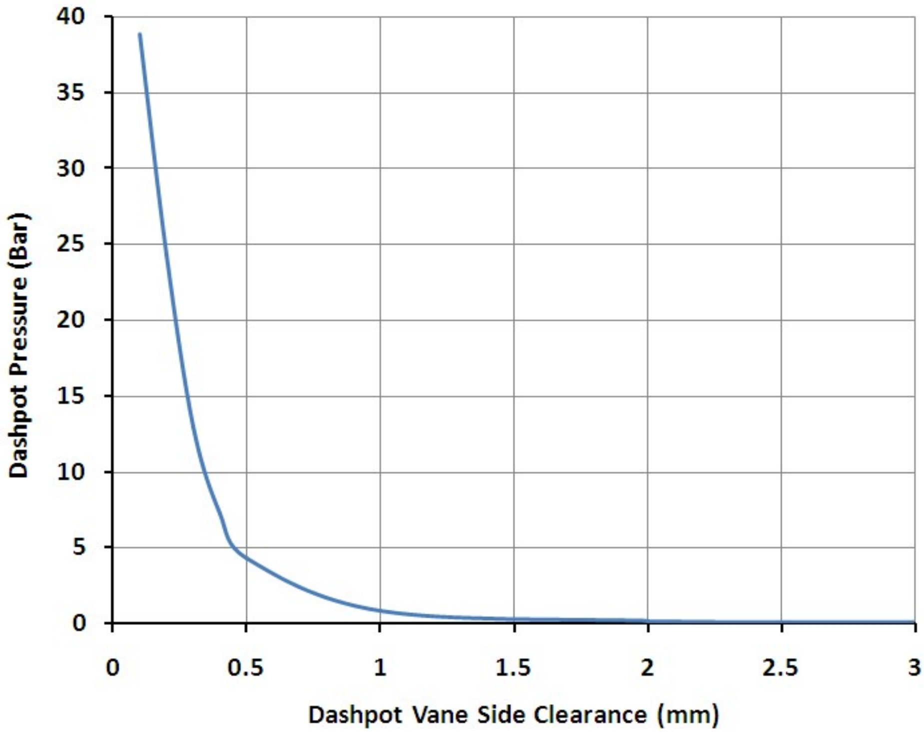

Fig. 3.25 Effect of dashpot vane side clearances on dashpot pressure

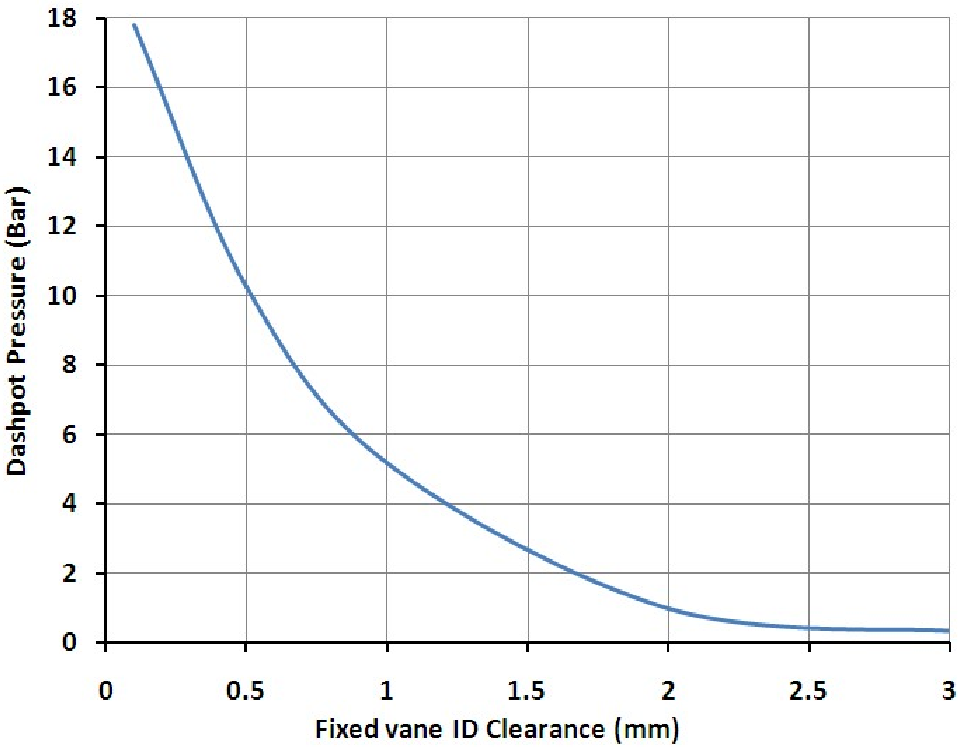

Fig. 3.26 Effect of fixed vane ID clearance on dashpot

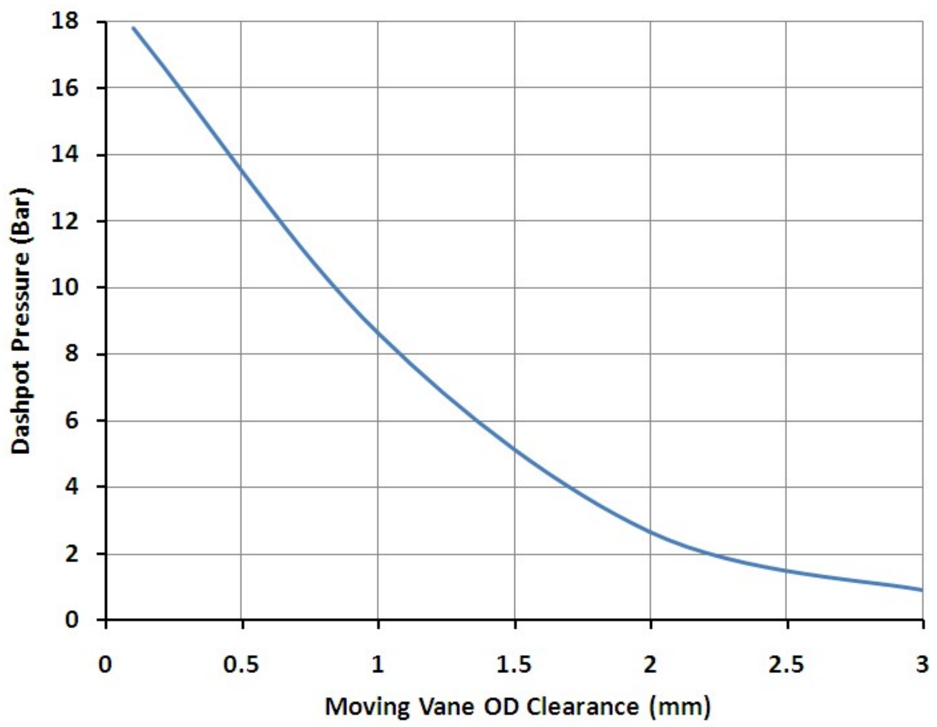

Fig. 3.27 Effect of moving vane OD clearance on dashpot pressure

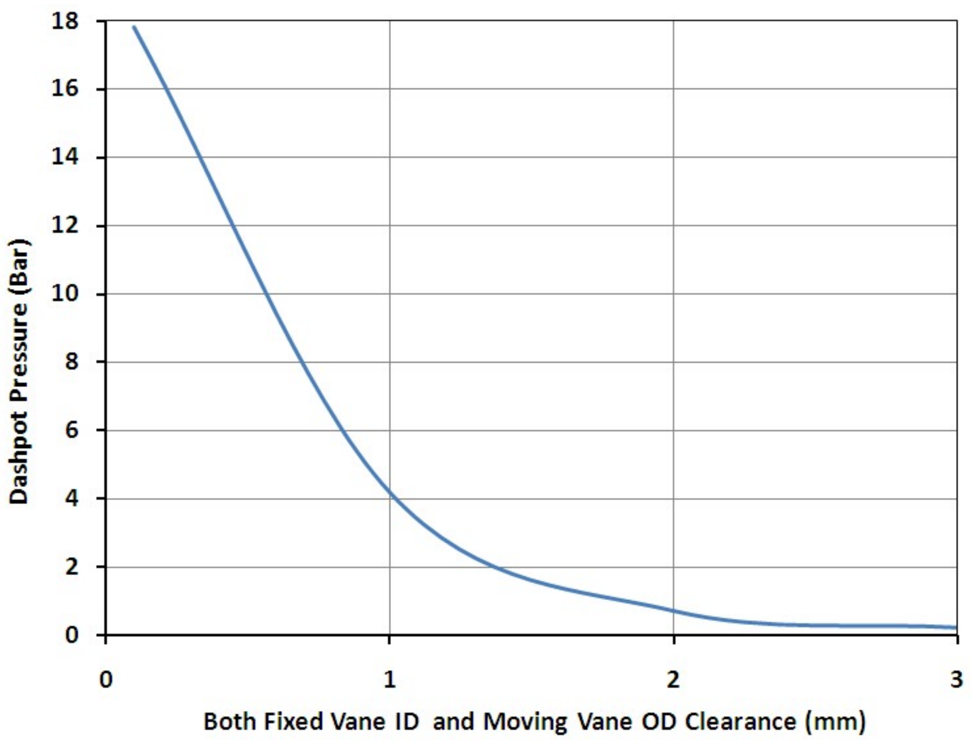

Fig. 3.28 Combined effect of fixed vane ID and moving vane OD clearance on dashpot pressure

3.6 Sensitivity and Uncertainty Analysis

Sensitivity analysis is done to look into the most effective parameters of hydraulic dashpot. This information is useful in designing the passive temperature compensating hydraulic dashpot. Sensitivity is defined as:

$$\text{Sensitivity} = \frac{\text{Rate of change of output parameter}}{\text{Rate of change of input parameter}}$$

In this analysis the output parameter is the pressure in the hydraulic dashpot chamber. As given in the closed form equation (Eq. 3.5), pressure is mainly dependent on viscosity (μ), clearance thickness (c) and depth of clearance (L) for a particular value of vane velocity. Other parameters are fixed throughout the study. Sensitivity of the Eq. 3.5 can be derived as:

$$\frac{d\Delta p}{dc} = 12\mu LU\left[(r_v - r_s)\frac{b}{L_c}\left(\frac{-3}{c^4}\right) + \frac{1}{2}\left(\frac{-2}{c^3}\right)\right] \tag{3.6}$$

Regression analysis of the Eq. 3.5 is done and the standardized regression coefficients of the input parameters are plotted in Fig. 3.29. Standardized regression coefficient is the ratio of parameter’s standard deviation to its mean. Fig. shows that the clearance thickness is the most effective input parameter in the study.

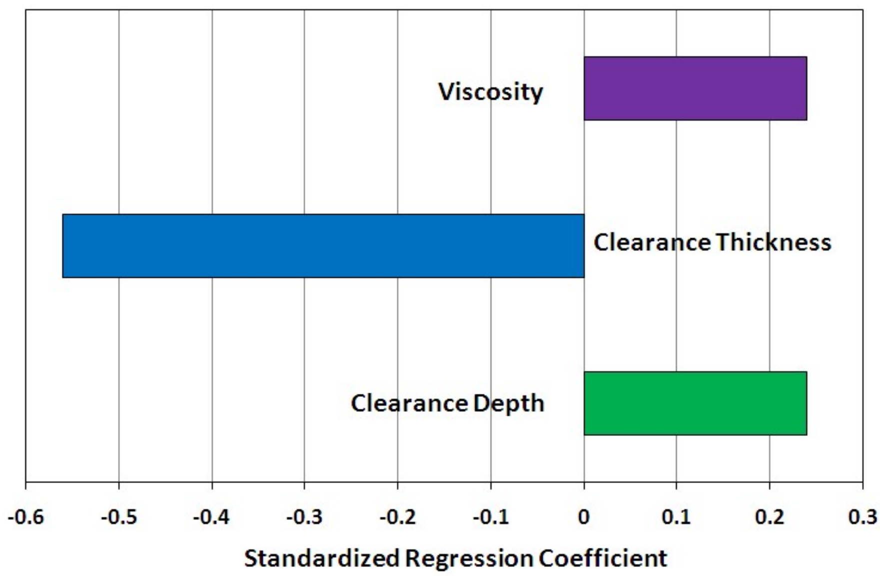

Fig. 3.29 Standardized regression coefficients of input parameters

As the clearance thickness is the most effective input parameter to affect the output pressure, so the effects of all the clearance thicknesses are compared in the Fig. 3.30. The parameters of AHWR's hydraulic dashpot as per Table 3.4 are used to generate the Fig. 3.30. This gives the comparison of actual pressure results obtained from the CFD analysis. It is clear from the Fig 3.30 that the side clearance thickness is the most effective and the dashpot pressure becomes negligible with the clearance thickness of more than 1.5 mm.

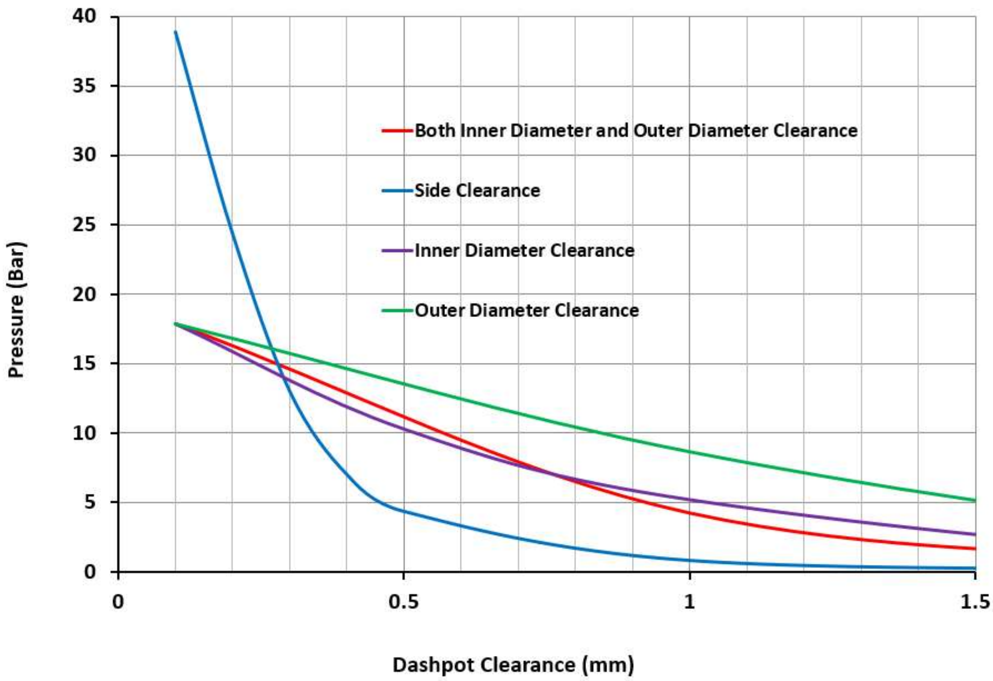

Fig. 3.30 Comparison of effects of all dashpot clearances

Uncertainties in the analysis and experiments are also analyzed. Uncertainties can come from:

1. Instrumental Uncertainty
2. Random Uncertainty
3. The effects of Assumptions
4. Uncertainty in Boundary conditions

Instrumental uncertainty is analyzed in detail, while others are not considered in this case. Uncertainty can be classified as:

(i) Absolute uncertainty

(ii) Relative uncertainty

If A is a value with ± dA variation, then dA is absolute uncertainty and dA/A is relative uncertainty.

Uncertainty in measuring instruments will lead to an overall measuring uncertainty. Different instruments have accuracy as below:

(i) Tacho-generators (Make: Servo-tek, Accuracy: 0.571%)

(ii) Pressure transducer (Make: Schaevitz, Accuracy: 0.059%)

(iii) Potentiometer (Make: Duncan, Linearity: 0.15%)

(iv) Viscosity measurements: (Accuracy:<1%)

Relative uncertainty of a product of measured values is approximately equal to the sum of the individual relative uncertainties as given by Brookes and Kagan [71]. This gives the total uncertainty in measurements as less than 2%.

3.7 Closure

Dashpot parameters pertaining to fluid flow have been analyzed in detail and it was revealed that the dashpot force is highly dependent on clearance thickness. Further it was revealed that the reduction in viscosity makes the dashpot under-damped and we see the impact in the hydraulic dashpot. To study the dashpot performance further it is necessary to model the hydraulic dashpot by multi-body dynamics, so that the dashpot performance with varying mechanical parameters can be studied. Hydraulic dashpot model will help in impact assessment with variation of different parameters.

Chapter IV

MULTI-BODY DYNAMICS MODELING, SIMULATION AND EXPERIMENTAL VALIDATION

This chapter is about the multi-body dynamics modeling of hydraulic dashpot. The dashpot is modeled as a hinge joint with moving and fixed vanes as rigid bodies. Study is focused on obtaining dashpot responses in terms of relative rotation, relative angular velocity and relative angular acceleration at various environmental temperatures.

4.1 Introduction

In the previous chapter the detailed CFD study of hydraulic dashpot has been carried-out to see the effects of fluid flow on dashpot performance. To study the effects of parameters like moment of inertia, constraint (mechanical stopper) angle in the dashpot and constant torque (due to shut-off rod weight) on the dashpot shaft, it is necessary to model the hydraulic dashpot using multi-body dynamics. This study is aimed at getting the effects of above parameters on dashpot performance.

4.2 Set-Up Description

The present study was carried-out on a prototype SRDM and full-scale test set-up meant to qualify the shut-off rod drive mechanism of 'Critical Facility' reactor. Shut-off drive mechanism comprises of following sub-assemblies; Motor Sub-Assembly, Worm Gear Sub-Assembly, EM Clutch Sub-Assembly, Reduction Unit-I Sub-Assembly, Mechanism Housing Sub-Assembly, Sheave Shaft Sub-Assembly, Position

Indication Unit Sub-Assembly, Reduction Unit-II Sub-Assembly, Hydraulic Dashpot Sub-Assembly, Limit Switch Sub-Assembly, Top Limit Switch Sub-Assembly, Push Tube Sub-Assembly, Absorber Rod (SOR) Sub-Assembly, Disc Spring Sub-Assembly.

Internal arrangement and working of drive mechanism is similar to that of AHWR's drive mechanism as given in the previous chapter. Shut-off rod of 'Critical Facility reactor falls in air, so there are no opposing forces in the guide tube. Fig. 4.1 gives the internal arrangement of the shut-off rod drive mechanism for 'Critical facility' reactor. Internal details of hydraulic dashpot are given in Fig. 4.2. All the parameters of the hydraulic dashpot under study are given in Table 4.1

Table 4.1: Study set-up parameters

Parameter	**Value for 'Critical Facility' reactor**					
Drive mechanism overall size (mm)	210 x 196 x 750					
Hydraulic dashpot vane size (mm)	20 ID x 60 OD x 64.6 Length					
Rod travel (mm)	2400					
Rod weight (Kg.)	8					
Free fall (mm)	2160 (in air)					
Approximate volume of the oil (cc)	162					
Hydraulic dashpot rotation (degree)	120					
Mechanical shaft seal	on one side					
No. of dashpot vanes	two moving vanes/two fixed vanes					
Shaft and moving vane material	SS 17.4 PH					
Housing and fixed vane material	SS 17.4 PH					
Viscosity of oil used at 25°C (cst)	1500					
Mass of moving vane (kg)	0.53					
Equivalent moment of inertia (kg.m^2)	0.1929					
Spring constant (N.m/rad)	0.93					
Applied moment (N.m)	5.24					
Environment Temperature (°C)	35	45	55	65	75	85
Damping coefficient (N.m.sec/rad)	4.51	4.11	3.30	3.22	3.16	3.11
Initial angular velocity acquired by the dashpot (rad/sec)	32.90	35.74	38.55	42.77	45.02	45.6
Relative angular velocity while moving vane hits the stopper (rad/sec)	2.3	3.8	7.74	9.02	10.47	12.56

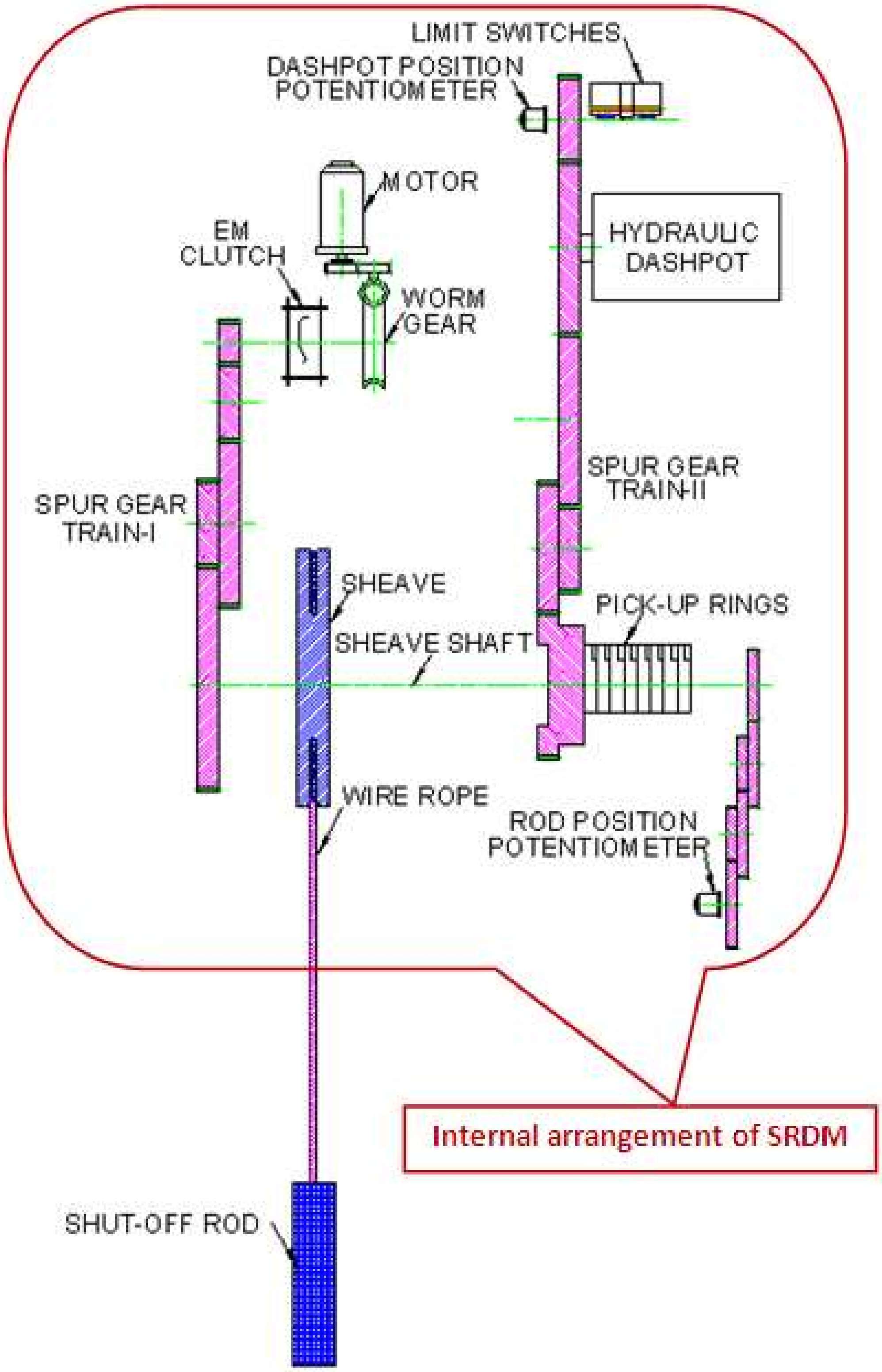

Fig. 4.1 Internal arrangement of shut-off rod drive mechanism for 'Critical Facility' reactor.

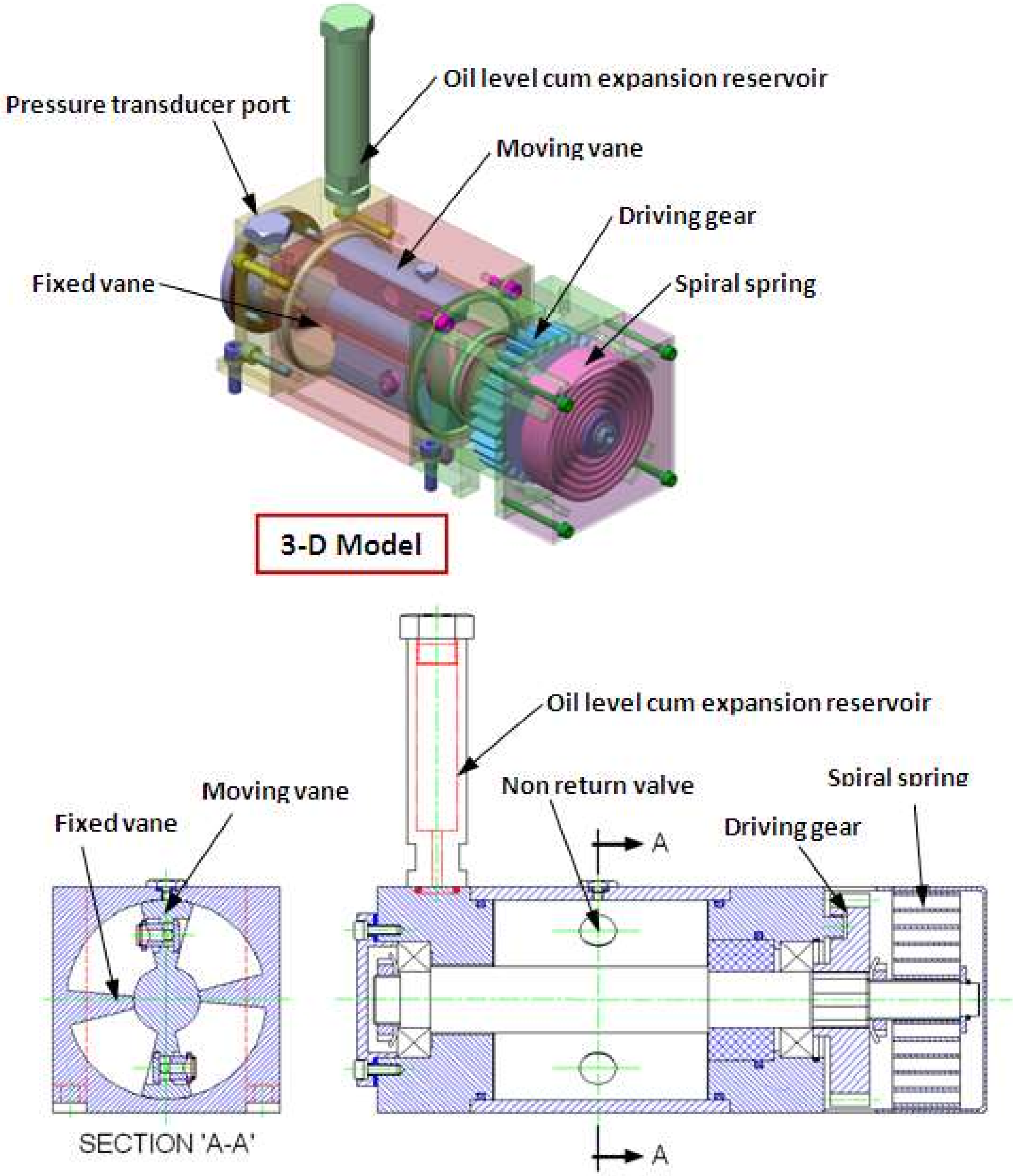

Fig. 4.2 Internal details of hydraulic dashpot for 'Critical Facility' reactor.

For multi-body dynamics analysis, we require equivalent moment of inertia at the dashpot shaft, damping coefficient and spring constant of the hydraulic dashpot. For calculating the equivalent moment of inertia at the dashpot shaft, the moment of inertia of each and every rotating component is resolved into the moment of inertia at the dashpot shaft as given in Taliyan et al. [5].

Damping coefficients of dashpot at various temperatures have been calculated from the experimental and CFD results. Values of pressure and relative angular rotation are taken from the experimental results. The values of damping coefficients are calculated as below:

$$c_\theta = T_q/\omega \tag{4.1a}$$

$$c_\theta = p.A.R/\omega \tag{4.1b}$$

Where, c_θ is the damping coefficient (N.m.sec/rad), T_q is torque (N.m), ω is the angular velocity (rad/sec), p is the pressure (N/m^2), A is the total vane area (m^2) and R is the torque arm (m), which is the distance between axis of dashpot shaft and vane center.

For a particular experimental result, damping coefficients are calculated at different time steps. The values of the damping coefficients at different time steps of the dashpot operation are plotted and the mean value of the damping coefficient is taken into consideration. Fig. 4.3 gives the variation of damping coefficient vs time at 35°C. The value of spring constant (N.m/rad) is measured experimentally with the help of a torque wrench. Values of equivalent moment of inertia, spring constant and damping coefficients at different environmental temperatures are also given in Table 4.1.

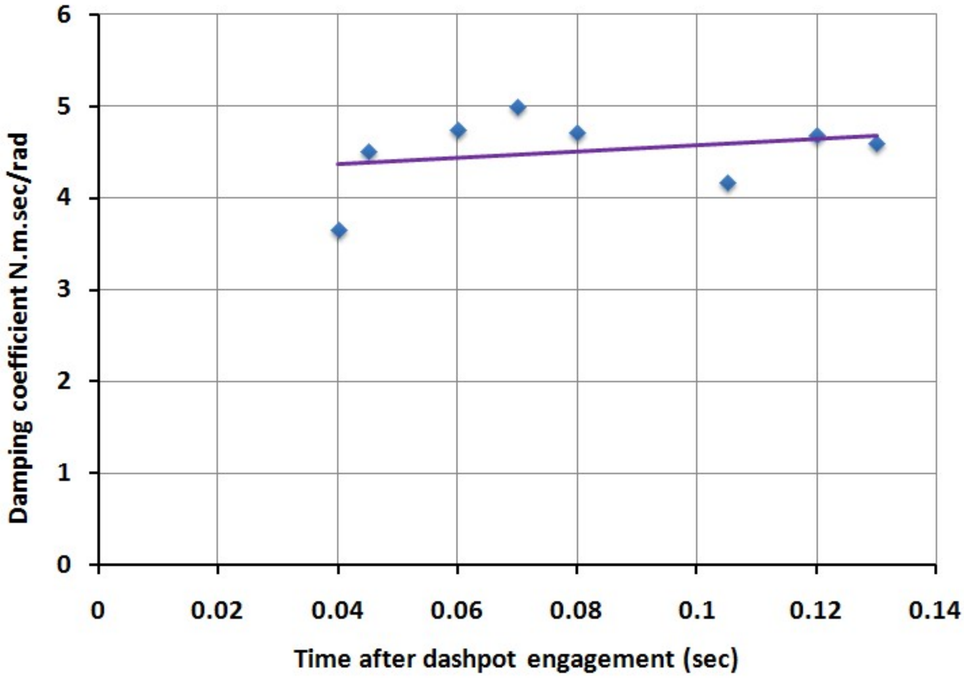

Fig. 4.3 Variation of damping coefficient vs time at 35°C

4.3 Modeling and Simulations

4.3.1 Modeling Procedure

Commercial software COMSOL Multiphysics 5.1 (based on finite element method) is used to model the hydraulic dashpot; COMSOL 5.1 documentation ([64] and tutorials [65] and [72]. Fixed vanes in the hydraulic dashpot are attached to the housing and the moving vanes are attached to the rotating shaft and there is no axial movement along the axis of the shaft. These vanes are modeled as two arms of a hinge joint where the fixed vanes are modeled as fixed arms. The hinge joint, also known as a revolute joint has one rotational degree of freedom between the two components. The two components are free to rotate relative to each other about the axis of the joint. Spring and damper is applied between the arms of the hinge joint. Rotation of the arm is also constrained to 120° as there is a mechanical stopper in the dashpot at 120°. To see the effects of all relative motion (including vane side relative motion) in the hydraulic dashpot, the modeling is done for 3-D geometry. Energy variation in the dashpot operation is also studied. Local increase in temperature during operation is also studied. Time dependent study is performed. Fig. 4.4 shows the multi-body dynamic model of hydraulic dashpot. Based on requirements, analysis strategy has been formulated in which following two physics aspects have been solved simultaneously:

(i) Multi-body dynamics

(ii) Heat transfer in solids

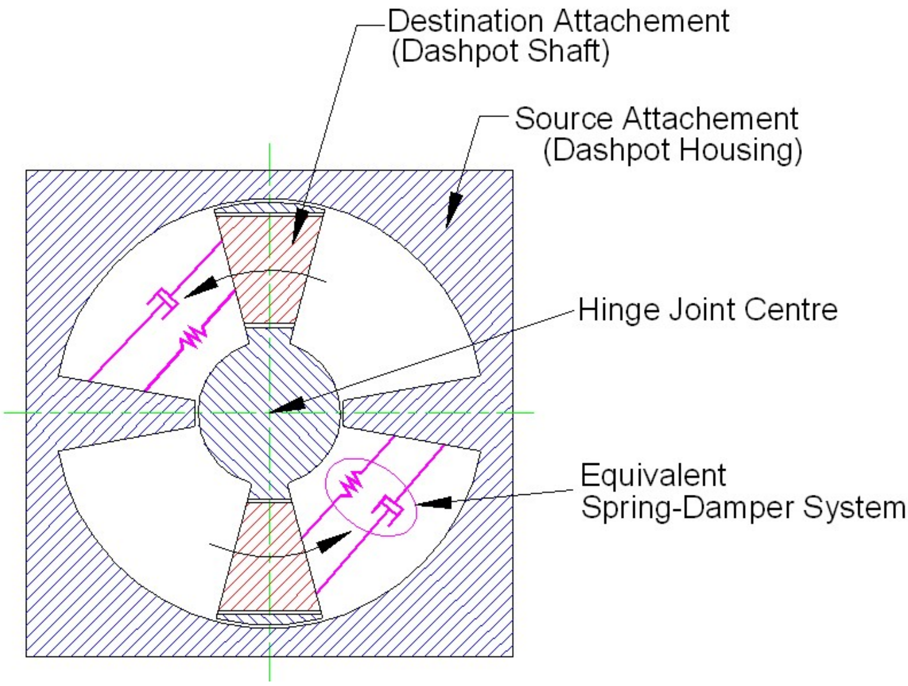

Fig. 4.4 Multi-body dynamic model of hydraulic dashpot

4.3.2 Theory of Multi-body Dynamics and Governing Equations

An attachment is a set of boundaries on a flexible component used to connect it to another flexible component or a rigid component through a joint. The attachment center of rotation is the centroid of its selected boundaries. In a joint, it is possible to select the attachment center of rotation as the center of the joint. The forces and moments on an attachment are computed by summing the reaction forces on the selected boundaries. These forces and moments are used to evaluate the joint forces.

For finite rotations, however, any choice of three rotation parameters is singular at some specific set of angles. For this reason, a four-parameter *quaternion* representation is used for rotations in COMSOL. The connection between the quaternion parameters and rotation matrix (R) is established. Under pure rotation, a vector from the center of rotation (X_c) of the attachment to a point X on the undeformed solid will be rotated into:

$$x - X_c = R\,(X - X_c) \tag{4.2a}$$

Where, x is the new position of the point, originally at X.

The displacement is by definition

$$u = x - X = (R - I)\,(X - X_c) \tag{4.2b}$$

Where, I is the unit matrix.

Scheme of position vectors under pure rotation is shown in Fig. 4.5. All position vectors are defined w.r.t. origin.

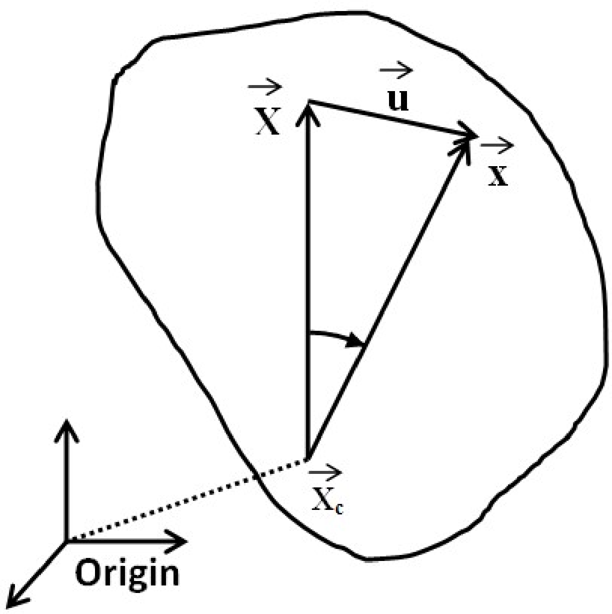

Fig. 4.5 Scheme of position vectors under pure rotation

When the center of rotation of the attachment also has a translation u_c, then the complete expression for the displacements of the solid is

$$u = (R - I)(X - X_c) + u_c \qquad (4.2c)$$

Scheme of position vectors under combined rotation and translation is shown in Fig. 4.6. $\mathbf{X'_c}$ is the new position of centre of rotation of the attachment after translation.

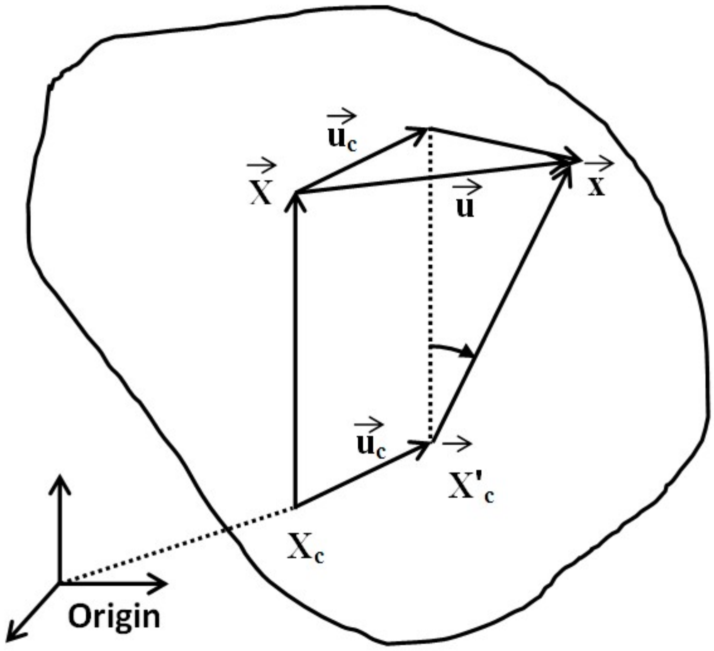

Fig. 4.6 Scheme of position vectors under combined rotation and translation

For a hinge joint, the destination attachment is free to rotate relative to the source attachment about the joint axis. The relative rotation about the joint axis (θ) is the degree of freedom. To formulate this kind of connection, the motion of destination attachment is prescribed in terms of the motion of the source attachment as follows:

$$u_{c.dest} = u_{c.src} \qquad (4.2d)$$

$$\Phi_{dest} = \Phi_{src} + \theta \qquad (4.2e)$$

$$u_{c.src} = u_{src} + (R_{src} - I)(X_c - X_{c.src}) \qquad (4.2f)$$

$$u_{c.dest} = u_{dest} + (R_{dest} - I)(X_c - X_{c.dest}) \qquad (4.2g)$$

Forces and moments at center of joint due to input parameters will be balanced by the damper moment. Damper moment can be given as:

$$M = - k_{\theta}(\theta - \theta_0) - c_{\theta}\left(\frac{\partial \theta}{\partial t}\right) \qquad (4.3)$$

Where, M is the damping moment (N.m), k_{θ} is the spring constant (N.m/rad), c_{θ} is the damping coefficient (N.m.sec/rad), $u_{c.src}$ and $u_{c.dest}$ are the displacement vectors for source and destination attachments and u_{src} and u_{dest} are the displacements at the centroid of the source and destination attachments. X_c is the joint center, $X_{c.src}$ and $X_{c.dest}$ are the positions of centroids for source and destination attachments. R_{src} and R_{dest} are the rotation matrices describing the rotation of source and destination attachments, Φ_{src} and Φ_{dest} are the rotation about the axis for source and destination attachments. I is the unit matrix. θ is relative rotation (rad) and θ_0 is the pre-deformation (rad).

The equations (4.2d)-(4.2g) are general equations for hinge joint, while equation (4.3) is equation for spring damper system. COMSOL 5.1 documentation [64]

The constraint on the relative displacement is enforced using a stiff spring between the components. COMSOL 5.1 Documentation [64]. The stiffness of the spring is defined by the penalty factor. The kinetic energy will be stored as spring potential energy at maximum penetration. By equating kinetic energy and potential energy, we get the equation for penalty factor p_u in (N.m/rad). The penalty factor (p_u) is evaluated as below:

$$p_u = \left[\frac{\frac{d\theta}{dt}}{\delta\theta\_max}\right]^2 I_e \qquad (4.4a)$$

Where θ is the relative rotation, t is the time. The numerator in the equation (4.4a) is an assumed angular velocity (rad/sec) between the components when the constraint is applied, and the denominator is the maximum allowable penetration (rad). This ratio of the relative angular velocity and the maximum allowable penetration decides the required stiffness of the spring (the penalty factor). The factor I_e in the eq. (4.4a) is the effective moment of inertia at the joint, defined as:

$$I_e = \frac{(I_{src} I_{dest})}{(I_{src} + I_{dest})} \tag{4.4b}$$

Where I_{src} and I_{dest} are source and destination moment of inertias (kg.m^2).

Total kinetic energy lost in the dashpot will be converted into heat and give temperature rise. To get the energy variation and temperature rise during the dashpot operation, energy equation is solved. Time dependent energy equation is:

$$\rho C_p \frac{\partial T}{\partial t} + \rho C_p u_2 . \nabla T = \nabla.(k \nabla T) + Q \tag{4.5}$$

Where, ∇ is divergence, ρ is density of dashpot fluid (kg/m^3), C_p is specific heat capacity of fluid at constant pressure (J/kg.K), k is coefficient of thermal conductivity (W/m.K), T is the absolute temperature (K), u_2 is the velocity vector (m/sec) and Q is heat sources (W/m^3).

Heat generated per second will be the kinetic energy lost in the dashpot operation and will give rise to the local temperature. Energy stored in shock absorber will be multiplication of spring constant and its rotation. All these parameters are defined in the variables.

4.3.3 Boundary Conditions

The multibody dynamics interface of COMSOL is solved to get the dashpot response in the operation. The stresses in the dashpot component are not of interest in present study, so the dashpot moving vane along with shaft and dashpot fixed vane along with housing are modeled as rigid domain. Dashpot housing along with fixed vanes (rigid domain 2) is given as fixed constraint boundary condition. Moving vanes along with shaft (rigid domain 1) is given the initial values equal to the initial angular velocity acquired by the moving vane. Moment equivalent to weight of the absorber element constantly acting on the dashpot shaft is given as applied moment. Variation of the gravity is neglected for the applied moment. Mass of the dashpot shaft and the equivalent moment of inertia of all rotating parts derived on the dashpot shaft are also given in boundary conditions.

A hinge joint is applied between the two rigid domains. Rigid domain 2 (fixed vane) is given as source attachment while rigid domain 1 (moving vane) is given as destination attachment. Spring and damper system is applied between the two rigid domains. Rotational constraint boundary condition for 120° is applied in the hinge joint to restrict the rotation beyond 120°. The constraint on the relative displacement is enforced using a stiff spring between the components. The stiffness of the spring is defined by the penalty factor.

(i) Rigid Domain 1 Boundary Conditions:

(a) Initial values (Translational):

Displacements at the center of rotation (u); u = 0, v = 0, w = 0

Velocity at the center of rotation $\left(\frac{\partial u}{\partial t}\right)$;

$$\frac{\partial u}{\partial t} = 0,\ \frac{\partial v}{\partial t} = 0 \text{ and } \frac{\partial w}{\partial t} = 0,$$

(b) Initial values (Rotational):

Angular velocity (ω);

$\omega_x = 0$

$\omega_y = 0$

$\omega_z = \omega$ (Axis of rotation)

Where ω is the initial angular velocity acquired by the dashpot. (Derived experimentally, as given in the Table 4.1)

(c) Applied Moment (N.m):

$M_x = 0$

$M_y = 0$

$M_z = 5.24$ (As given in Table 4.1)

(d) Mass (kg) and Moment of Inertia (kg.m^2):

Mass = 0.53 kg (As given in Table 4.1)

Moment of Inertia (I);

$I_x = 0$, $I_y = 0$ and $I_z = 0.1929$ kg.m^2 (As given in Table 4.1)

(ii) Rigid Domain 2 Boundary Conditions:

Fixed constraint; All displacements are zero.

$u = 0$, $v = 0$ and $w = 0$

(iii) Hinge Joint Boundary Conditions:

(a) Spring and Damper:

Spring constant (k_θ) = 0.93 N-m/rad (As given in Table 4.1)

Pre-deformation (θ_0) = 0

Damping coefficient (c_θ) = As per Table 4.1

(b) Constraints:

Maximum relative rotation (θ_{max}) = $2\pi/3$ rad

Minimum relative rotation (θ_{min}) = 0

Penalty factor (p_u);

For the penalty factor computing, angular relative velocity $\left(\frac{\partial\theta}{\partial t}\right)$ between moving vane and stopper at the time of hitting is derived experimentally as given in Table 4.1.

Maximum allowable penetration ($\delta\theta\_max$) = 10^{-3} rad (Assumed value)

Effective moment of inertia (I_e) = 0.1929 kg.m^2 (As given in Table 4.1)

Only dashpot shaft is free to rotate, so the effective moment of inertia will be that of dashpot shaft only.

Moving and fixed domains in the model are assembled with identity pair. All the surfaces which are in relative motion are defined as identity pair. For heat transfer in solids, pair boundary heat source boundary condition is applied on the identity pair, as this is the source of heat generation.

(iv) Boundary Conditions for Heat Transfer in Solids:

(a) Initial Values:

Temperature (T) = 293.15 °K

(b) Pair Boundary Heat Source:

$\nabla.(-k\nabla T) = Q_b$

Where, Q_b is the Boundary heat source and $Q_b = \frac{Q}{A}$

Where, Q is the overall heat transfer rate and A is the contact surface area of the moving vane.

4.3.4 Grid Independence and Convergence Methods

A mesh sensitivity study was performed to find the mesh size that was sufficiently fine so that solution does not change by further refining the mesh. Tetrahedral mesh with varying mesh density as shown in Fig. 4.7 (size in meters) is used for study, response curves and energy variation were evaluated at different mesh sizes. No appreciable change has been found beyond 108095 numbers of elements. So, this is considered as the optimized mesh size for this study. Both multi-body dynamics and heat transfer in solids interfaces are solved simultaneously. Time dependent iterative (geometric multigrid) solvers are used with segregated approach. Temperature is kept in segregated step 1 while other variables are kept in segregated step 2. Nonlinear method used for both segregated approach is constant (Newton). All the solutions were considered to be fully converged when the sum of absolute value of residuals was below 10^{-5}. Convergence was achieved on a work station with system descriptions as: Processor; 3.40 GHz, 64-bit operating system and 64.0 GB RAM and the CPU time was 1 hour 31 minutes.

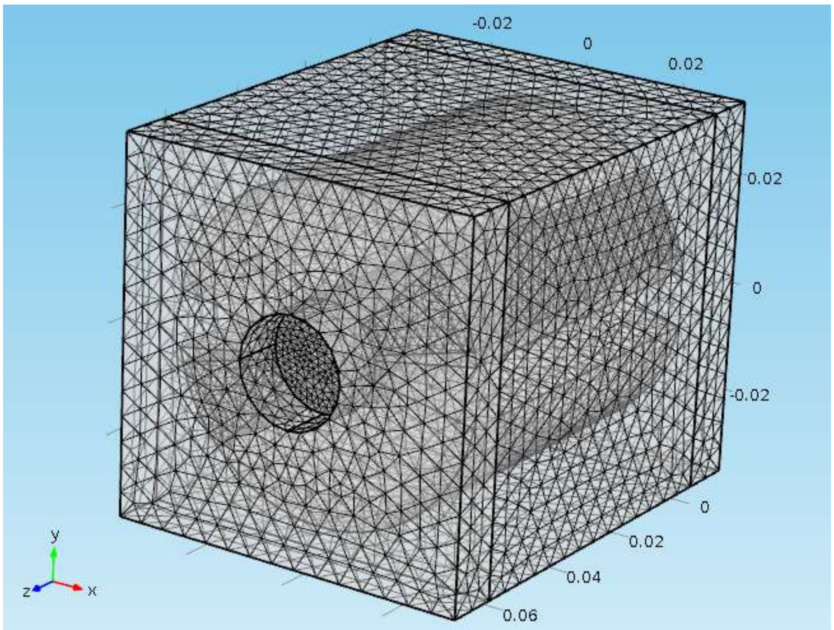

Fig. 4.7 A typical mesh of the hydraulic dashpot assembly

4.3.5 Simulation Results

Simulation results are shown in Figs. 4.8 - 4.14. Fig 4.8 shows the 3-D temperature profile of the hydraulic dashpot. Fig. 4.9 gives relative vane rotation vs. time, Fig. 4.10 gives relative angular velocity vs time, Fig. 4.11 gives relative angular acceleration vs time and Fig. 4.12 gives the variation of the energy at 35°C. As shown in Fig. 4.9, the relative rotation of the vane at 35°C is fast initially, and then it rotates slowly towards the end of the travel because by this time the energy is absorbed in the dashpot and vane rotates only because of absorber element weight. It is clear from the relative angular velocity curves that, at 35°C, the vane rotation is smooth at the end of the dashpot rotation and the vane velocity goes smoothly to zero. The relative angular acceleration curve at 35°C (Fig. 4.11) shows that the vane decelerates fast initially and then stops smoothly. There is a slight kink when the vane stops with terminal velocity, which is very small at 35°C. There is a constraint applied in the simulation at 120° of rotation which is equivalent to the mechanical stopper in the dashpot. The moving vane hits the constraint and re-bounces at the environmental temperatures of 55°C and 85°C when dashpot oil viscosity reduces. Further vane moves forward due to constant applied torque by the shut-off rod weight and finally stops at the mechanical stopper. The energy variation is analyzed in Figs. 4.12- 4.14, we can see that, initially the kinetic energy is acquired by the moving vane, which gets converted into the heat and absorbed in the dashpot. So, as the kinetic energy reduces with time, energy absorbed by the dashpot increases and saturates. Energy absorbed by the dashpot is more than the kinetic energy, because some heat is also generated due to constant applied moment on the dashpot shaft. Some energy is also stored in the spiral spring as shown in the energy variation curves (Figs 4.12-14). Overall energy balance is satisfied. At 55°C and 85°C the vane movement sees the impact, as the relative rotation, angular velocity and acceleration curves are not smooth. This shows that the moving vane is hitting the stopper. Relative angular acceleration curves at 55°C and 85°C show erratic acceleration/deceleration behavior as the vane hits the stopper and we see the impact. The impact is more severe at 85°C than that at 55°C. At 55°C and 85°C, the energy variation curves also have kink, because of the impact in the dashpot. As shown in Fig. 4.8, the temperature rise in dashpot vanes is high at local surfaces which are in relative motion. The highest temperature rise observed is 5°C, at time = 0.01 sec. The temperature rise is local, while the bulk temperature of dashpot components remains nearly constant. Local temperature rise also reduces gradually with time and found to be negligible at the end of dashpot operation. This temperature analysis is done with the assumption that whole damper heat is transferred to the dashpot components, if some heat goes into the dashpot oil then this temperature rise will be less. The important simulation results are given in Table 4.2.

Table 4.2: Simulation results

Temper-ature (°C)	Time taken for 120° rotation (sec)	Initial kinetic energy (J)	Total energy loss in shock absorber (J)	Impact in the dashpot	Vane hitting velocity (rad/sec)
35	0.86	104	115	No	-
45	0.52	123	134	No	-
55	0.15	144	156	Yes	5.4
65	0.10	176	190	Yes	8.9
75	0.08	196	212	Yes	13.2
85	0.07	201	216	Yes	15.1

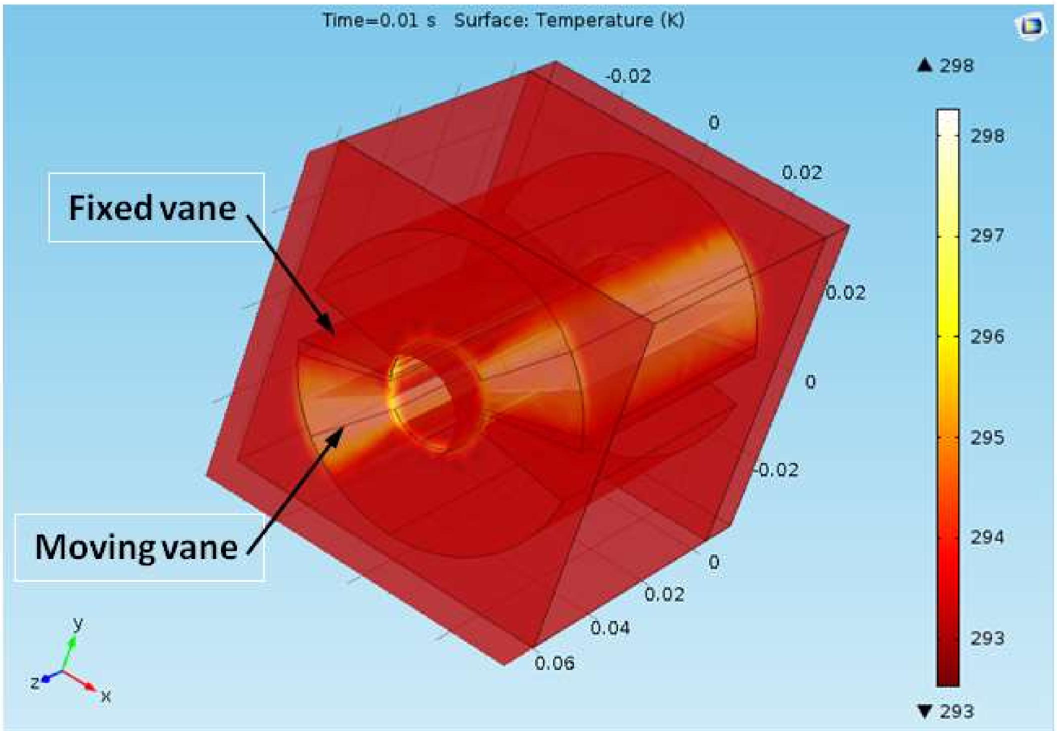

Fig. 4.8 3-D Temperature profile of hydraulic dashpot

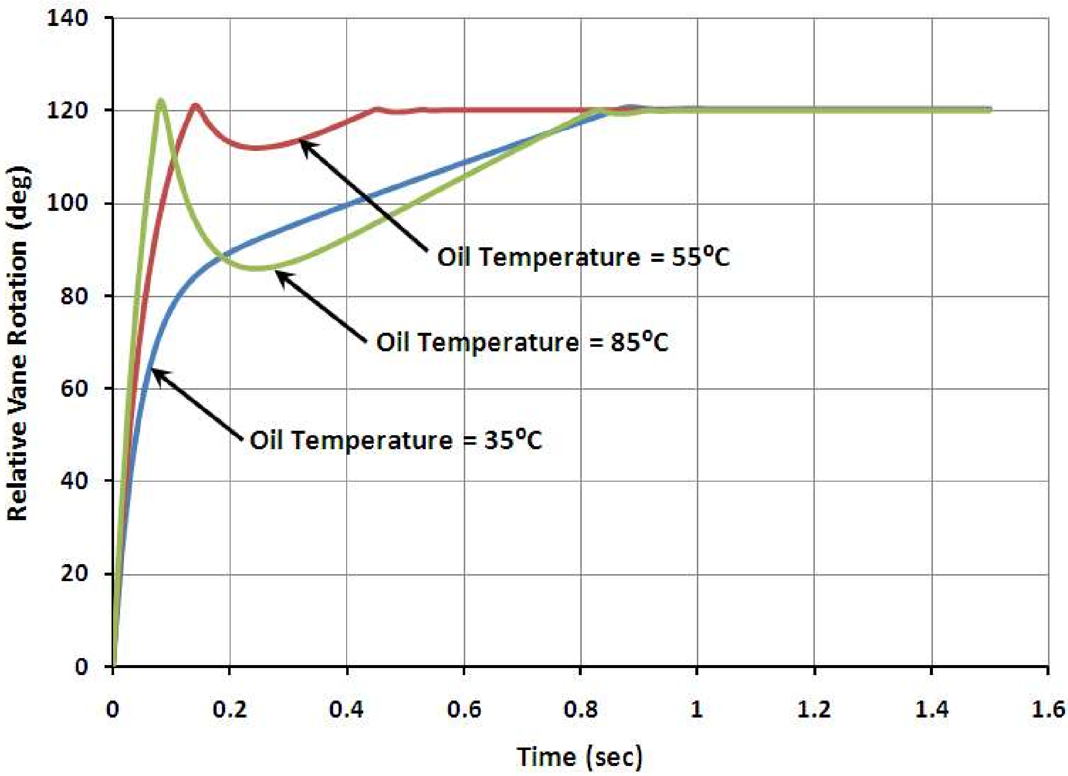

Fig. 4.9 Relative vane rotation vs time

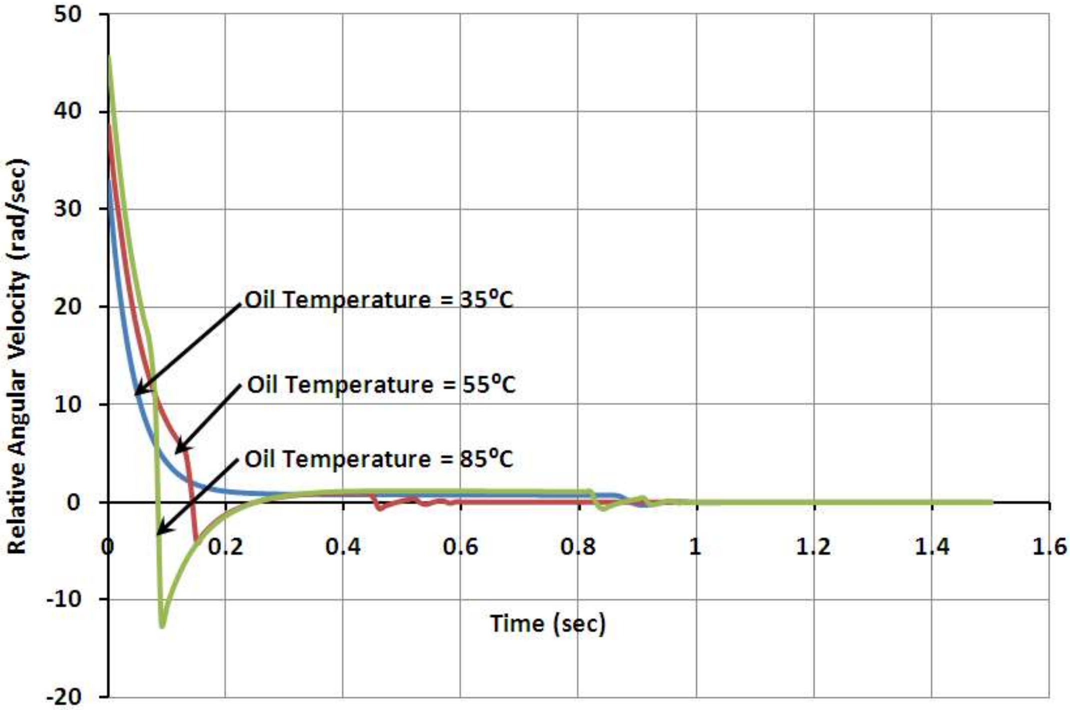

Fig. 4.10 Relative angular velocity vs time

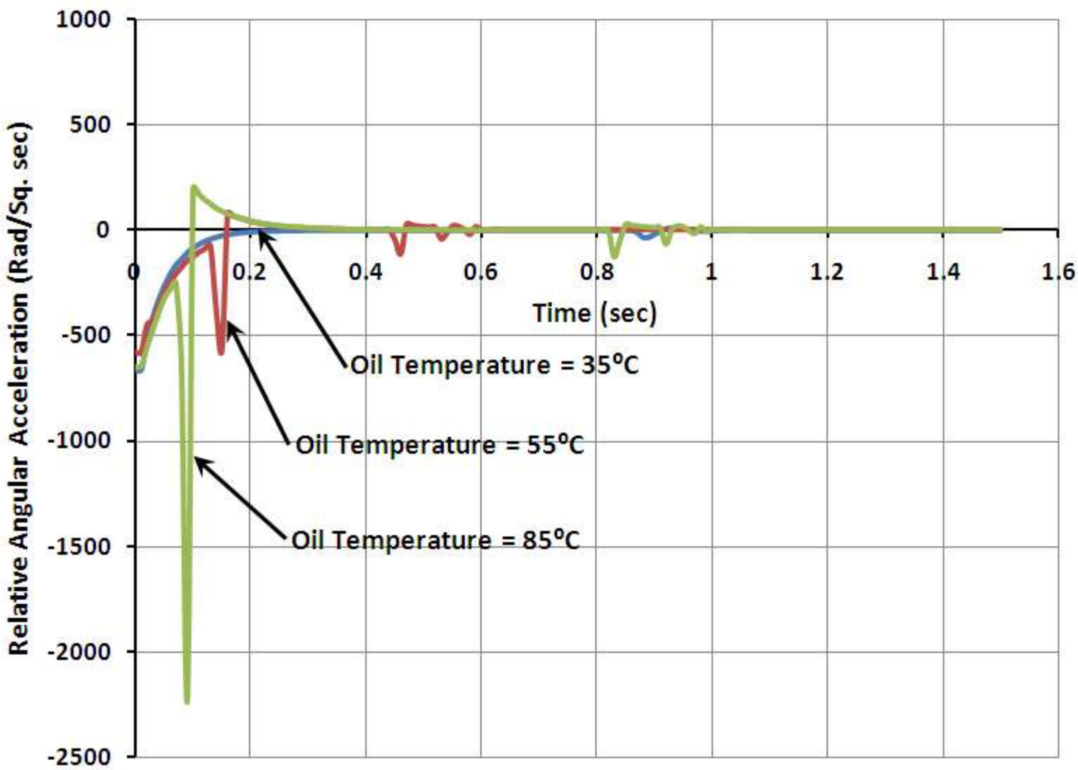

Fig. 4.11 Relative angular acceleration vs time

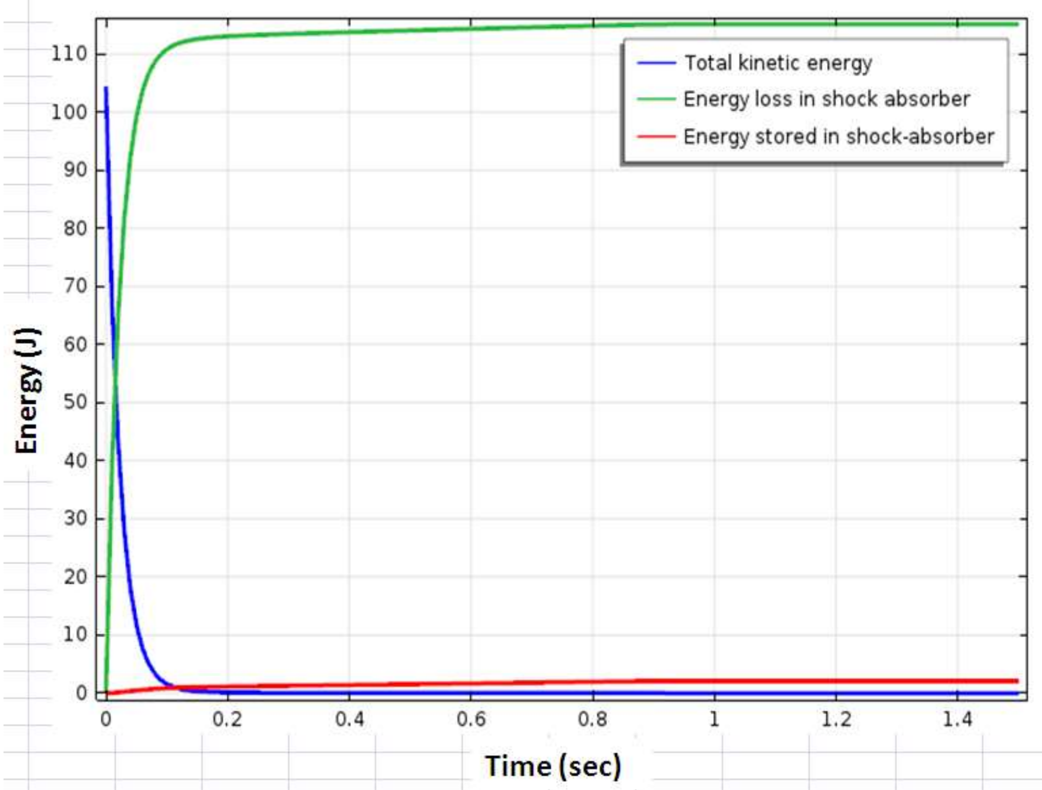

Fig. 4.12 Variation of energy vs time at 35°C

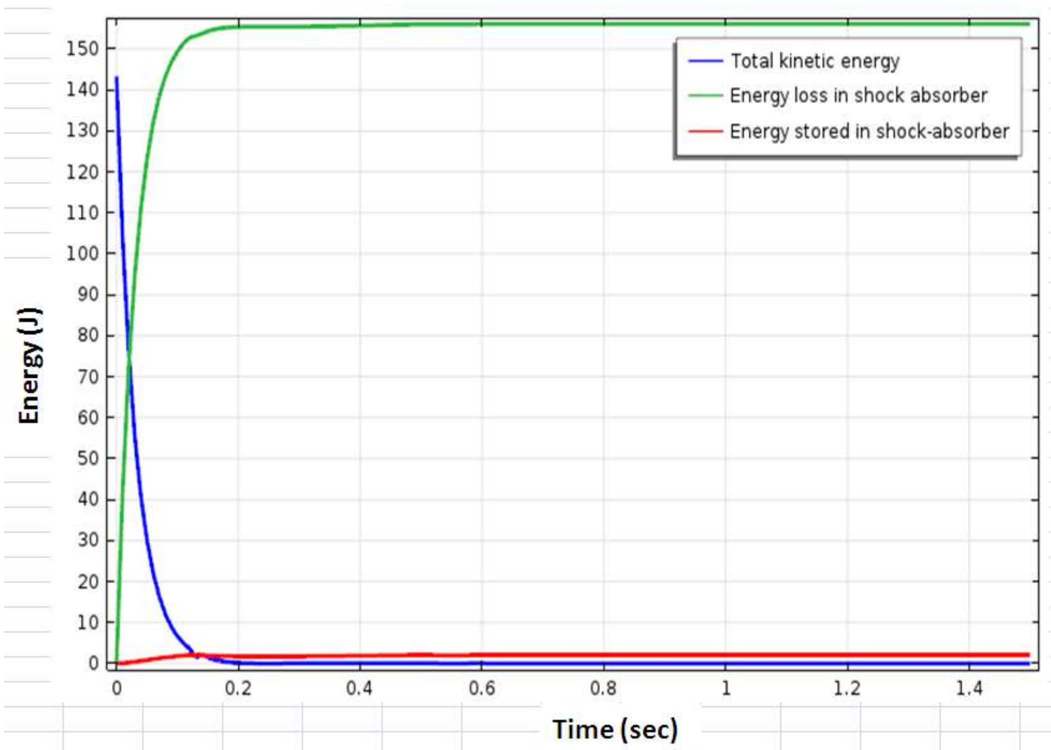

Fig. 4.13 Variation of energy vs time at 55°C

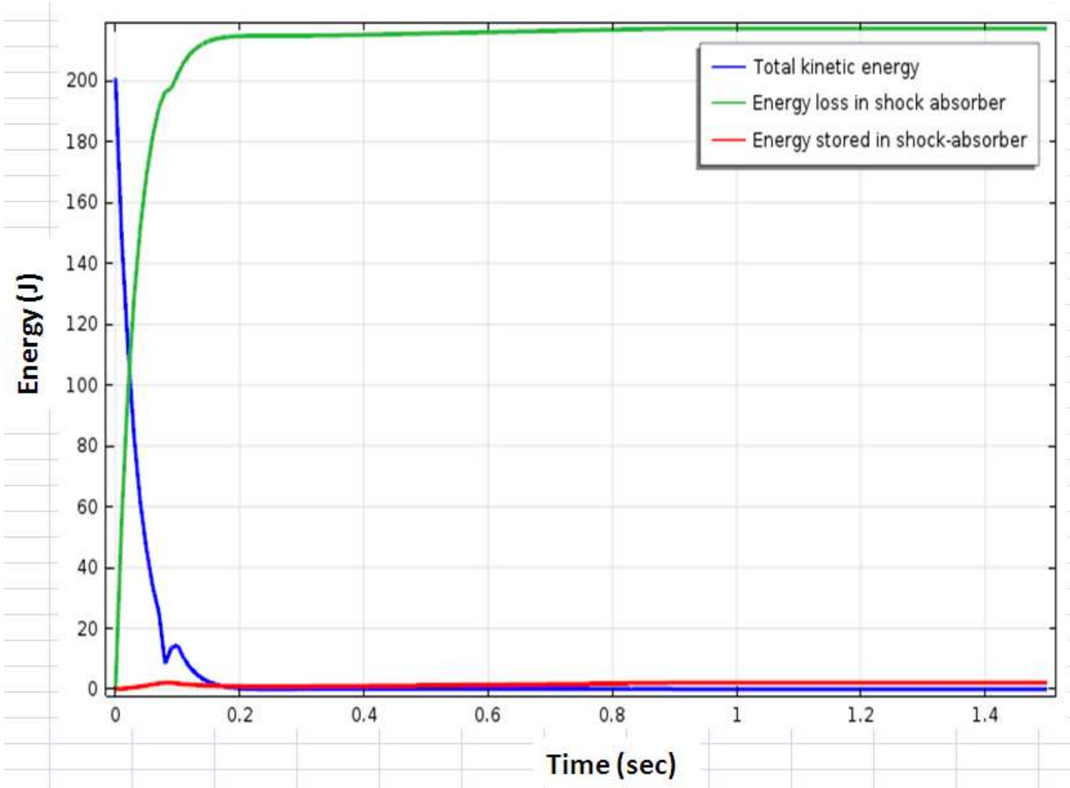

Fig. 4.14 Variation of energy vs time at 85°C

4.4 Experimental Studies

In order to study the dynamics of the hydraulic dashpot experiments were conducted on a full-scale test station. Shut-off rod drive mechanism and full-scale test station of 'Critical facility' reactor has been used to conduct the experiments. Fig.4.15 shows the full-scale test-station along with the test console, recorder and heating oven. Heating oven was used to conduct the experiments at elevated temperatures. Once the temperature reached the desired value, experiments were conducted and the dashpot speed and the pressure rod positions were measured. Tacho-generators (Make: Servo-tek, Accuracy: 0.571%) are mounted on the mechanism to measure the sheave shaft and dashpot speeds. A servo-mount potentiometer (Linearity: 0.15%) is mounted on the sheave shaft to measure the rod position at any time. A pressure transducer (Make:

Schaevitz, Accuracy: 0.059%) is mounted on the hydraulic dashpot to measure the pressure inside the oil chamber. A test console is used to operate the SRDM. A PC based recorder (data-logger, Make: DEWEsoft) is used to plot the output voltage of tacho-generators, potentiometer and pressure transducer against time. The output voltages are converted into the sheave shaft angular velocity / hydraulic dashpot angular velocity, rod position and hydraulic dashpot pressure. Experiments were conducted at room temperature as well as at elevated temperatures. Because of limitations of sensors and switches in the drive mechanisms, the experimental study was restricted up to 85°C. Sensor constants are given below:

Tacho-generator: 1000 RPM/7Volt

Potentiometer Voltage variation for full dashpot movement: 3.95 Volts

Pressure Transducer: 2.5 Bar/Volt

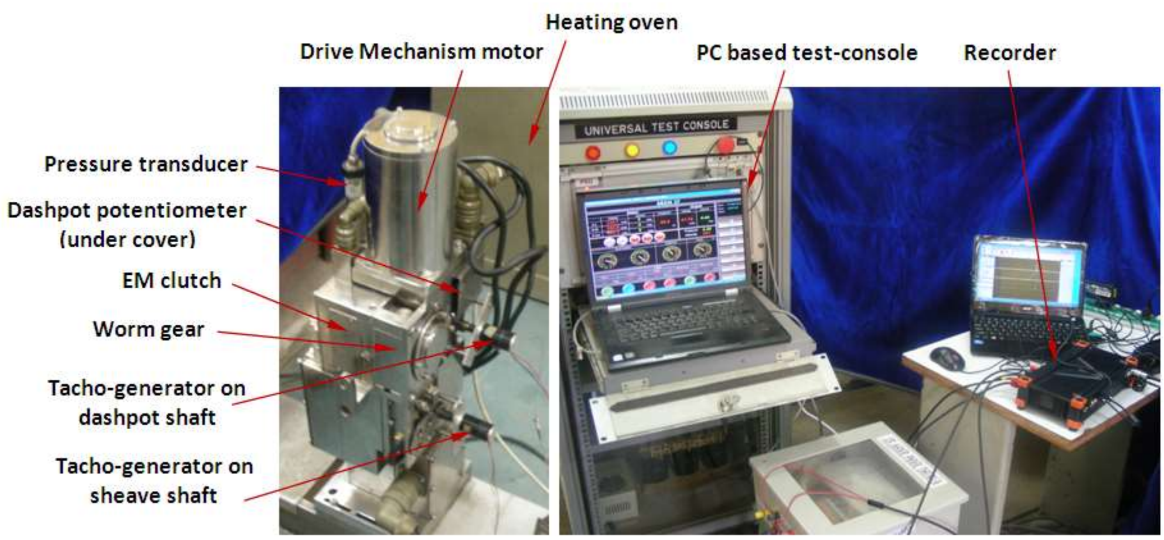

Fig. 4.15 Test set-up for experimental studies

4.4.1 Experimental Validation

Experimental validation is done by comparing numerical and experimental results as shown in Figs. 4.16 - 4.21. Results are compared at room temperature (35°C) as well as at elevated temperatures of 55°C and 85°C. A comparison shows that the results are in close proximity at 35°C all throughout as shown in Figs. 4.16 and 4.17. While at elevated temperatures of 55°C and 85°C where we see the impact in the dashpot operation, the experimental values never cross the 120° as it bounces back from the mechanical stopper. Numerically there is a constraint at 120° and the movement of the dashpot vane is restricted to 120° and the vane oscillates. The trend of oscillation is very similar to that of experimental results. This trend can be seen in Figs. 4.18 – 4.21. Minor variation in numerical and experimental results is due to error in values of input parameters for the model.

Both numerical and experimental results show that the dashpot becomes under damped beyond 55°C and the impact is seen in the damper responses. This means the modeling of hydraulic dashpot predicts the impact in dashpot fairly accurate. Vane hitting velocity is also predicted by the model as given in Table 4.2 and the experimental values of vane hitting velocity are given in Table 4.3. The numerical and experimental values of vane hitting velocity are also in close agreement.

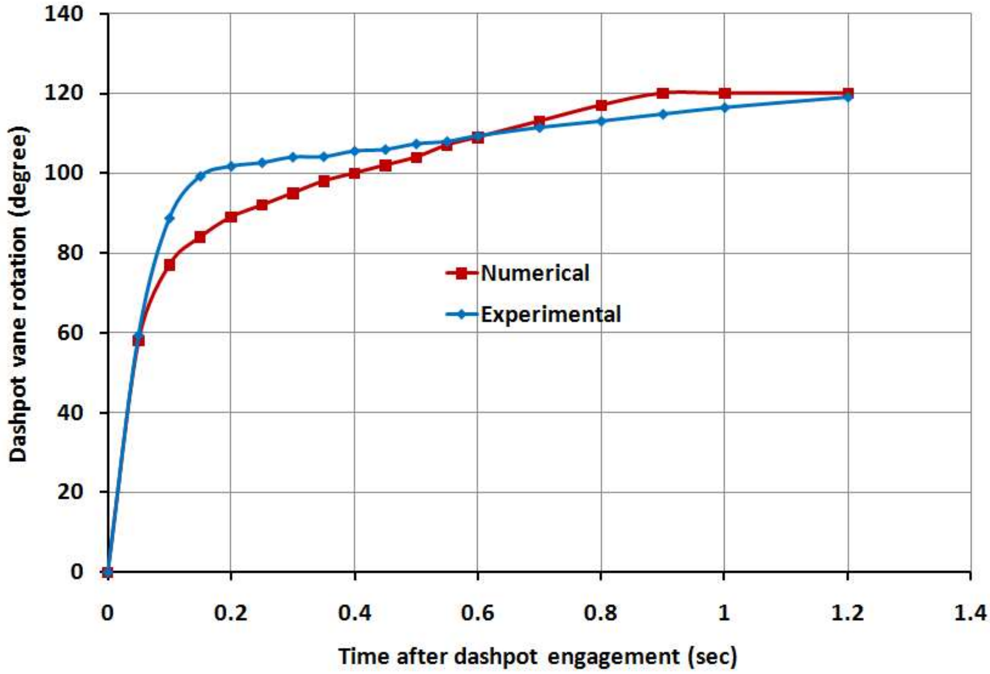

Fig. 4.16 Comparison of numerical and experimental dashpot vane rotation vs time at 35°C

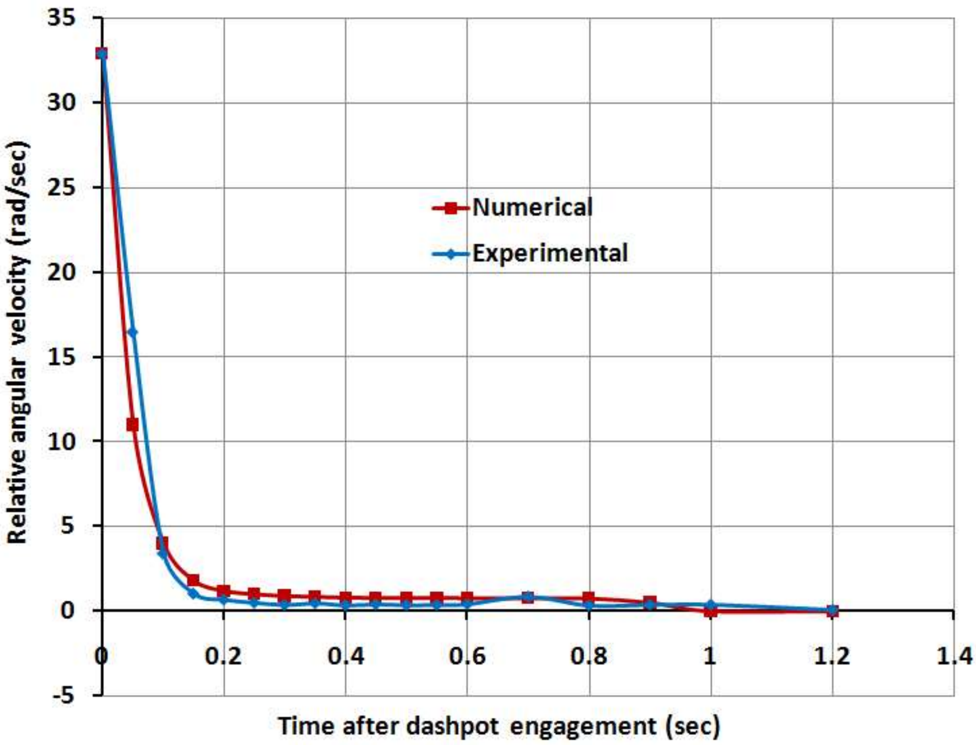

Fig. 4.17 Comparison of numerical and experimental relative angular velocity vs time at 35°C

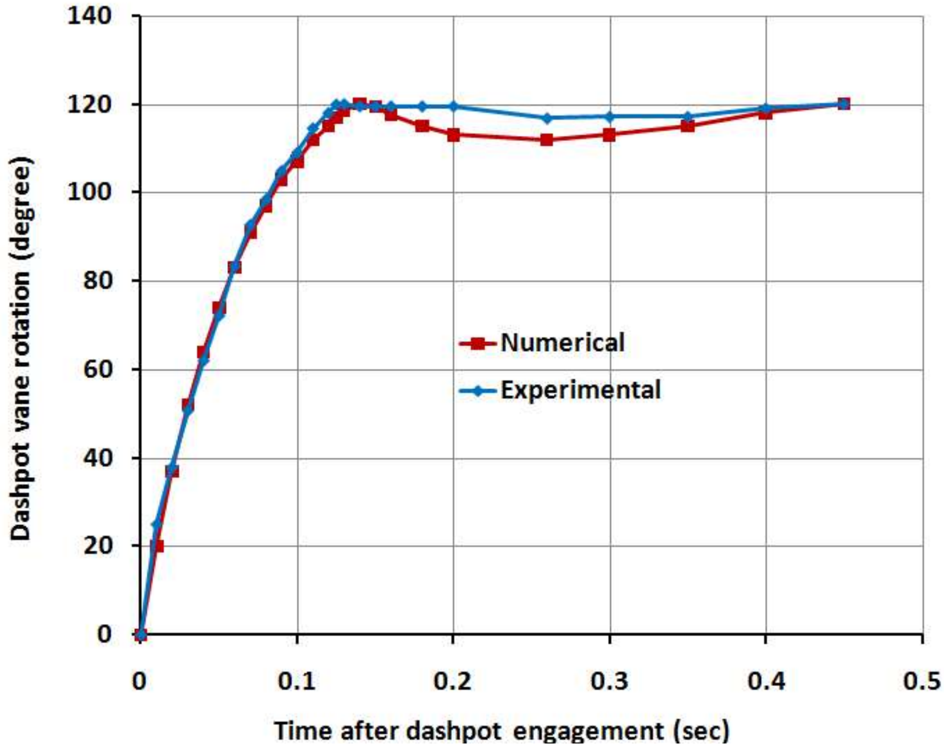

Fig. 4.18 Comparison of numerical and experimental dashpot vane rotation vs time at 55°C

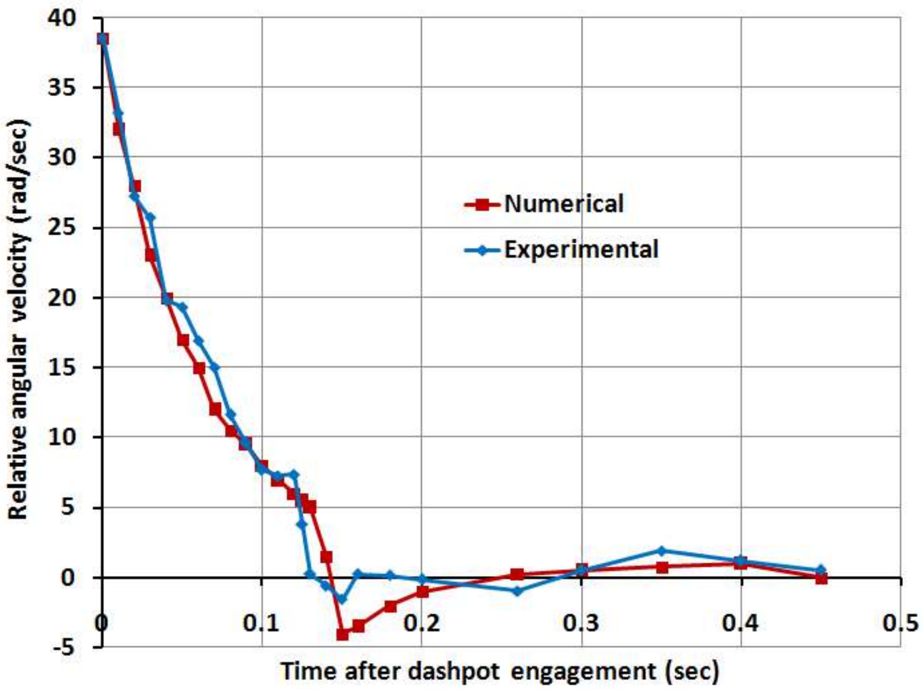

Fig. 4.19 Comparison of numerical and experimental relative angular velocity vs time at 55°C

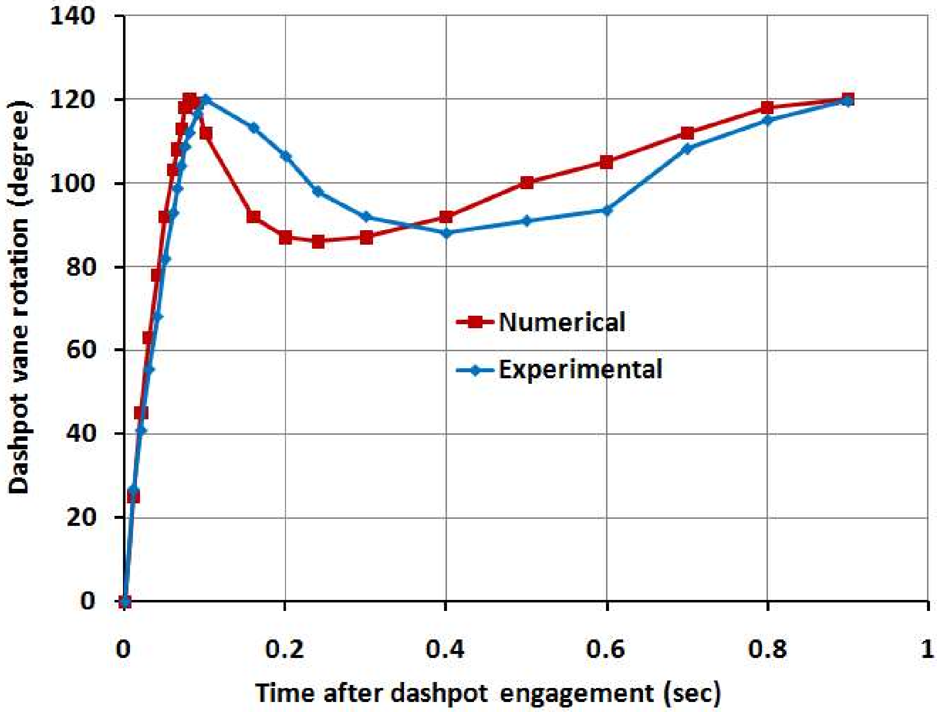

Fig. 4.20 Comparison of numerical and experimental dashpot vane rotation vs time at 85°C

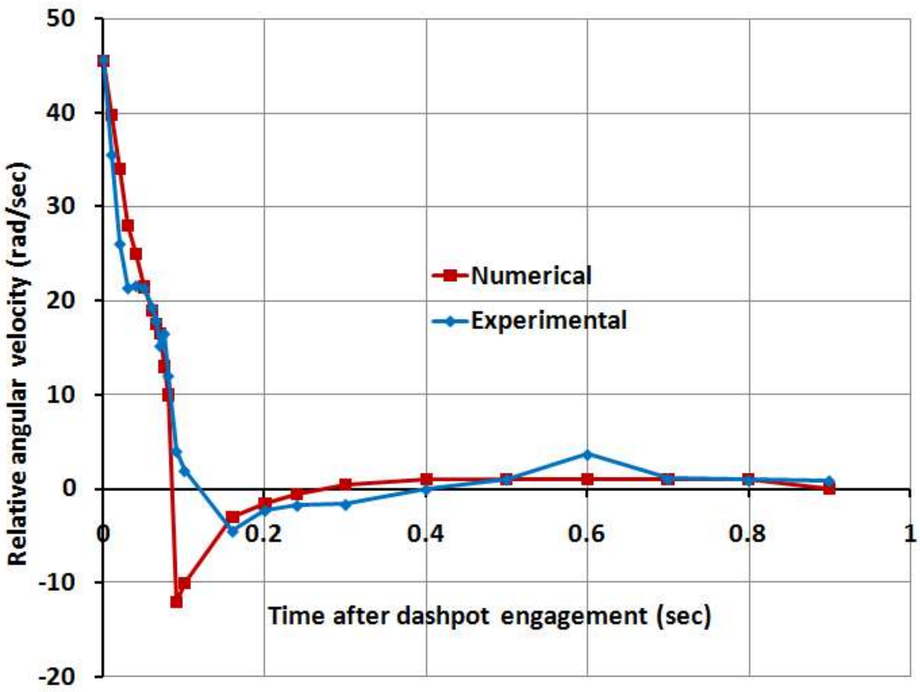

Fig. 4.21 Comparison of numerical and experimental relative angular velocity vs time at 85°C

4.4.2 Experimental Results

Experiments have been conducted at a temperature range from 35°C to 85°C to extract more useful data. Experimental results are given in Table 4.3 and corresponding experimental plots at 35°C, 55°C and 85°C are given in Figs. 4.22 – 4.25 with various conditions. Fig 4.22 shows the comparison of experimental sheave angular velocities vs time at 35°C, 55°C and 85°C. Impact/kink can be seen in the plots at oil temperature of 55°C and 85°C. The comparison of dashpot response (angular velocity) vs time at 35°C, 55°C and 85°C is given in Fig. 4.23 and comparison of dashpot moment due to pressure vs time at 35°C, 55°C and 85°C is given in Fig. 4.24 Fig 4.25 gives comparison of relative vane rotation respectively vs time at 35°C, 55°C and 85°C. Experimental results show that the impact is observed beyond 55°C as damping coefficient reduces at elevated temperature. Vane hitting velocity also increases with increase in environmental temperature.

A comparative study of torque due to inertial force and torque due to dashpot force is also done. The torque due to inertial force is the multiplication of moment of inertia and angular acceleration (as shown in Fig. 4.11), which is very high initially (127 N.m at 35°C). This inertial torque reduces sharply to zero as the pressure builds-up in the dashpot and the kinetic energy is absorbed. Torque (moment) due to dashpot pressure reaches a peak value of 67.17 at 35°C and this reduces very slowly as shown in the Fig. 4.24.

Table 4.3: Experimental Results

Environment temperature (°C)	Sheave shaft peak angular velocity (rad/s)	Dashpot peak angular velocity (rad/s)	Dashpot peak pressure (Bar)	Peak damping moment due to pressure (N-m)	Damping coefficient (N.m.s/rad)	Impact in the dashpot action	Vane hitting velocity (rad/sec)
35	71.01	32.67	12.97	67.02	4.51	No	-
45	70.74	35.50	11.85	61.24	4.11	No	-
55	70.86	38.30	10.85	56.07	3.30	Yes	7.74
65	71.45	42.48	9.57	49.45	3.22	Yes	9.02
75	71.31	44.72	9.00	46.51	3.16	Yes	10.47
85	72.12	45.31	8.90	45.99	3.11	Yes	12.56

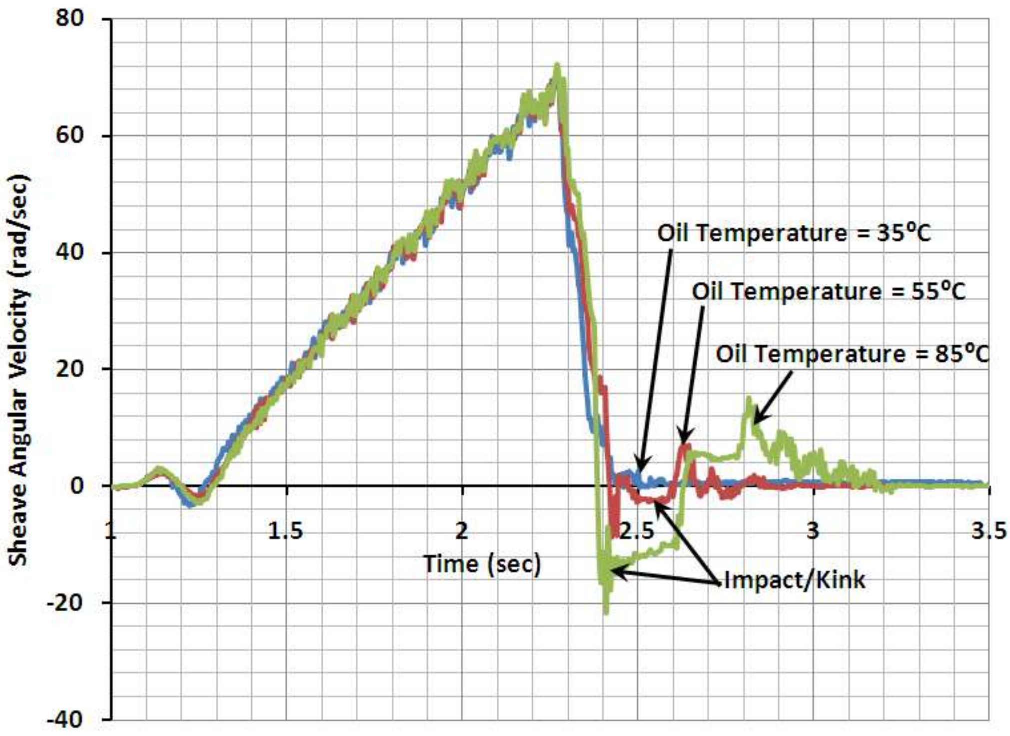

Fig. 4.22 Experimental sheave angular velocity vs Time

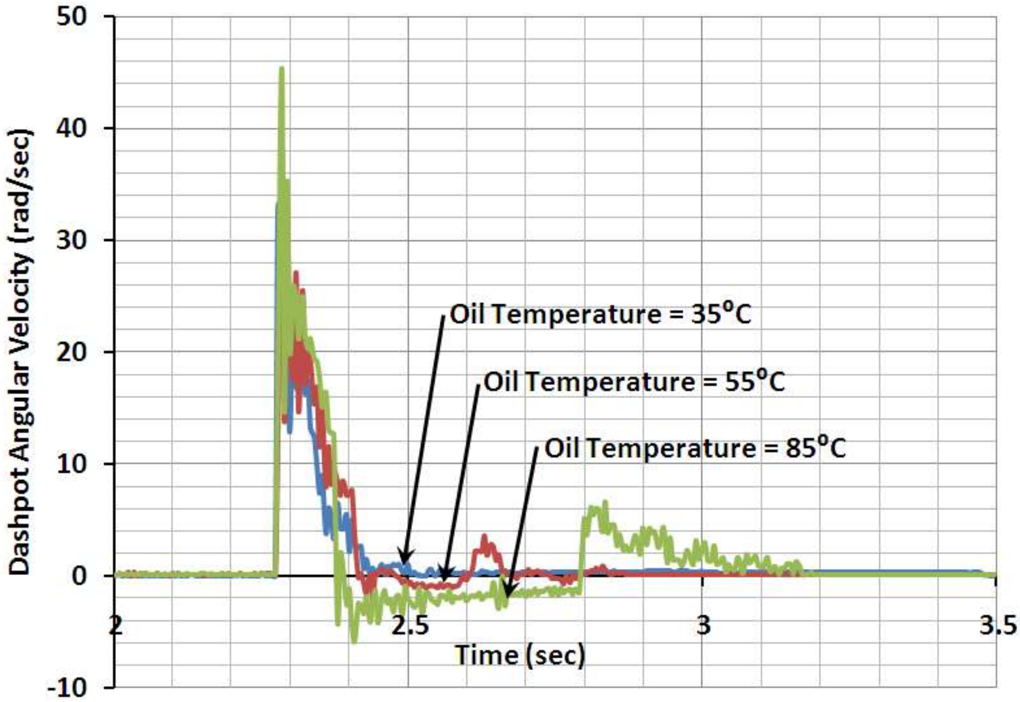

Fig. 4.23 Experimental dashpot response (angular velocity) vs Time

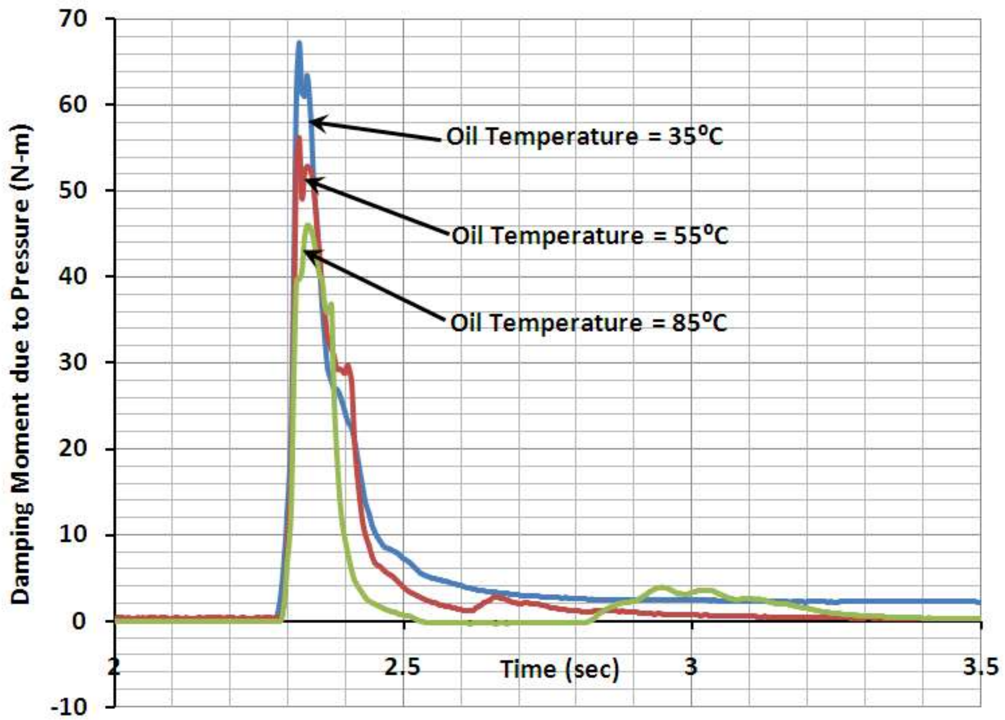

Fig. 4.24 Experimental variation of damping moment due to pressure vs Time

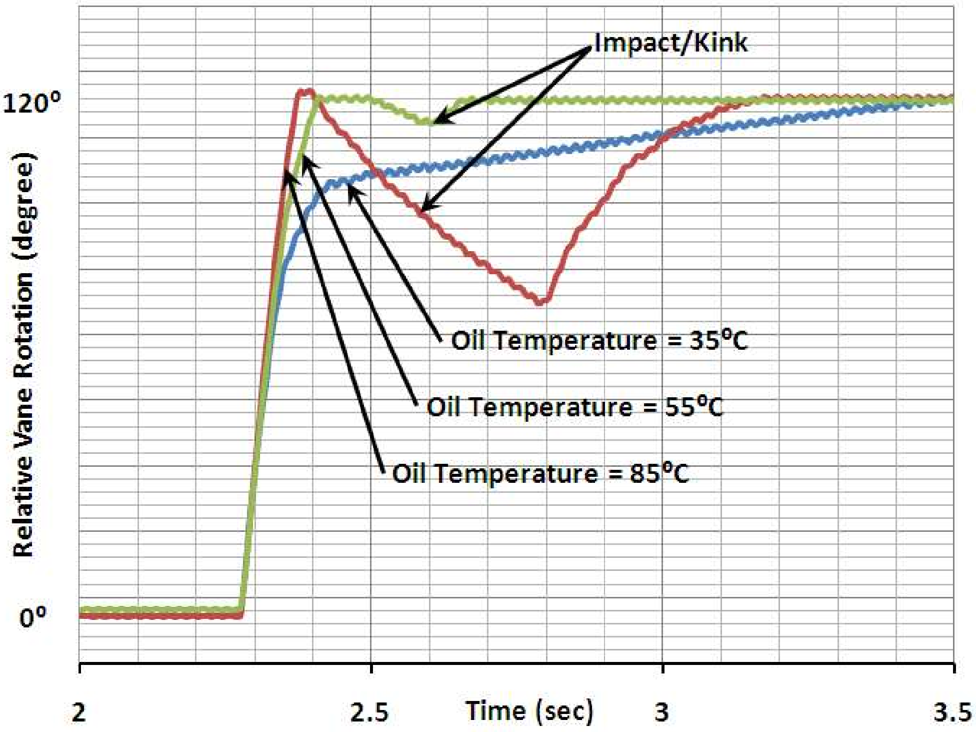

Fig. 4.25 Experimental dashpot relative vane rotation vs Time

4.5 Parametric Studies

The model of the hydraulic dashpot is used to extend the study further for various parameters. Fig. 4.26 shows the variation of dashpot vane rotation vs time with different values of equivalent moment of inertia at 35°C. It clearly shows that if, we increase the moment of inertia of the rotating components while keeping all other parameters same, the dashpot becomes under damped beyond a value of moment of inertia. Fig. 4.27 shows the variation of dashpot vane rotation vs time with different values of constraint angle at 35°C. The curve shows that if we reduce the constraint angle below a value, we get the impact in the hydraulic dashpot, as by that time the whole energy of the dashpot is not absorbed. Similarly, Fig. 4.28 shows the variation of dashpot vane rotation vs time with different values of applied moment at 35°C. The applied moment in the hydraulic dashpot shaft is due to the constant weight of the absorber rod which is always there in the dashpot action. One can see from the Fig. 4.28 that, beyond a value of applied moment the dashpot becomes under damped and we see the impact in dashpot operation.

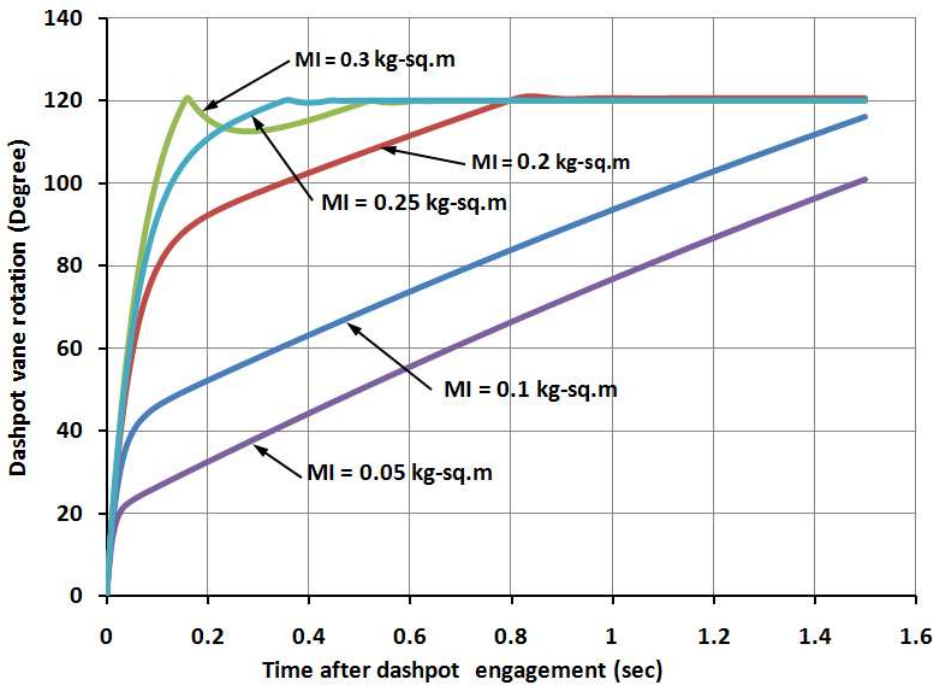

Fig. 4.26 Variation of dashpot vane rotation vs time with different values of moment of inertia at 35°C

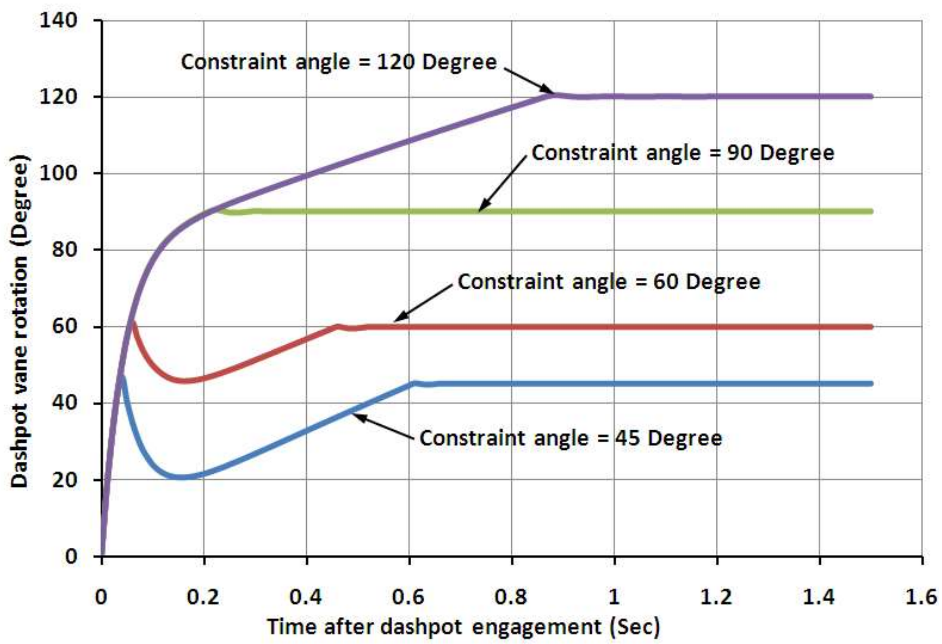

Fig. 4.27 Variation of dashpot vane rotation vs time with different values of constraint angle at 35°C

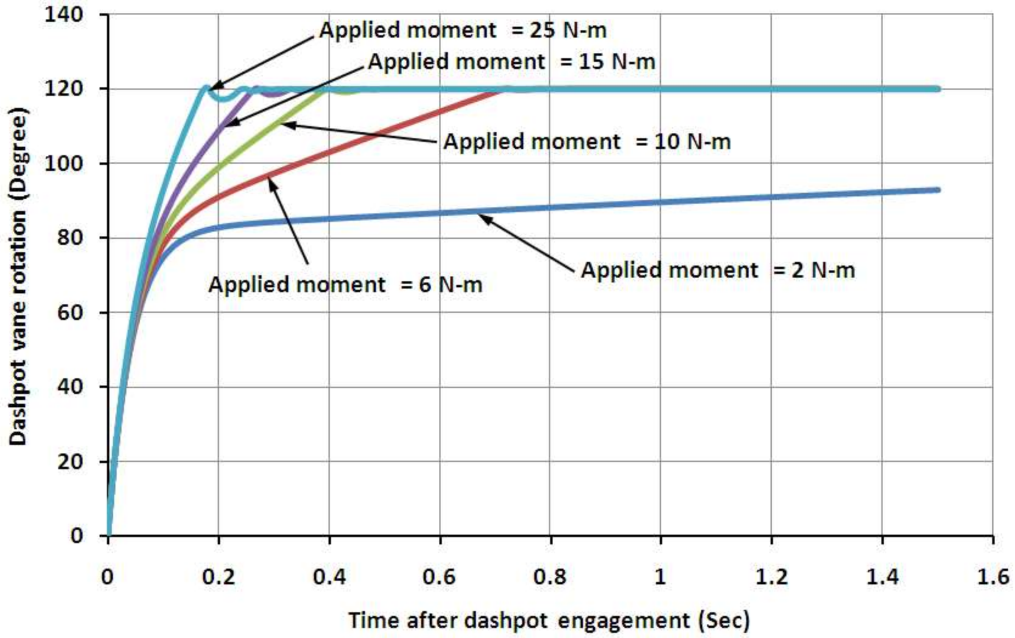

Fig. 4.28 Variation of dashpot vane rotation vs time with different values of applied moment at 35°C

4.6 Closure

Effects of mechanical parameters on dashpot performance are studied by multi-body dynamics modeling. It was revealed that apart from reduction in viscosity (as discussed in chapter 3), the dashpot can also become under damped with increase in moment of inertia, reduction in constraint angle and increase in constant applied moment. By now all the parametric effects on dashpot performance (both fluid flow and mechanical) have been studied in depth. From the study, it is learnt that the dashpot clearance thickness is the most critical parameter and should be controlled in a passive manner. With this information, passive ways of making hydraulic dashpot temperature compensating shall be studied further.

Chapter V

PASSIVE TEMPERATURE COMPENSATION IN HYDRAULIC DASHPOT

This chapter presents the methods studied for passive temperature compensation in the hydraulic dashpot. Fluid structure analysis is carried-out for temperature compensation.

5.1 Introduction

Passive temperature compensation study is focused on reducing the clearances of the hydraulic dashpot at elevated temperature which intern compensates for the reduction in viscosity of damping oil and the dashpot gives uniform performance for wide range of temperature variation. The temperature compensation effects are mainly due to difference in the thermal expansion of materials. Different combinations of materials are used to reduce the dashpot clearances at elevated temperature. Fluid-structure analysis (CFD/FEM) has been carried-out to study the thermal expansion and pressure generated in the hydraulic dashpot.

5.2 Study Set-Up Description

Passive temperature compensation effects are studied on a prototype SRDM and full-scale test set-up meant to qualify the shut-off rod drive mechanism of 'Critical Facility' reactor. The detailed set-up description is explained in chapter 4. The hydraulic dashpot shaft is modified to insert dissimilar material temperature compensating blocks. These block designs can be altered as per the methods used to get the clearance reduction. Fig. 5.1 gives the detailed construction of hydraulic dashpot studied for temperature compensation. Fig. 5.2 shows the details of internal components of the hydraulic dashpot while Fig. 5.3 shows the picture of a dashpot shaft with the brass blocks and deformed bimetallic strips at elevated temperature. The shaft in the dashpot (as shown in Fig. 5.1) is having brass blocks along with the bimetallic strips. These brass blocks (total 4 Nos.) have been mounted on the moving vane and the bimetallic strips are mounted on these brass blocks. Brass blocks are used, so that the combined temperature compensating effect of brass block and strip can be achieved. Design modifications in terms of block and bimetallic strip are done in the dashpot shaft only, so that the over-expansion of bimetallic strip will never lead to seizure of dashpot operation. All the parameters of the hydraulic dashpot under study are given in Table 5.1.

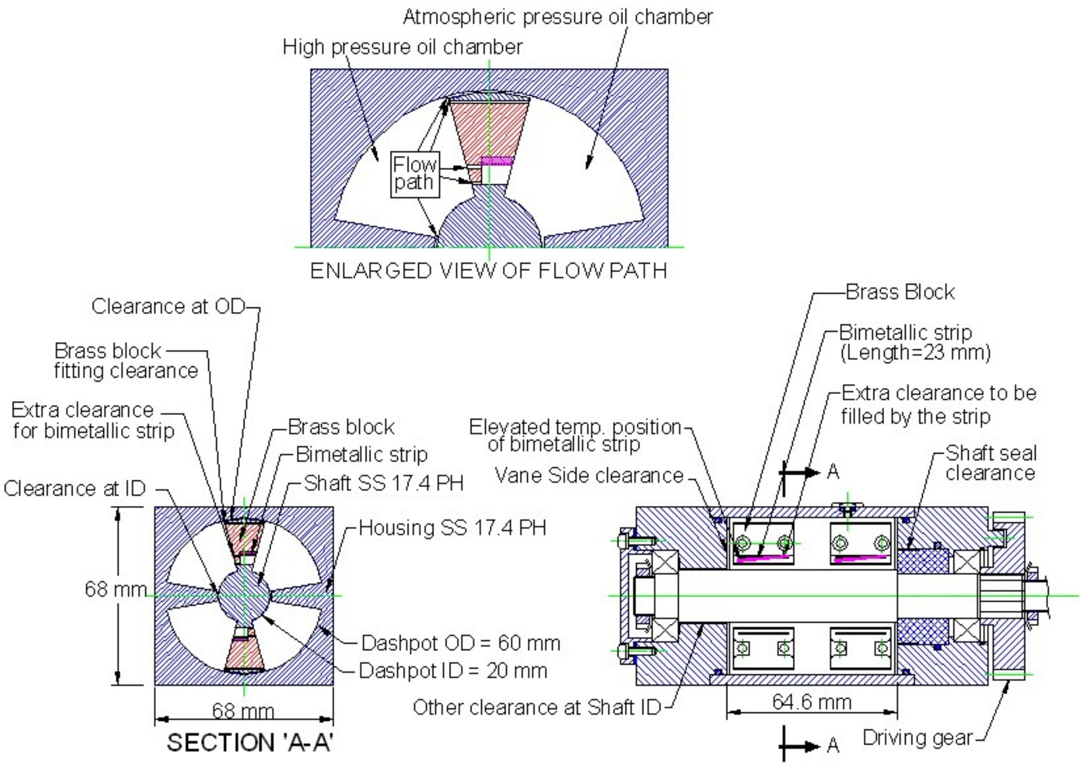

Fig. 5.1 Detailed construction of the hydraulic dashpot along with brass blocks and bimetallic strips.

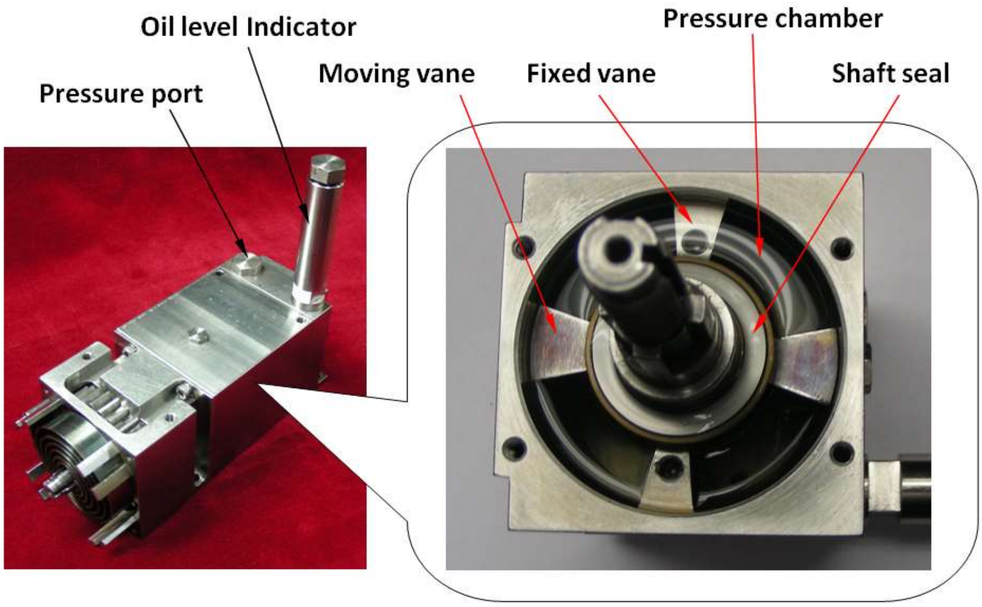

Fig. 5.2 Internal components of the hydraulic dashpot

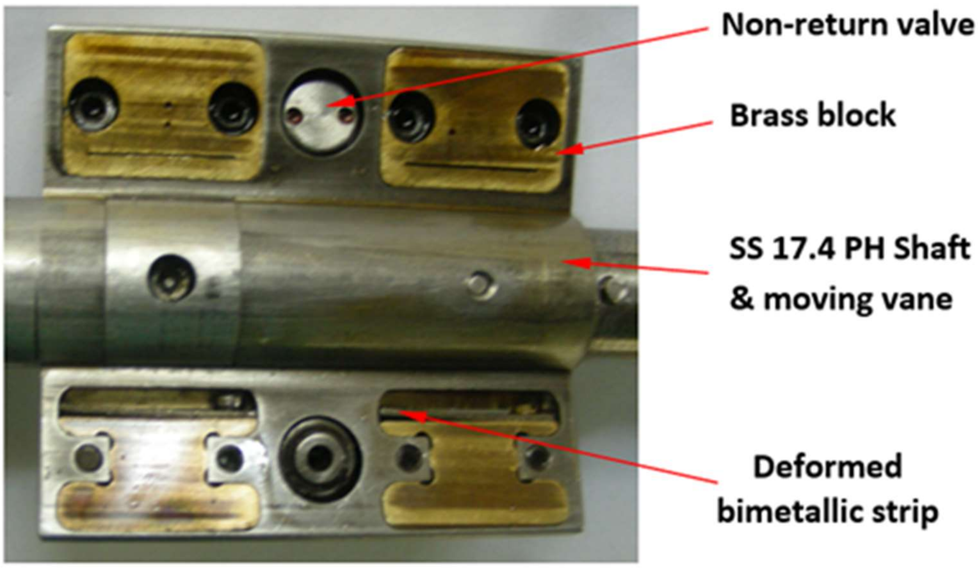

Fig. 5.3 Dashpot shaft with brass blocks and deformed bimetallic strips at the elevated temperature.

Table 5.1: Study set-up parameters

Parameter	**Value for 'Critical Facility' reactor**
Drive mechanism overall size (mm)	210 x 196 x 750
Rod travel (mm)	2400
Rod weight (kg)	8
Free fall (mm)	2160 (in air)
Hydraulic dashpot vane size (mm)	20 ID x 60 OD x 64.6 Long
Approximate volume of the oil (cc)	162
Hydraulic dashpot rotation (degree)	120
Mechanical shaft seal	On one side
No. of dashpot vanes	Two moving vanes/two fixed vanes
Clearance at OD (mm)	0.1
Clearance at ID (mm)	0.1
Brass block fitting clearance (mm)	0.1
Shaft seal clearance (mm)	0.3
Other clearance at shaft ID (mm)	0.3
Extra clearance for bimetallic strip (mm)	0.3
Brass block size (mm)	16 x 23
Bimetallic strip size (mm)	23 x 6 x 0.8 (Layer one, S1=0.4, Layer two, S2= 0.4)
Bimetallic strip material	Layer two: NiMn-steel and Layer one: Invar (Fe-Ni 36%)
Shaft and moving vane material	SS 17.4 PH
Housing and fixed vane material	SS 17.4 PH
Inserted block in moving vane	Brass
Viscosity of the oil used at 25°C (cst)	1500

5.3 Methods for passive temperature compensation

Hydraulic dashpot pressure is highly dependent on dashpot clearances, if the clearances are reduced, the dashpot force increases sharply. Efforts are made to reduce the clearances in a passive manner at elevated temperature, so that it can compensate for the effect of viscosity reduction. This can be achieved by using different combinations of dissimilar materials with different thermal expansion properties, like use of bimetallic strips, use of bimetallic washers and use of different material in 'C' groove. Detailed thermal expansion analysis is carried-out to see the reduction in the clearances at the elevated temperature. As the hydraulic dashpot size under study is small, the size of dissimilar material component is also limited; hence we get very less compensation in the dashpot pressure. Hence main focus of study was on utilizing bimetallic strips to reduce the dashpot clearances at the elevated temperature. Bimetallic strips can have good amount of deflection even in small lengths. These bimetallic strips are mounted on the brass blocks so that the combined effect of brass block and strip can be achieved. Results have been compared between dashpot shaft with only brass blocks and with bimetallic strips along with brass blocks.

5.4 Numerical Procedure

5.4.1 Analysis Methodology

Commercial code COMSOL Multiphysics 5.1 (based on finite element method) is used to solve the governing equations. COMSOL tutorial: Fluid damper [65]. The phenomenon in the hydraulic dashpot is such that, the dashpot components see the high temperature mainly due to environmental heat. Because of the high environmental temperature, the oil viscosity decreases, dashpot structural components expand and this phenomenon affects the fluid flow. Based on this, analysis strategy has been formulated in which following three physics aspects have been solved:

(i) Solid mechanics

(ii) Laminar flow

(iii) Moving mesh

Study has been divided into two stages; as the structural changes have taken place first, so in the study-1 only solid mechanics interface is solved for thermal expansion. In study-2, the output results of the study-1, i.e. solid mechanics deformations are taken as an input. Laminar flow and moving mesh interfaces are solved simultaneously to get the dashpot pressure in study-2. In this way it is a one way coupling of fluid and structural phenomenon. Based on increased dashpot pressure further structural changes in dashpot components can also be studied, but that is not included in the present study. Moving mesh interface in COMSOL utilizes Arbitrary Lagrangian Eularian (ALE) formulation, to analyze the fluid and structure interfaces. Souli et al. [57] and Hwa et al. [73]. COMSOL Multiphysics allows the coupled solving of structural deformations and fluid flow variables (velocity and pressure) in moving mesh geometry consisting of a solid deformable object surrounded by a fluid. Kuehne et al. [59] and Gao et al. [74].

The hydraulic dashpot geometry is complex with narrow clearances, so it is simplified to reduce the size of computational domain and also to get structured mapped mesh of the whole geometry with hexahedral elements. Actual X-section of the hydraulic dashpot geometry with dimensions is given in Fig. 5.4. Thermal expansion analysis as shown in the Fig. 5.5 has been done to validate the geometry simplifications. A round geometry with two fixed vanes and one moving vane as shown in Fig. 5.15 has been finalized for the study. Side walls of the dashpot are also modeled. Though for the pressure chamber modeling, only one moving vane and one fixed vane are sufficient, but for structural analysis considerations, two fixed vanes and one moving vane are considered. The blocks which are inserted in the dashpot shaft are having straight faces (for ease of manufacturing), while in the analysis they are modeled as round (for ease of modeling). As the length of the clearance is much higher as compare to the thickness of clearance, so the effect of curvature is negligible.

Hydraulic dashpot operation is a transient phenomenon; hence flow variables and computational domain changes with time. The present study has been carried-out in 3-D geometry, as it is not possible to resolve the geometry in 2-D. Because of 3-D geometry and fast transients, it is difficult to solve the transient equations with present computational set-up. So, alternatively the whole transient phenomenon has been divided into small time steps and the stationary equations are solved at different time steps (Similar to that in chapter 3). The computational domain (geometry) is also changed to that time step (by rotating the vane) every time.

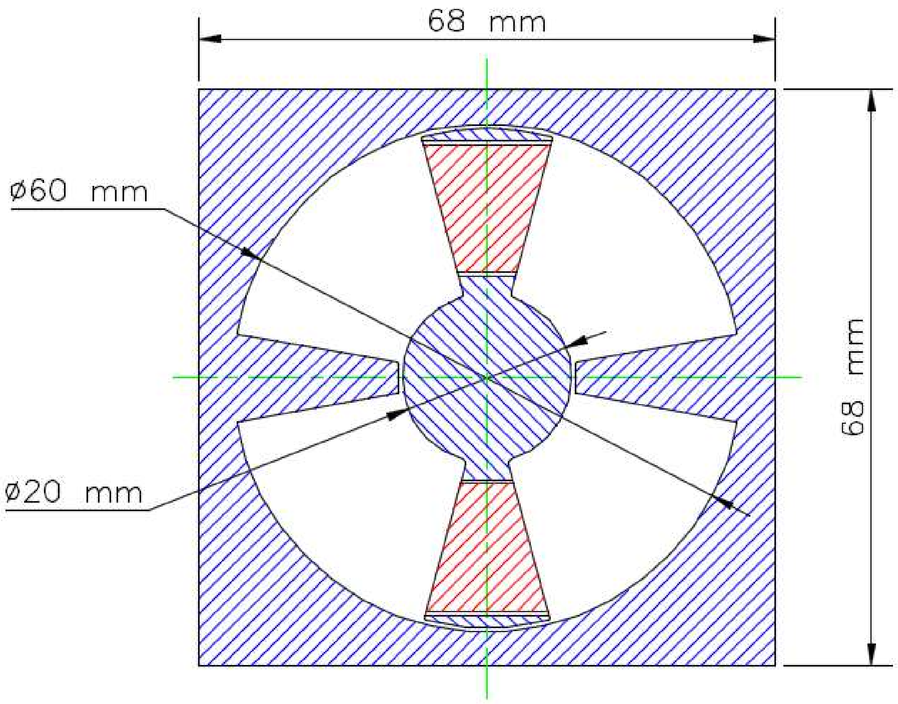

Fig. 5.4 Actual X-section of the hydraulic dashpot with dimensions

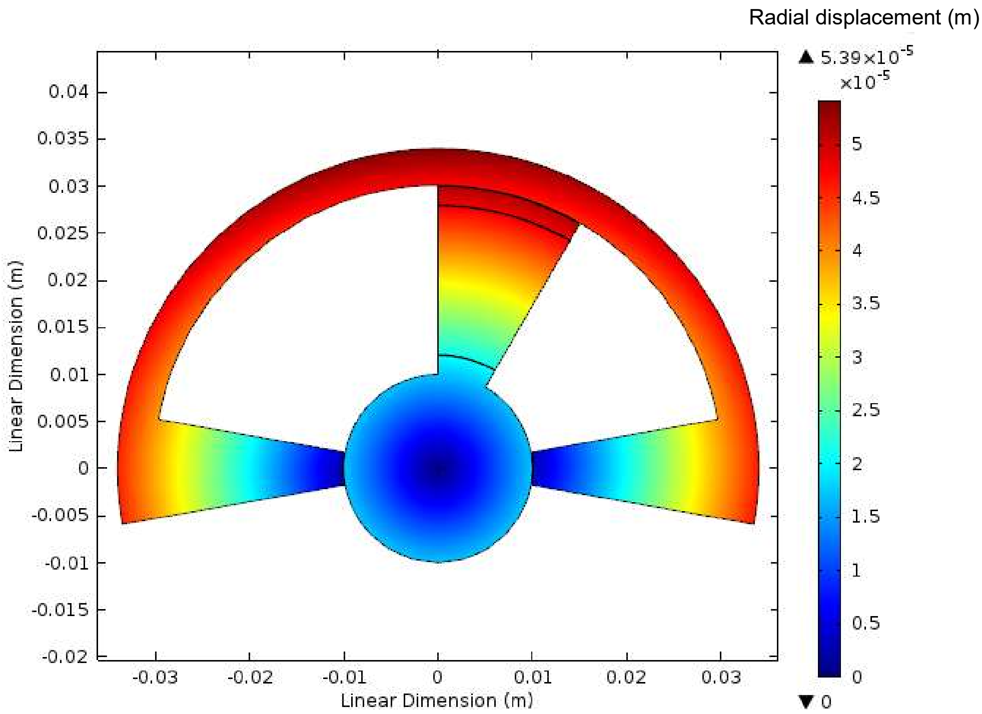

Fig. 5.5 Radial displacement contour for thermal expansion in simplified geometry of the hydraulic dashpot X-section

5.4.2 Theory of Thermal Expansion in Solids and Governing Equations

In study-1, only solid mechanics equations are solved. The equations (5.1a)-(5.1d) are general equations for linear elastic materials: COMSOL 5.1 Documentation [64]

$$-\nabla.\sigma = F_v \tag{5.1a}$$

$$\sigma = J^{-1}FSF^T \tag{5.1b}$$

$$F = (I + \nabla u) \tag{5.1c}$$

$$J = \det(F) \tag{5.1d}$$

Duhamel-Hookes law relates the stress tensor to the strain tensor and temperature as:

$$S - S_0 = C:(\epsilon - \epsilon_0 - \epsilon_{inel}), \tag{5.2a}$$

$$\epsilon_{inel} = \alpha\,(T - T_{ref}), \tag{5.2b}$$

$$\epsilon = \tfrac{1}{2}[(\nabla u)^T + \nabla u] \tag{5.2c}$$

Where σ is the normal Cauchy stress that relates stresses in the structure, F_v is the body force per unit volume, F is the deformation gradient tensor, S is the second Piola-Kirchhoff stress tensor that relates forces to area, J is the determinant of tensor F and called Jacobian matrix, ∇u is the material displacement gradient vector and I is the identity matrix, α is the thermal expansion tensor, C is the 4^{th} order elasticity tensor represented by Duhamel-Hooke's law is a function of modulus of elasticity and Poison's ratio, S_0 and ϵ_0 are the initial stress and strain, : is the double dot tensor product, T and T_{ref} in Eq. 5.2b are the environment temperature and the reference temperature respectively, at rest of the places T is transpose.

Fluid flow in the damper is described by the incompressible Navier-Stokes equations, solving for the velocity field $u_2 = (u_2,v_2,w_2)$ and the pressure. In this study the equations are solved as stationary at a particular time-step. Further the equations are solved at the next time-step with changed geometry and boundary conditions. As frequency of operation is very low in these types of dashpots, the effect of viscous heating has been neglected, He et al. [66], hence energy equation is not solved in this study. Continuity and momentum equations for incompressible flow solved in COMSOL Multiphysics for stationary conditions are:

$$\nabla . u_2 = 0 \tag{5.3}$$

$$\rho(u_2 . \nabla)\, u_2 = \nabla . [-pI + \mu (\nabla u_2 + (\nabla u_2)^T)] + F \tag{5.4}$$

Where, ∇ is the divergence, ρ is the density of fluid (Kg m^{-3}), u_2 is the velocity field (u_2,v_2,w_2) (m s^{-1}), p is the pressure (Pa), μ is the dynamic viscosity (Pa s), I is the identity matrix, T is the transpose and F is the volume force vector (N m^{-3}). The equations have been discretized and solved in COMSOL.

5.4.3 Thermal Expansion Analysis

Thermal analysis has been carried-out for the different methods to reduce the clearance at the elevated temperature. This analysis is useful in deciding the most effective ways of reducing the clearances in the hydraulic dashpot.

(a) Thermal Expansion in Bimetallic Washer

Bimetallic washers are made of two layers with different materials. As the two layers have different coefficient of thermal expansion, the washer will become convex (as shown in Fig. 5.7) at the elevated temperature. This phenomenon of washer can be utilized to reduce the clearances of dashpot at the elevated temperature. Fig. 5.6 gives a design in which 4 bimetallic washers are used and combined effects of their convexity are used to reduce the clearance. These washers will pull a spring-loaded lever at the elevated temperature thus reduce a given gap. This design can be implemented in form of a block, which can be inserted into the vane of the dashpot shaft. In present study the bimetallic washers of aluminum and copper layers are used.

Thermal expansion analysis results are shown in Figs. 5.7 and 5.8, where Fig. 5.7 gives the thermal expansion of a bimetallic washer while Fig. 8 gives the line graph of total displacement across the cross-section of bimetallic washer. Results indicates that, one washer can give a total deflection of 1.5 microns in lever and with 4 washers, we can maximum have 6 microns of deflection. This deflection will result into a clearance reduction by 6 microns.

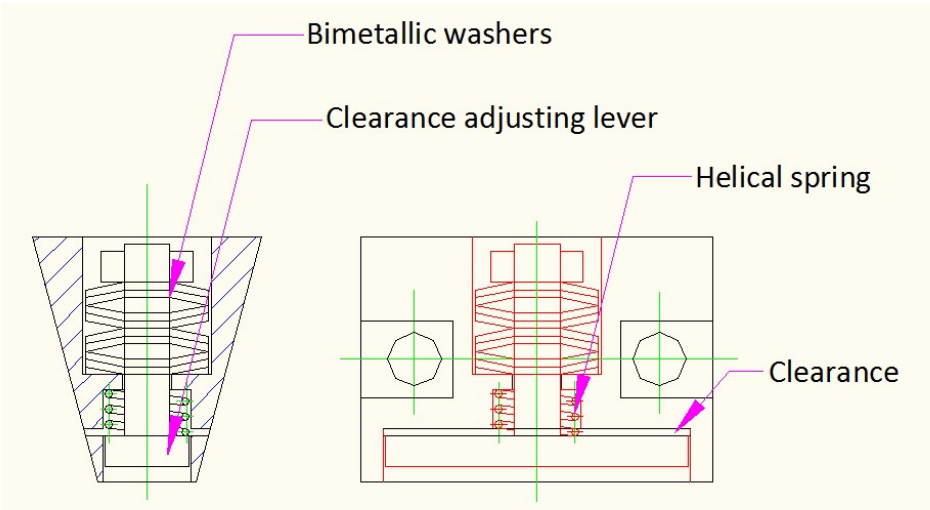

Fig. 5.6 Bimetallic washer based design to reduce the clearance

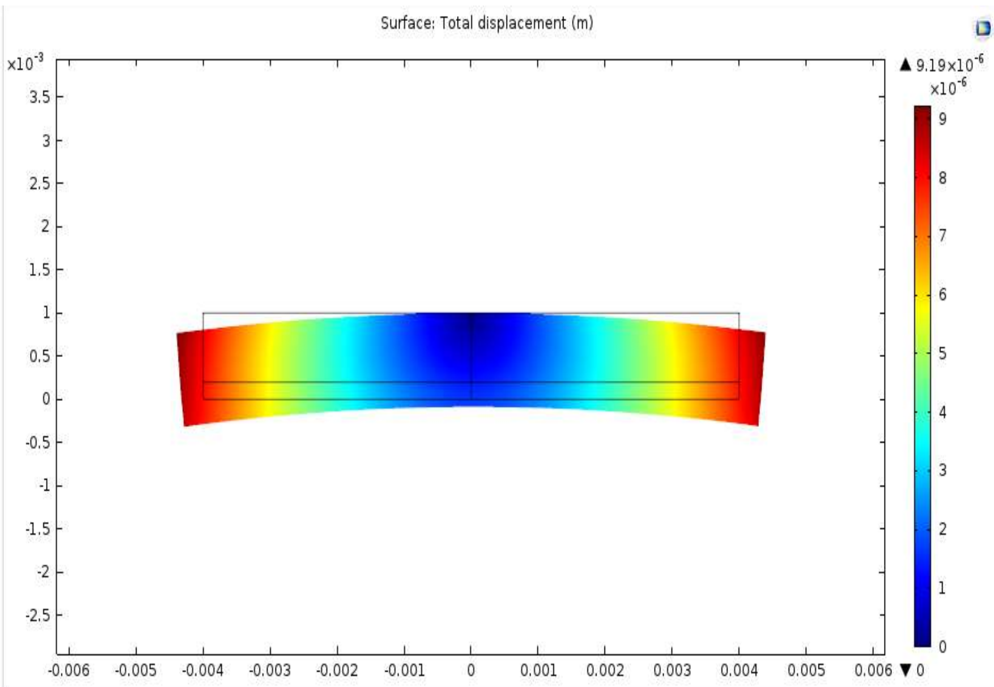

Fig. 5.7 Thermal expansion of a bimetallic washer

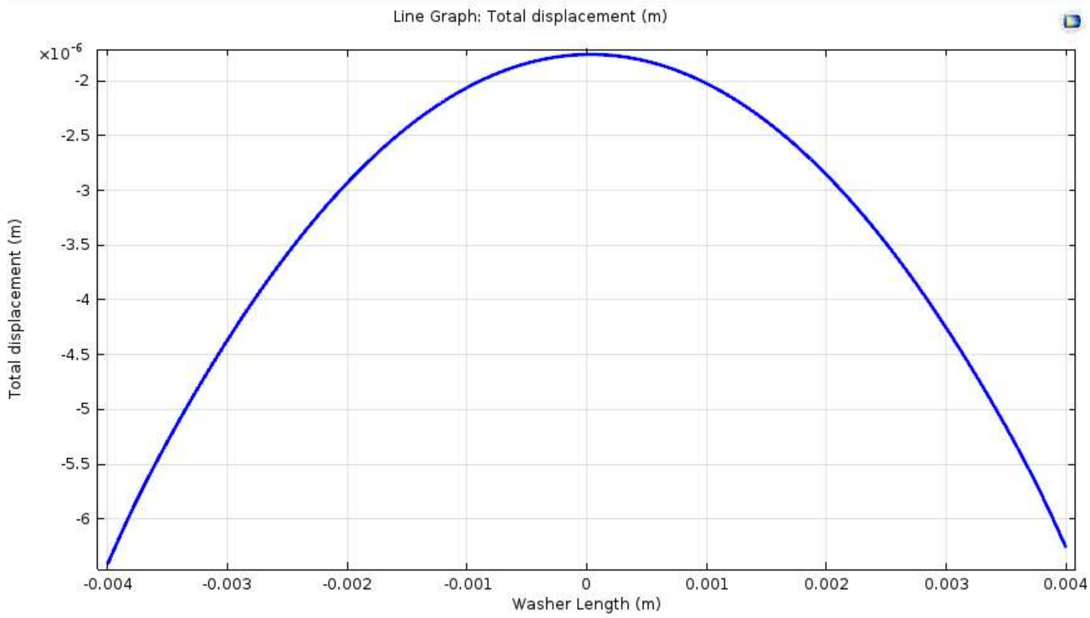

Fig. 5.8 Line graph of total displacement across cross-section of the bimetallic washer

(b) Thermal Expansion with Dissimilar Material Ring in Radial Gap

Thermal expansion analysis of the dashpot is done with a ring fitted in the seal clearance. These rings of material brass and aluminum have been analyzed. Analysis results show that with this we could get a reduction in clearance up-to 1-2 microns only.

(c) Thermal Expansion in Dashpot Shaft with Dissimilar Material in 'C' Groove

Thermal expansion analysis has been done with the dashpot shaft in which a block of brass/aluminum is fitted in the 'C' groove location. This block of brass/aluminum will reduce the depth of 'C' groove at the elevated temperature.

Analysis shows that by this method, a reduction in depth of 'C' groove by 10 microns is possible. Analysis results are shown in Figs 5.9 and 5.10.

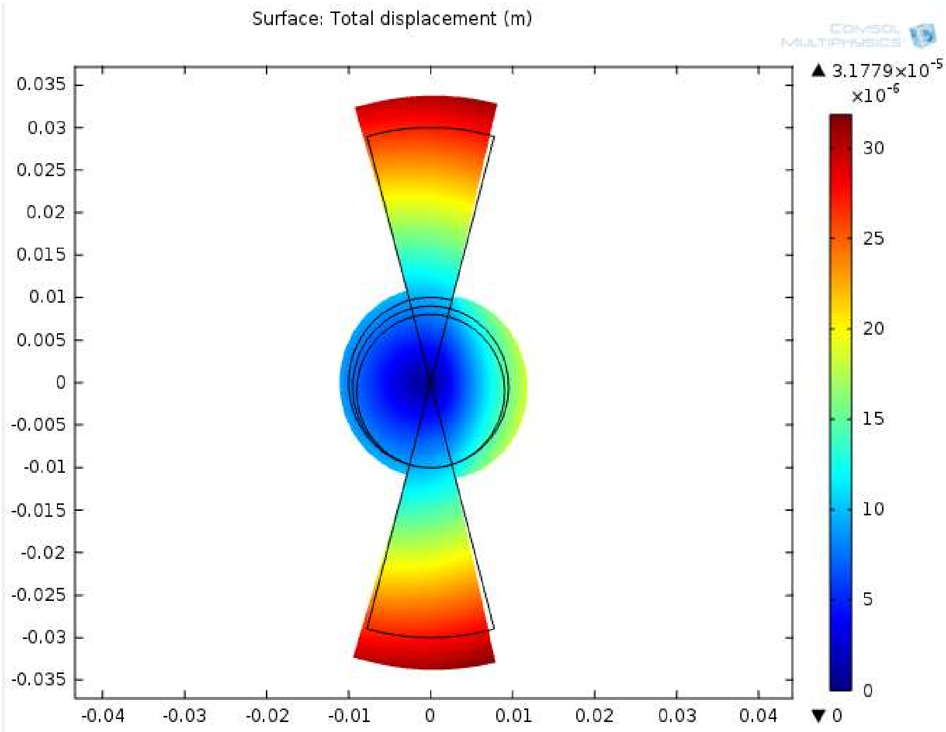

Fig. 5.9 Thermal expansion of dashpot shaft with dissimilar material in the 'C' groove

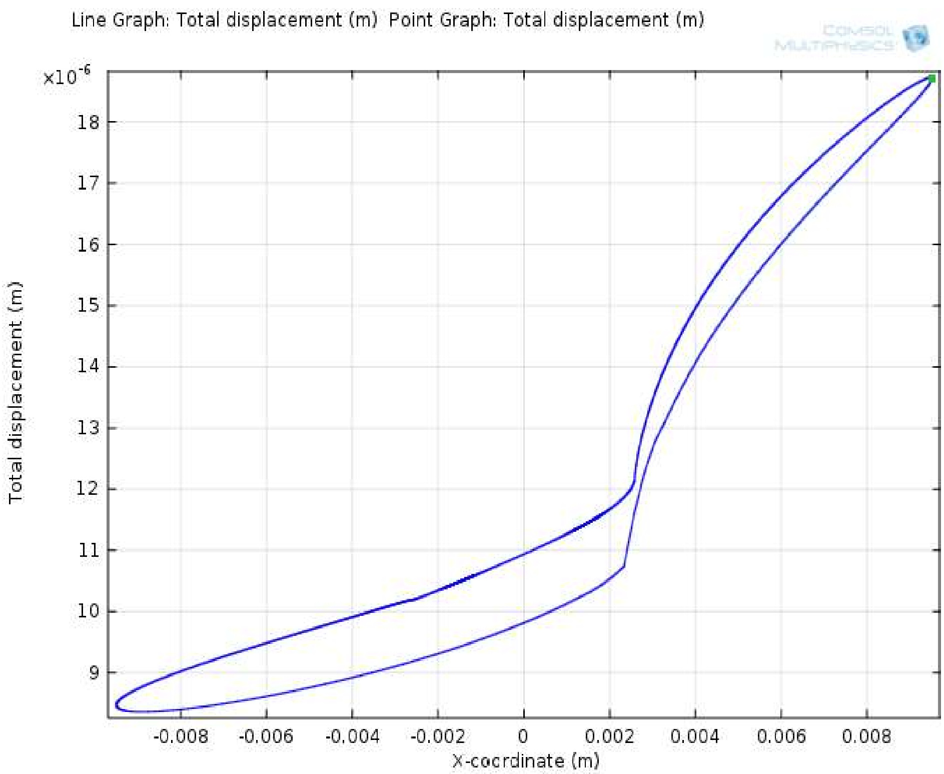

Fig. 5.10 Line graph of total displacement across the cross section of the dashpot shaft

(d) Thermal Expansion in Dissimilar Material Blocks in the Moving Vane

Thermal expansion analysis of the dashpot shaft with blocks of dissimilar material (with higher coefficient of thermal expansion) has been done. These blocks give appreciable reduction in fitting clearance. The detailed study which is also used for scheme and code validation is given in chapter 5.4.7

(e) Thermal Expansion in Bimetallic Strip

Thermal expansion analysis of bimetallic strip is done to see the deflection in bimetallic strip, which in turn will reduce the clearance. The maximum length of bimetallic strip possible in our study is limited to 23 mm and one end of the bimetallic strip is kept as fixed.

Thermal analysis results as shown in Figs 5.11 and 5.12 show that with the bimetallic strip we can have a good deflection, which can be used to reduce the clearance at the elevated temperature. Thermal expansion study of bimetallic strip is done in depth.

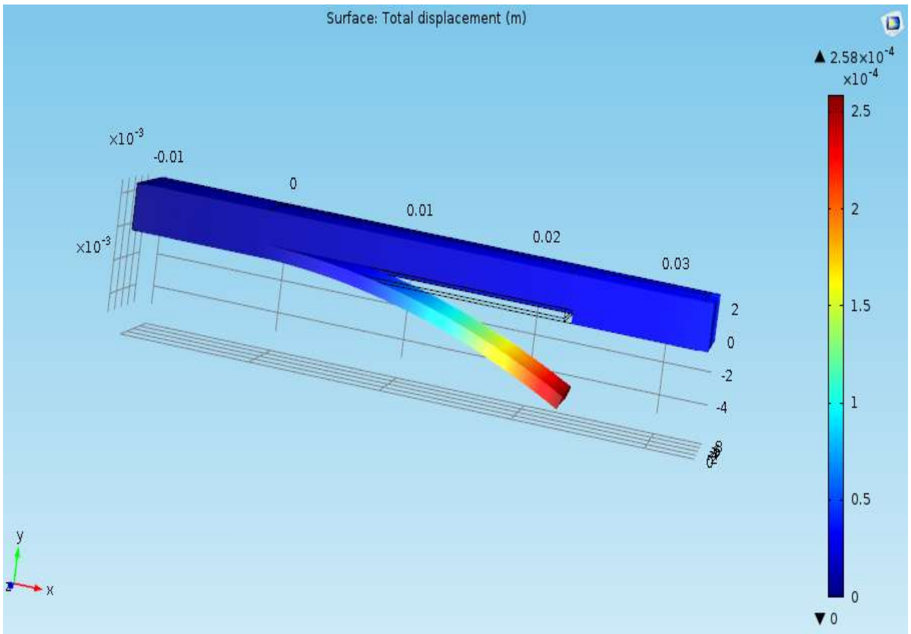

Fig. 5.11 Thermal expansion of a bimetallic strip

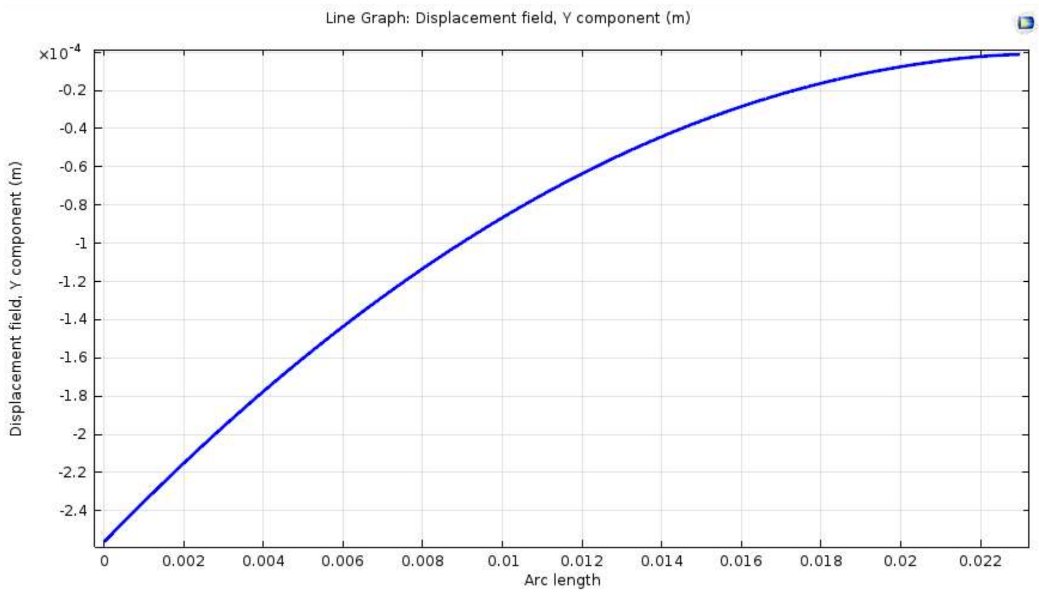

Fig. 5.12 Line graph of total displacement of a bimetallic strip

Studies have been done on deflection of a bimetallic strip and the same was also measured experimentally with the help of eddy current probe. Fig. 5.13 gives the construction and deflection of a bimetallic strip, while Fig. 5.14 gives the experimental set-up for the measurement of bimetallic strip deflection. Studies for the bimetallic strip deflection have been carried-out with various strip materials and layer thicknesses. Approximate area reduction in the clearance due to bimetallic strip deflection is also calculated.

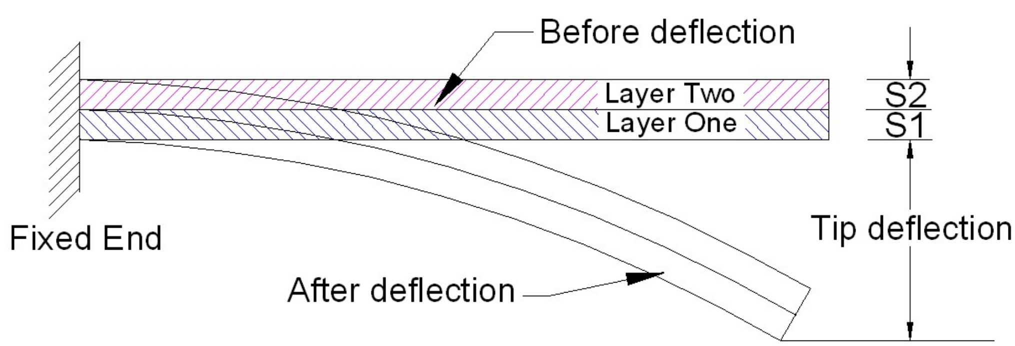

Fig. 5.13 Construction and deflection of a bimetallic strip

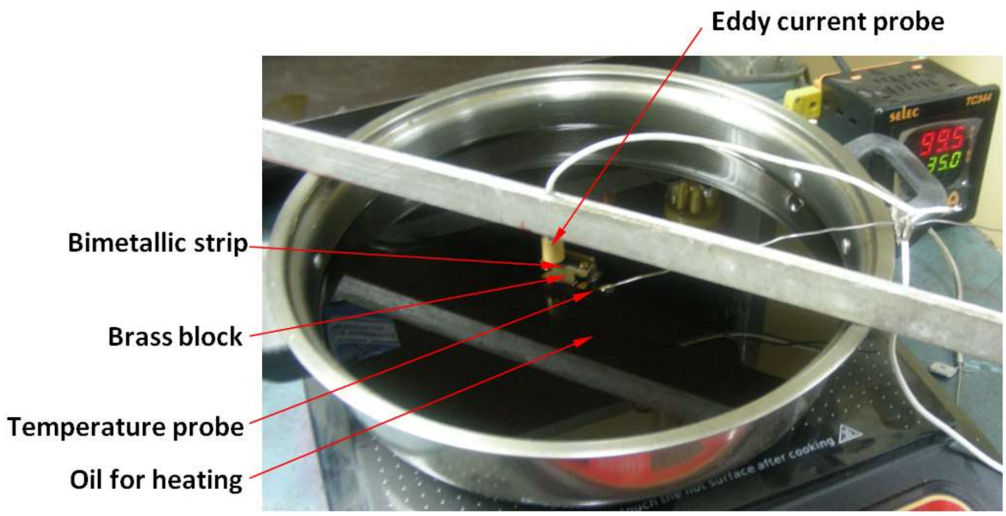

Fig. 5.14 Experimental measurement of deflection in a bimetallic strip

Tables 5.2, 5.3 and 5.4 give the bimetallic strip deflection results in different material/size conditions. Numerical results have been compared with the experimental results as shown in Table 5.2. Studies of the bimetallic strip deflection have been carried-out with variation in strip material and layer thickness.

(a) Bimetallic Strip Deflection with Variation in Temperature

Fixed material: Layer Two: NiMn-steel and Layer One: Invar (Fe-Ni 36%)

Fixed Thickness: S1=S2=0.4 mm, Reference temperature=25°C

Table 5.2: Bimetallic strip deflection results with the variation of temperature

Environment temperature (°C)	**Tip deflection (m)**		**Approx. clearance area reduction (m^2) (Numerical)**
	Numerical results (COMSOL)	**Experimental measurement**	
85	3.25×10^{-4}	3.12×10^{-4}	3.73×10^{-6}
75	2.65×10^{-4}	2.55×10^{-4}	3.04×10^{-6}
65	2.20×10^{-4}	2.12×10^{-4}	2.53×10^{-6}
55	1.60×10^{-4}	1.53×10^{-4}	1.84×10^{-6}
45	1.10×10^{-4}	1.06×10^{-4}	1.01×10^{-6}
35	0.55×10^{-4}	0.52×10^{-4}	0.63×10^{-6}

(b) Bimetallic Strip Deflection with Variation in Layer Thickness

Fixed material: Layer Two: NiMn-steel and Layer One: Invar (Fe-Ni 36%)

Fixed temperature: 85°C, Reference temperature: 25°C

Table 5.3: Bimetallic strip deflection results with variation of layer thickness

Strip layer thickness (mm)		Tip deflection numerical results (COMSOL)	Approx. clearance area reduction (m^2) (Numerical)
S1 (Layer one)	**S2(Layer Two)**		
0.4	0.4	3.25×10^{-4}	3.73×10^{-6}
0.2	0.6	2.40×10^{-4}	2.76×10^{-6}
0.3	0.5	3.10×10^{-4}	3.56×10^{-6}
0.5	0.3	3.15×10^{-4}	3.62×10^{-6}
0.6	0.2	2.50×10^{-4}	2.87×10^{-6}

(c) Bimetallic Strip Deflection with Variation in Layer Material

Fixed environment temperature: 85°C

Fixed strip layer thickness: S1=S2=0.4 mm, Reference temperature: 25°C

Table 5.4: Bimetallic strip deflection results with variation of layer materials

Material of bimetallic strip		Tip deflection numerical results (COMSOL)	Approx. clearance area reduction (m^2) (Numerical)
S1 (Layer one)	**S2 (Layer two)**		
36 Ni (Invar)	NiMn-steel	3.25×10^{-4}	3.73×10^{-6}
36 Ni (Invar)	Mn NiCu	3.45×10^{-4}	3.96×10^{-6}
40 Ni	NiMn-steel	2.55×10^{-4}	2.93×10^{-6}
42 Ni	NiMn-steel	2.05×10^{-4}	2.35×10^{-6}
46 Ni	NiMn-steel	1.50×10^{-4}	1.72×10^{-6}

5.4.4 Moving Mesh (Arbitrary Lagrangian Eularian Formulation)

Moving mesh interface utilizes Arbitrary Lagrangian Eularian (ALE) formulation to analyze fluid and structure interfaces. Fluid equations are converted into ALE form to accommodate the moving mesh due to thermal expansion at elevated temperature. As inherent problem with the pure Eulerian formulation is that it can't handle moving domain boundaries. Since the physical quantities are referred to the fixed points in space, while the set of spatial points currently inside the domain boundaries changes with time. Therefore, to allow moving boundaries, the Eulerian equations must be rewritten so as to describe all physical quantities as function of some coordinate system in which the domain boundaries are fixed. Rewriting physics equations in this way, on a freely moving mesh, results in an ALE method. The ALE method is therefore an intermediate between the Lagrangian and Eulerian methods, and it combines the best features of both; it allows moving boundaries without the need of the mesh movement to follow the material. COMSOL 5.1 Documentation [64]

5.4.5 Boundary Conditions

The whole computational domain is divided in solid and liquid domains. Solid mechanics boundary conditions are given for solid domains, while laminar flow and moving mesh boundary conditions are given for liquid domains. Equations are not coupled for the solid mechanics and the laminar flow; they are solved separately in two different studies.

In study of solid mechanics interface, the only load is the environmental temperature for thermal expansion. The centerline of the shaft is given as fixed constraint boundary condition. The shaft along with moving vane is given as rotating frame. In case of analysis with bimetallic strips, the geometry of bimetallic strip and a layer of fluid below it are modeled as assembly with identity pair to the rest of geometry, so that it can have a free deflection. These strips have material continuity boundary condition on one end and are free on the other end.

For laminar flow the moving walls are rotated along with rotor as moving wall boundary condition. Outlet boundary conditions are given to the faces which connects the liquid domain to the low-pressure chamber. Fictitious forces (Centrifugal and Coriolis) are also given as volume force to the whole liquid domain, though the effect is negligible. The numerical model is solving the flow in the clearance near the bimetallic strip considering it as a part of liquid domain.

The solid mechanics displacements in the dashpot geometry are taken as input to the second study for the pressure analysis. In order to find pressure with deformed geometry, both laminar flow and moving mesh interface are to be solved. In moving mesh (ALE) interface the mesh at common boundaries of liquid and solid are displaced according to the output displacements of solid mechanics interface and given as prescribed mesh displacement boundary condition.

Computational domain and the boundary conditions are shown in Fig. 5.15 while, Fig. 5.16 shows the structural hexahedral mesh for full domain and Fig. 5.17 shows the partially shown mesh, where one side wall and one fixed wall are hidden.

(i) Solid Mechanics Boundary Conditions:

(a) Thermal Expansion Boundary Conditions:

Temperature (T) = Environmental temperature in °K

Reference temperature (T_{ref}) = 293.15 °K

(b) Initial Values:

Displacement field (u); u = 0, v = 0, w = 0

Structural velocity field $\left(\frac{\partial u}{\partial t}\right)$; $\frac{\partial u}{\partial t} = 0$, $\frac{\partial v}{\partial t} = 0$, $\frac{\partial w}{\partial t} = 0$,

(ii) Laminar Flow Boundary Conditions:

(a) Initial values:

Velocity field (u_2); $u_2 = 0$, $v_2 = 0$, $w_2 = 0$

(b) Fixed Wall (No Slip) Boundary Conditions:

Velocity field (u_2); $u_2 = 0$, $v_2 = 0$, $w_2 = 0$

(c) Moving Wall Boundary Conditions:

Velocity of moving wall (u_w);

$(u_w)_x = 0$ (as, x is the axis of dashpot)

$(u_w)_y$ = moving wall velocity in y direction

$(u_w)_z$ = moving wall velocity in z direction

(d) Sliding Wall Boundary Condition:

Velocity of sliding wall (u_{sw});

$(u_{sw})_x = 0$ (as, x is the axis of dashpot)

$(u_{sw})_y$ = sliding wall velocity in y direction

$(u_{sw})_z$ = sliding wall velocity in z direction

(e) Outlet Boundary Condition:

Pressure (p) = 0

(iii) Moving Mesh Boundary Conditions:

Prescribed mesh displacements on common solid liquid boundaries:

$d_x = u$ (mesh displacements equal to the solid mechanics displacement)

$d_y = v$ (mesh displacements equal to the solid mechanics displacement)

$d_z = w$ (mesh displacements equal to the solid mechanics displacement)

Where d_x, d_y, d_z are the mesh displacements in x, y and z directions respectively.

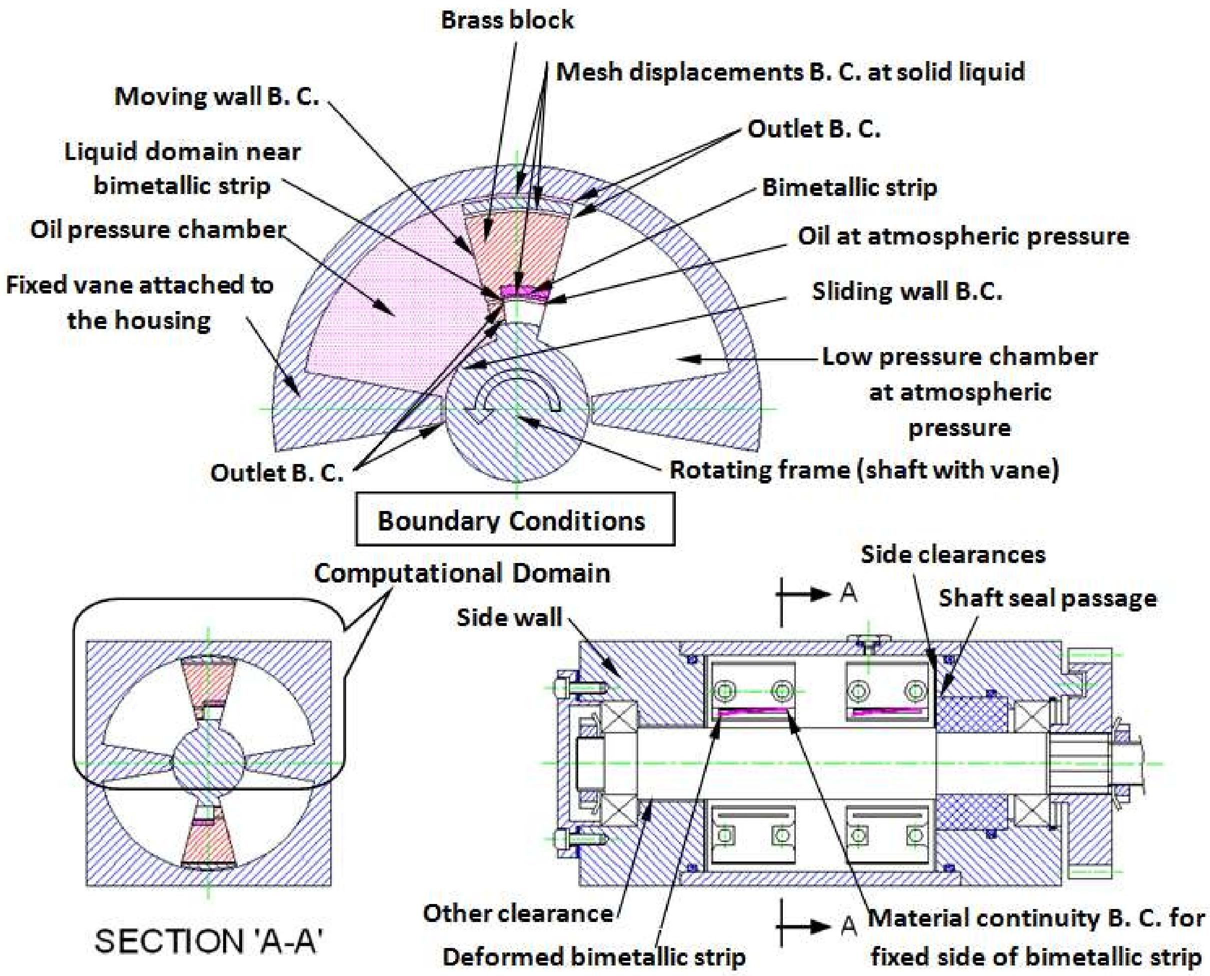

Fig. 5.15 Computational domain and boundary conditions in the hydraulic dashpot

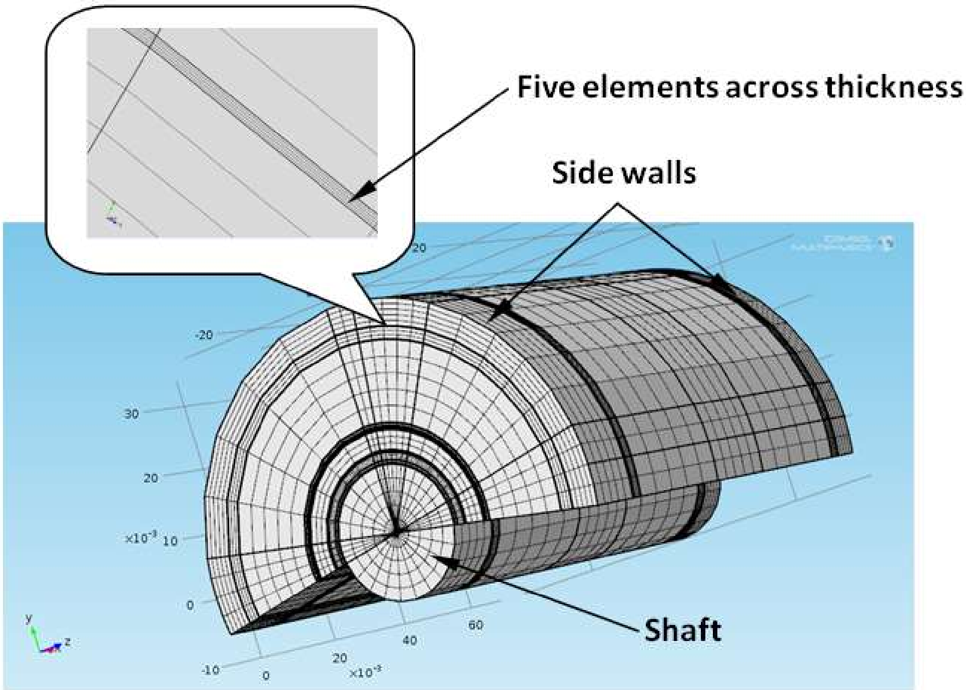

Fig. 5.16 Structured hexahedral mesh for the full domain

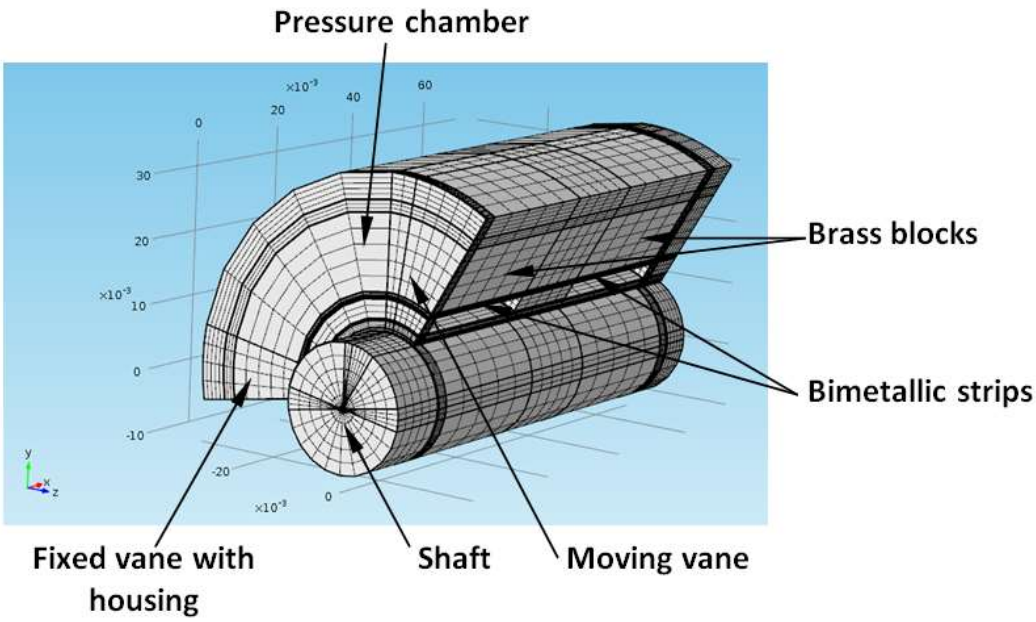

Fig. 5.17 Structured hexahedral mesh (shown partially)

5.4.6 Mesh Sensitivity and Convergence Methods

A mesh sensitivity study has been performed to find the mesh size that is sufficiently fine so that solution does not change by further refining the mesh. Pressure generated in the oil pressure chamber i.e. dashpot pressure is evaluated using COMSOL Multiphysics at a particular time-step. At this time-step keeping other parameters unchanged, numbers of elements in the mesh are increased. Fig. 5.18 shows the dashpot pressure variation against the total number of elements in the mesh. No appreciable change has been found beyond 155719 numbers of elements. Hence, this is considered as the optimized mesh size for this geometry. In this mesh size, there are minimum 5 elements across the thickness of the clearance (in fluid flow) as shown in the Fig. 5.16. In the study-1 for solid mechanics, direct solvers are used with fully coupled approach and double dogleg as nonlinear method. In study-2 for laminar flow and moving mesh, direct solvers are used with segregated approach. Spatial coordinates (material) are kept in one segregated step while velocity field and pressure are kept in another segregated step. Nonlinear method used for both segregated approach is constant (Newton). All the solutions were considered to be fully converged when the sum of residuals was below 10^{-3}. Convergence is achieved on a work station with system descriptions as: Processor; Intel core i7 3.40 GHz, 64-bit operating system and 64.0 GB RAM and the CPU time is 19 minutes for the study-1 and 5 minutes for the study-2.

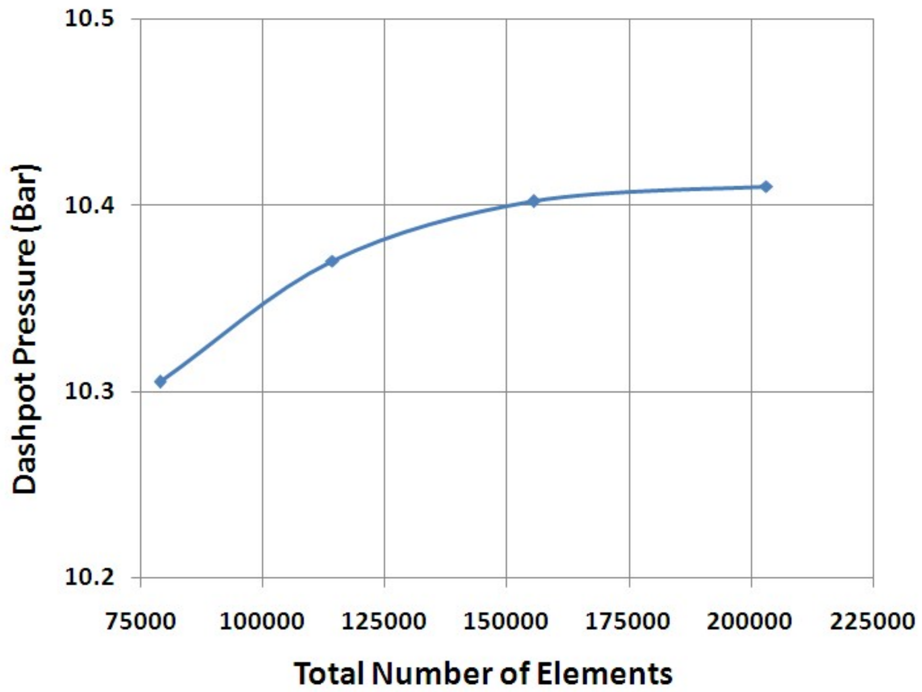

Fig. 5.18 Mesh sensitivity study on dashpot pressure at a fixed time-step

5.4.7 Scheme Validation with Pressure Analysis in 2-D

In order to validate the applicability of the code and scheme followed, an analysis has been done initially in 2-D geometry. The dashpot model in 2D is not simulating all the actual clearances (like vane side clearances), so analytical results can't be compared with experimental results. In this code validation analysis, a block is inserted in the moving vane as shown in Fig. 5.19. The analysis is performed at a vane velocity (ω) = 10 rad/sec and environment temperature of 85°C. The analysis is performed in three stages: in first stage, the material of block is kept as brass. Brass block expands more as compare to SS 17.4 PH (parent material of moving vane) and reduces the fitting clearances. In the second stage of analysis this block is replaced with the SS 17.4 PH material, same as parent material of moving vane. The SS 17.4 PH material block will expand less as compared to brass block and will not reduce the fitting clearances.

Pressure results have been obtained in both cases. The pressure in case of brass block is found to be more in comparison to the SS 17.4 PH block with same conditions (as shown in Table 5.5); it shows the temperature compensation by brass block by reducing the clearance. In third stage the SS 17.4 PH block size has been increased equivalent to the difference in coefficient of thermal expansion of brass and SS 17.4 PH (called as compensated SS 17.4 PH block) and pressure results have been obtained. Pressure results obtained in the compensated SS 17.4 PH block are very near to the results obtained from the brass block. This proves the applicability of code and analysis methodology. These results are given in Table 5.5 and pressure field is shown in Fig. 2.20.

Table 5.5: Pressure analysis results in 2-D geometry

Environment temperature (°C) (Reference temperature 20°C)	Dynamic Viscosity of oil at environment temperature (Pa.sec)	Pressure (Pa) (With brass block in the rotating vane)	Pressure (Pa) (With SS 17-4 PH block in the rotating vane)	Pressure (Pa) (With compensated SS 17-4 PH block in the rotating vane)
85	0.543	5.4272×10^7	5.2612×10^7	5.4121×10^7
75	0.626	6.1133×10^7	5.9482×10^7	6.0765×10^7
65	0.726	6.7674×10^7	5.9491×10^7	6.0764×10^7
55	0.851	8.0845×10^7	7.9574×10^7	8.0703×10^7
45	1.007	9.3441×10^7	9.2369×10^7	9.3431×10^7
35	1.206	1.1232×10^8	1.1154×10^8	1.1201×10^8

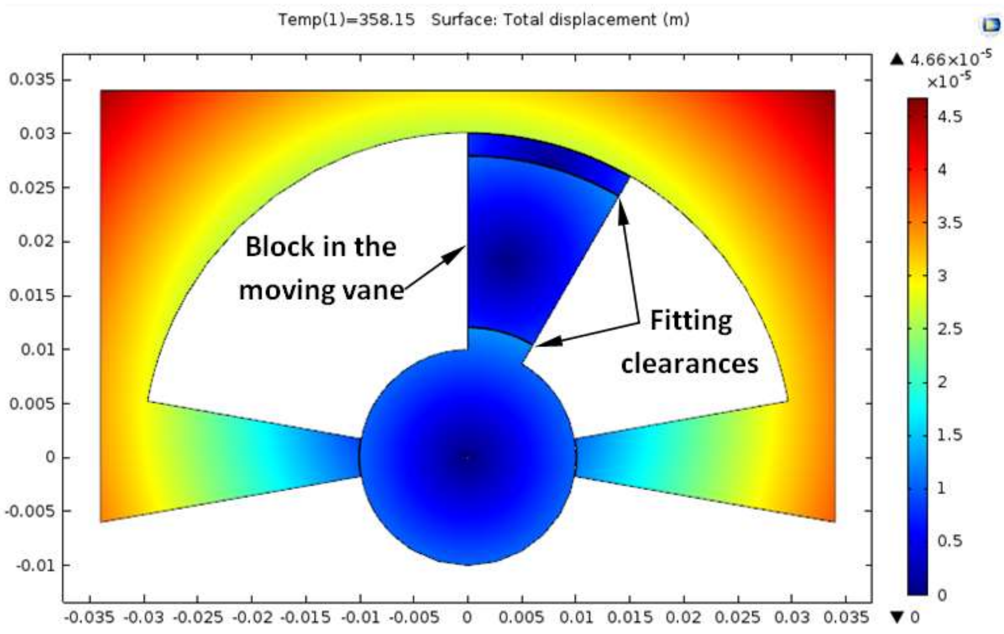

Fig. 5.19 2-D Thermal expansion with brass block in moving vane

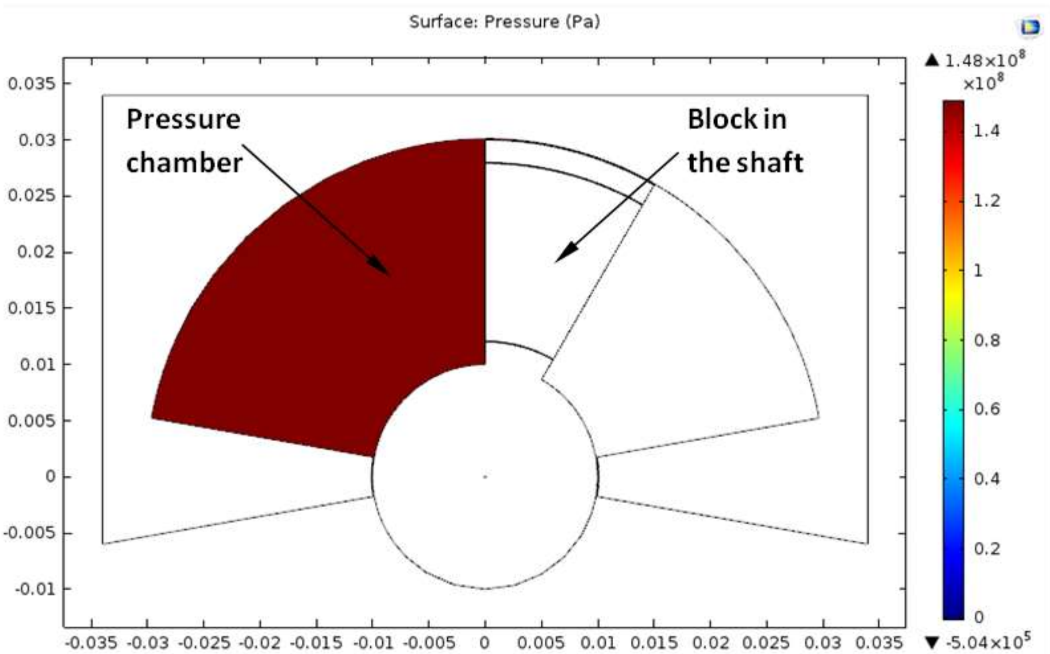

Fig. 5.20 2-D Pressure field in the dashpot pressure chamber

5.5 Experimental Study

In order to study the passive temperature compensation in the hydraulic dashpot experiments were conducted on a full-scale test station. Shut-off rod drive mechanism and test station of 'Critical facility' reactor has been used to conduct the experiments. Description of test set-up is given in chapter 4. Experiments are conducted to do the experimental validation as well as to extract more useful data for analysis.

5.5.1 Experimental Validation

Numerical and experimental results are compared in Figs. 5.21-5.24. Results are compared at the room temperature (35 °C) as well as at 85°C. Comparison shows that the results are in close proximity. The vane velocity in the numerical simulations is set with the dashpot RPM values measured in the experiments. Analysis of these results shows that the pressure values are initially low, though there is high vane speed at the start of dashpot operation. The reason is, at the start of operation the dashpot volume is more, hence we get low pressure comparatively, further we get the pressure peak when volume reduces. Towards the end of operation, the dashpot vane speed reduces as the energy is absorbed by that time hence pressure reduces. High temperature plots (85°C) as shown in Figs 5.22 and 5.24 are drawn for the time up-to impact seen by the dashpot. Further numerical and experimental results are discussed in the section 5.6.

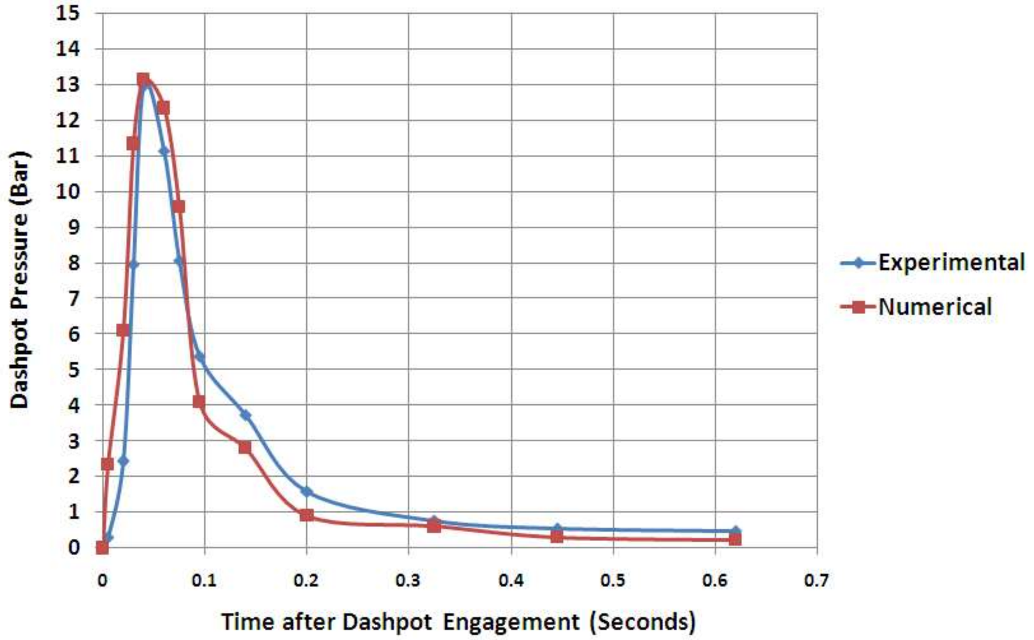

Fig. 5.21 Dashpot pressure without bimetallic strips at the room temperature (35°C)

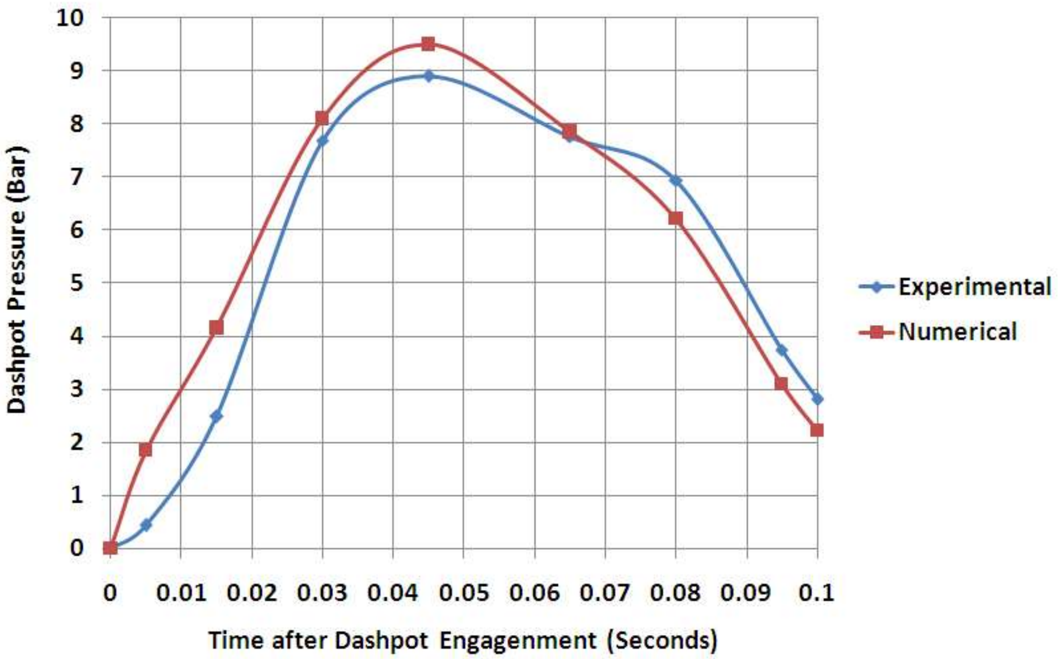

Fig. 5.22 Dashpot pressure without bimetallic strips at 85°C

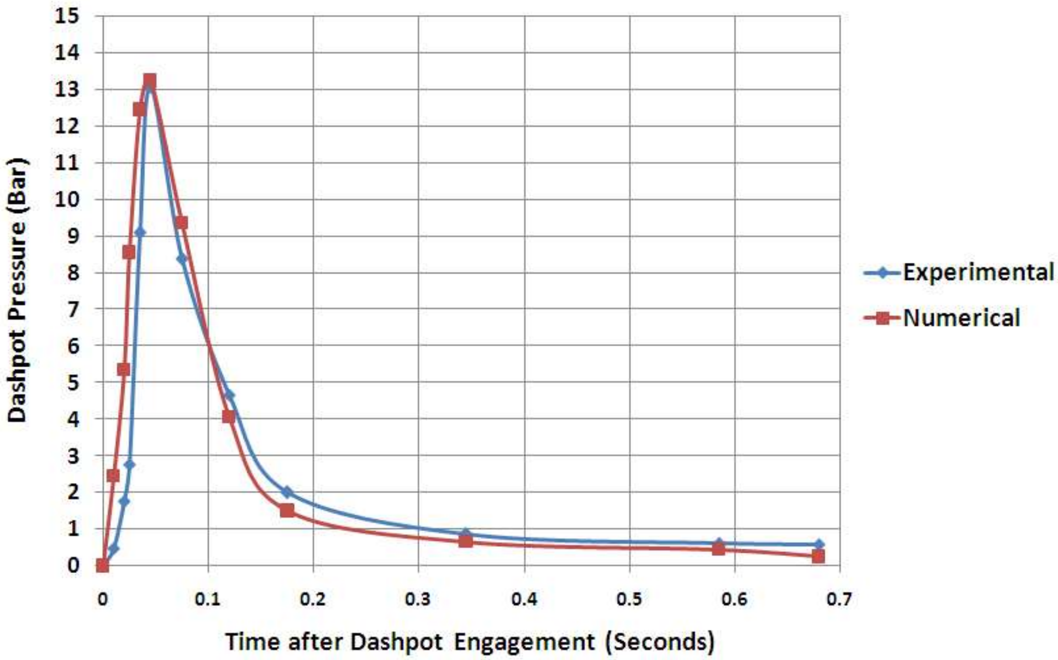

Fig. 5.23 Dashpot pressure with bimetallic strips at the room temperature (35°C)

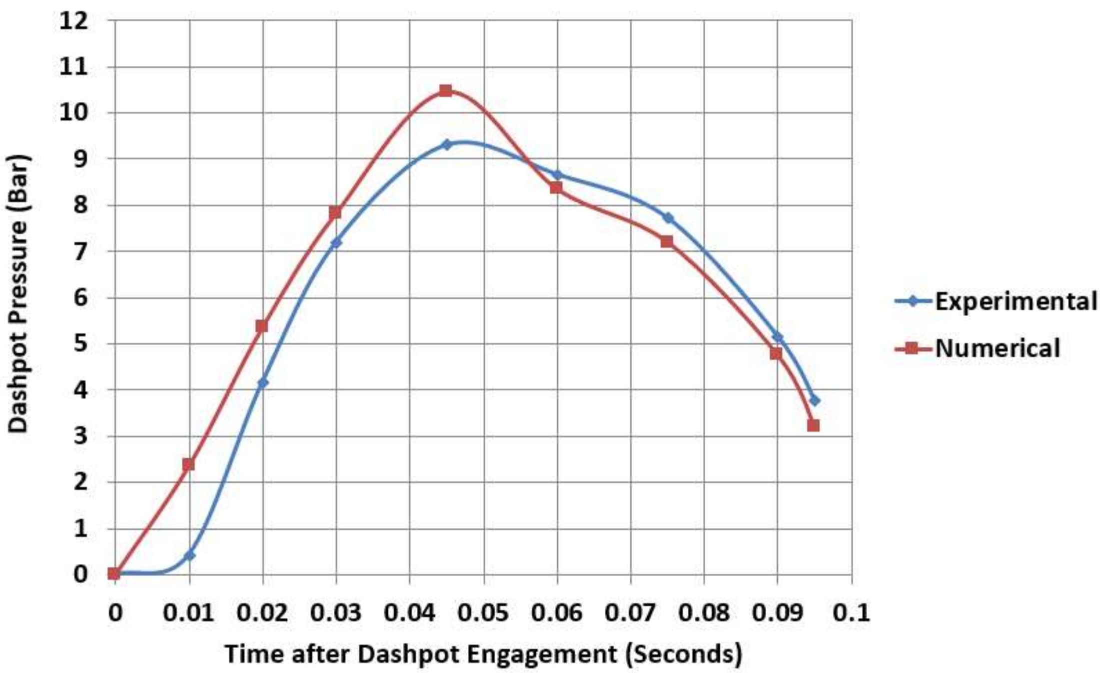

Fig. 5.24 Dashpot pressure with bimetallic strips at 85°C

5.5.2 Experimental Results

Experimental studies have been done by inserting brass blocks inside the moving vane with and without bimetallic strips. Experimental results are given in Table 5.6 and corresponding experimental plots are given in Figs. 5.25-5.36 with various conditions. Figs. 5.25-5.28 compare various dashpot parameters at room temperature (35°C), Figs. 5.29-5.32 at room temperature (55°C) and Figs. 5.33-5.36 at room temperature (85°C). Comparison of results in Figs 5.25-5.28 clearly shows that the values of pressure generated in the hydraulic dashpot and other parameter values with and without bimetallic strip are almost very near to each other at room temperature (35°C) as there is very little deflection of bimetallic strip at this temperature. Further, if the temperature increases to 55°C as shown in Figs. 5.29-5.32, the difference in pressure with and without bimetallic strip increases, it shows that the bimetallic strip helps in increasing the pressure in the dashpot. Moreover, if we compare the Figs. 5.29-5.32 then it is clearly visible that, there is an impact (kink in the plots) in the hydraulic dashpot operation without bimetallic strip at this temperature, which is not there in plots with bimetallic strips. In case of blocks with bimetallic strips, impact (kink) starts at 65°C (as given in Table 5.6). Figs. 5.33-5.36 give the results at 85°C. At this temperature the difference in the pressure obtained is further increased, hence we are getting more compensation in terms of pressure. Although there is an impact in both cases (with and without bimetallic strip), but severity of impact is more in case of results without bimetallic strip.

Table 5.6: Experimental Results

Envir-onment temp-erature (°C)	Experimental results without bimetallic strip in the moving vane						Experimental results with bimetallic strip in moving vane					
	Sheave shaft peak RPM	**Dash-pot peak RPM**	**Dashpot RPM at peek press-ure**	**Dashpot peak press-ure (Bar)**	**Dashpot peak pressure position (% of travel)**	**Impact in the dashpot action and vane hitting velocity (rad/sec)**	**Sheave shaft peak RPM**	**Dash-pot peak RPM**	**Dashpot RPM at peek press-ure**	**Dashpot peak pressure (Bar)**	**Dashpot peak pressure position (% of travel))**	**Impact in the dashpot action and vane hitting velocity (rad/sec)**
35	682.8	314.2	141.8	12.97	94.52	No Impact	682.7	304.2	134.5	13.07	94.68	No Impact
45	680.2	341.4	145.4	11.85	94.55	No Impact	680.0	325.4	143.2	11.97	94.47	No Impact
55	681.4	368.3	148.2	10.85	94.65	6.24	681.4	350.0	147.0	11.05	94.45	No impact
65	687.1	408.5	150.1	9.57	96.15	9.16	683.1	388.5	149.3	9.90	94.55	6.83
75	685.7	430.0	158.4	9.00	96.84	11.14	685.8	416.8	151.4	9.40	96.95	9.38
85	693.5	435.7	159.2	8.90	96.94	14.94	692.8	421.4	154.2	9.30	96.75	12.61

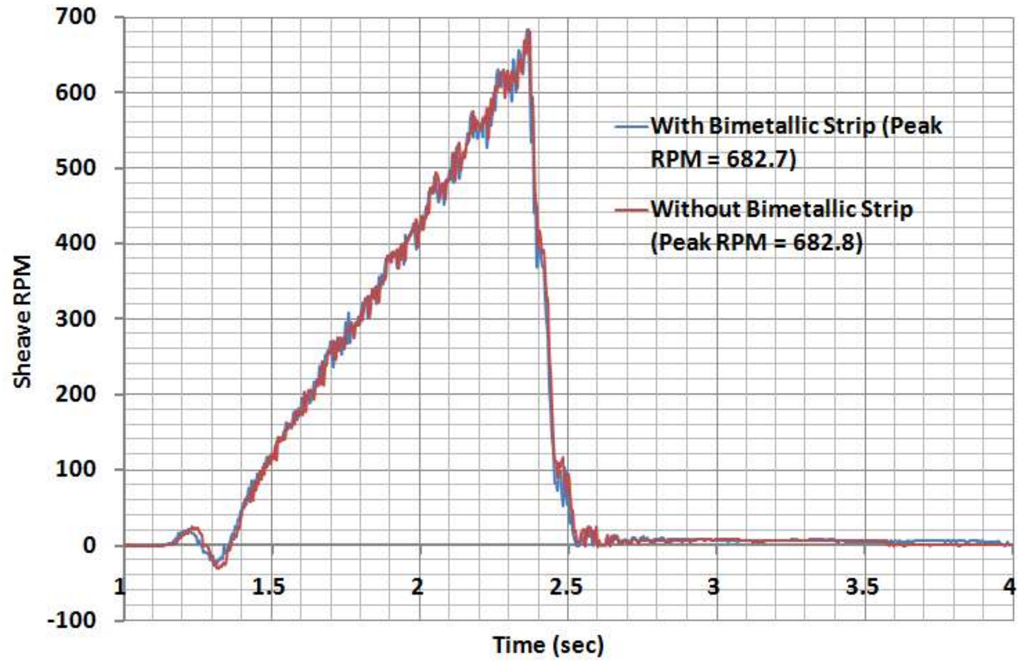

Fig. 5.25 Experimental sheave RPM vs time with and without bimetallic strips at 35°C

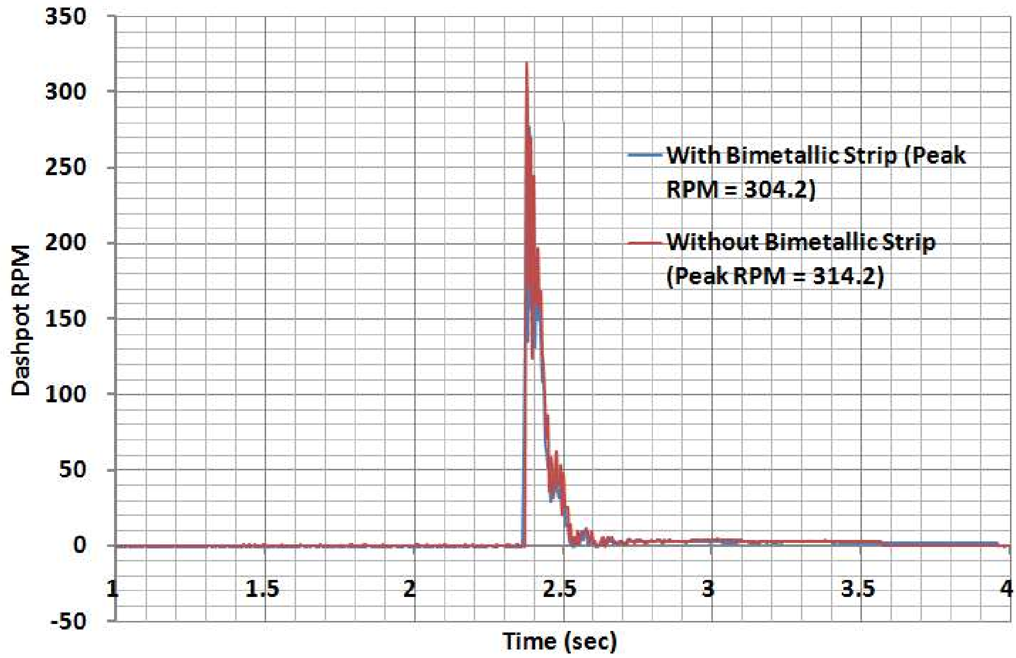

Fig. 5.26 Experimental dashpot RPM vs time with and without bimetallic strips at 35°C

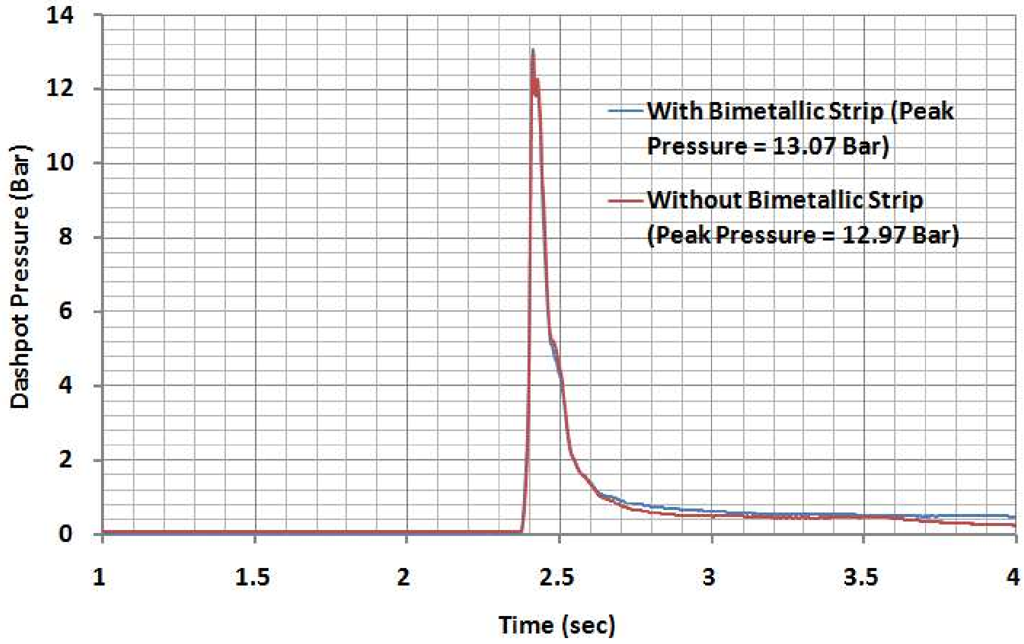

Fig. 5.27 Experimental dashpot pressure vs time with and without bimetallic strips at 35°C

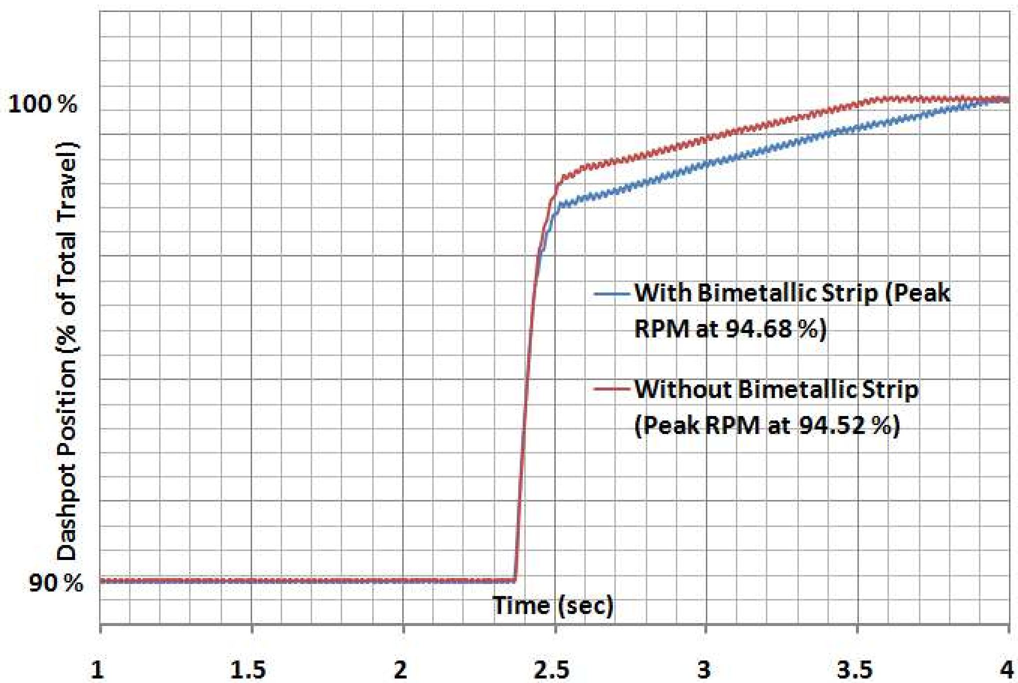

Fig. 5.28 Experimental dashpot position vs time with and without bimetallic strips at 35°C

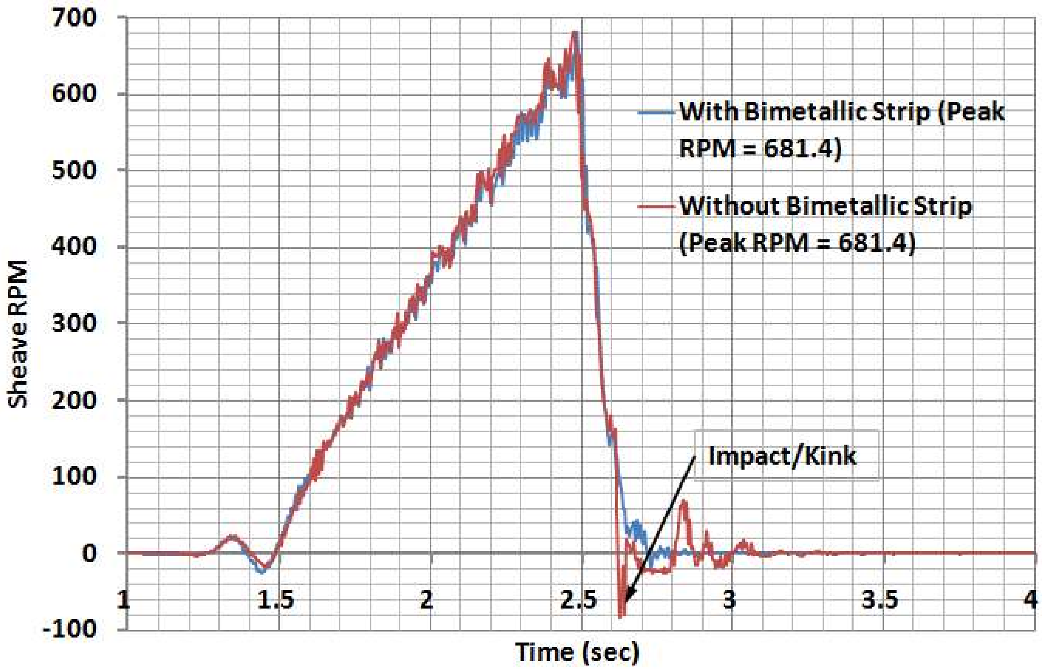

Fig. 5.29 Experimental sheave RPM vs time with and without bimetallic strips at 55°C

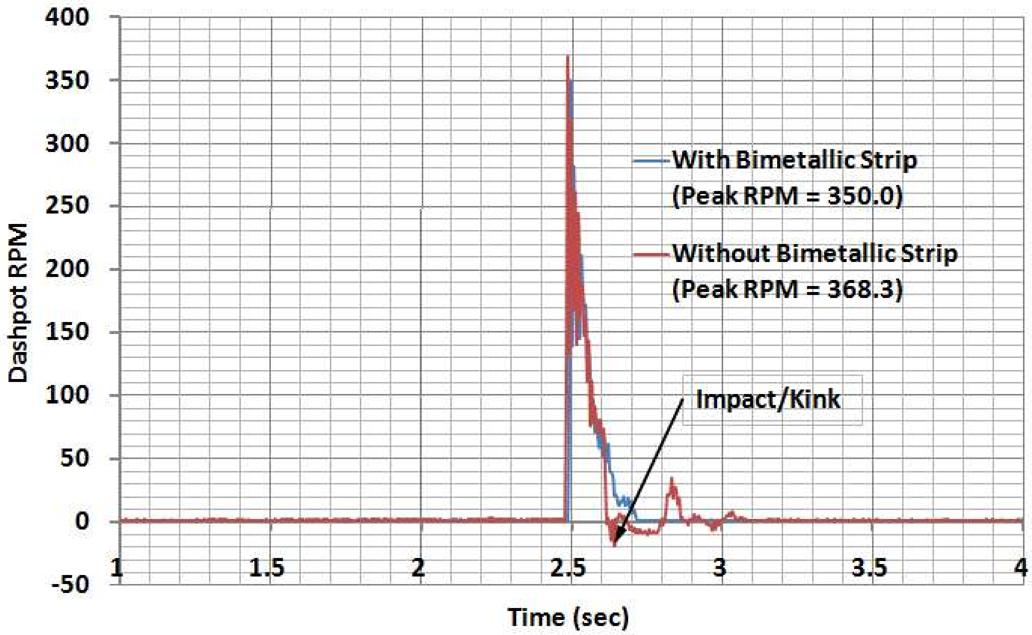

Fig. 5.30 Experimental dashpot RPM vs time with and without bimetallic strips at 55°C

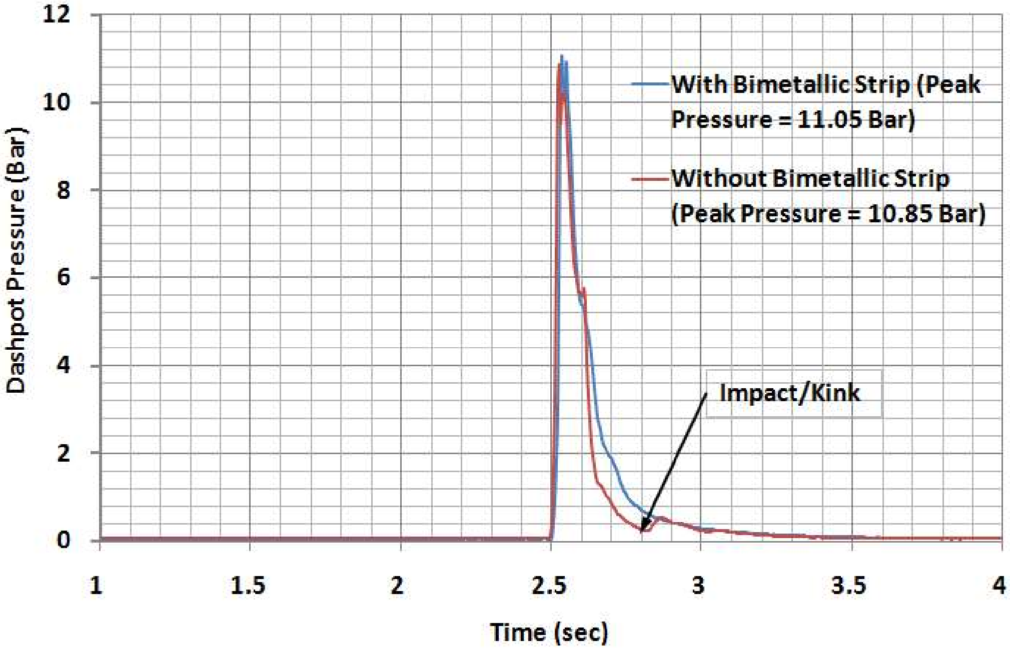

Fig. 5.31 Experimental dashpot pressure vs time with and without bimetallic strips at 55°C

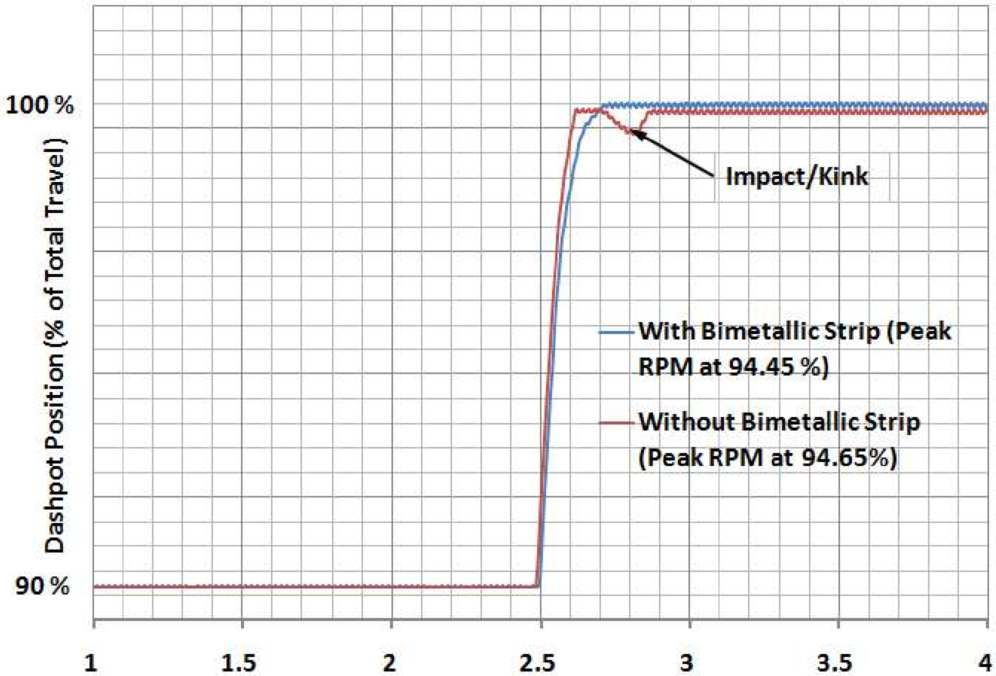

Fig. 5.32 Experimental dashpot position vs time with and without bimetallic strips at 55°C

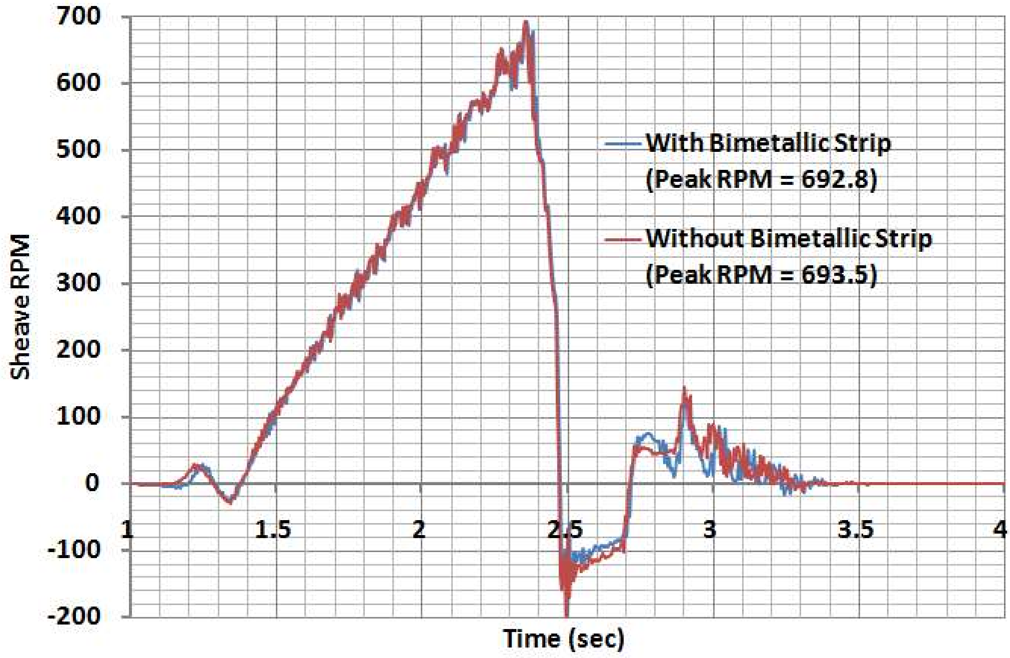

Fig. 5.33 Experimental sheave RPM vs time with and without bimetallic strips at 85°C

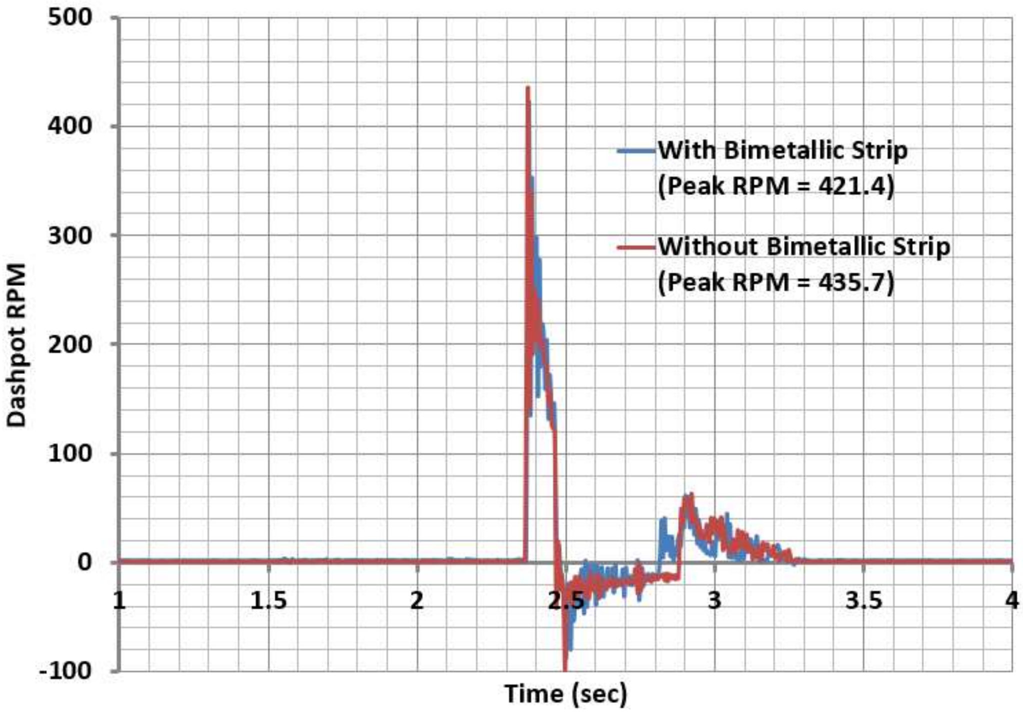

Fig. 5.34 Experimental dashpot RPM vs time with and without bimetallic strips at 85°C

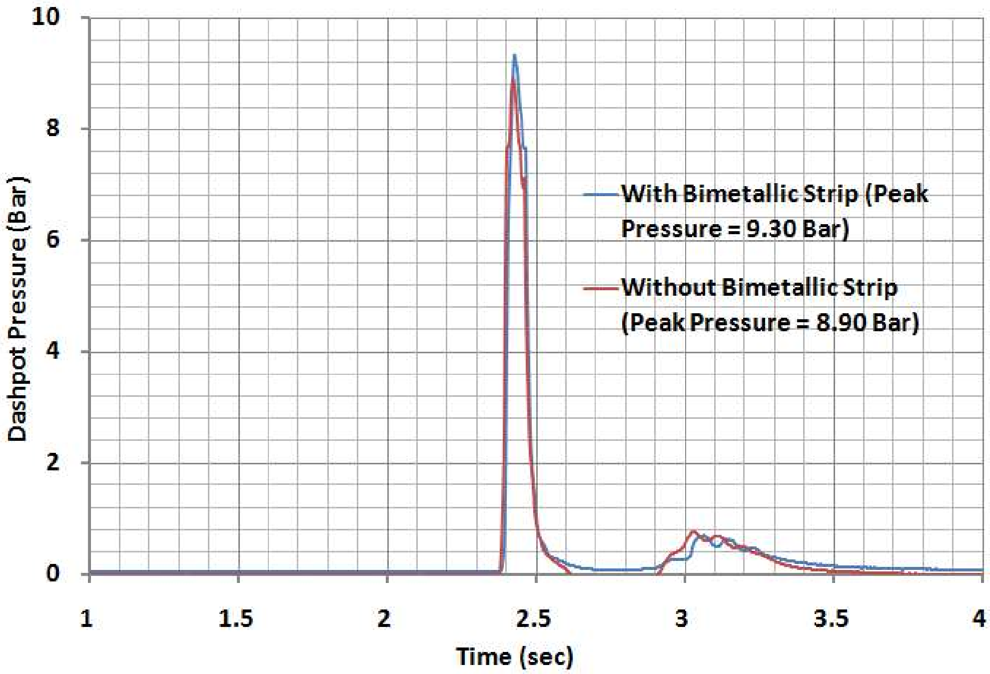

Fig. 5.35 Experimental dashpot pressure vs time with and without bimetallic strips at 85°C

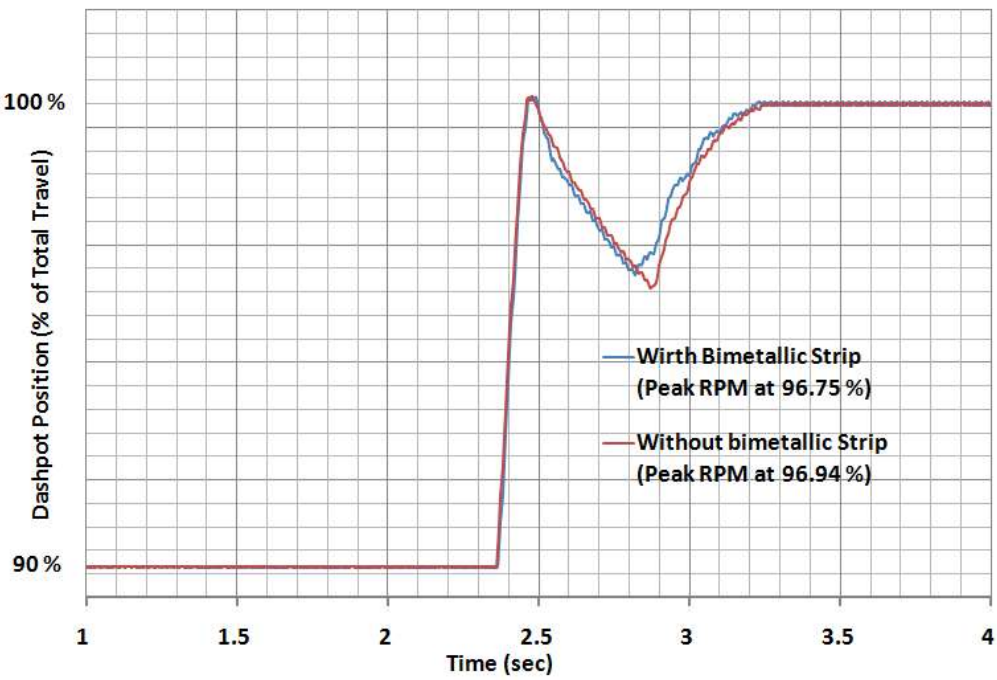

Fig. 5.36 Experimental dashpot position vs time with and without bimetallic strips at 85°C

5.6 Results and Discussion

After validation of numerical model with experimental results, the parametric study of temperature compensating hydraulic dashpot has been done. Numerical results are given in Figs. 5.37-5.40. Fig. 5.37 gives the thermal expansion (y component in cut view) of the hydraulic dashpot by coupled fluid structure analysis. It is clearly visible from the Fig. 5.37, how the deflected bimetallic strip blocks the clearance near it. Fig. 5.38 gives the velocity field (cut view) in the clearance near to the bimetallic strip. Figs. 5.39 and 5.40 give the pressure field inside the hydraulic dashpot at two different moving vane positions.

The performance improvement of the hydraulic dashpot with present system parameters is limited. In order to improve it further, the study has been extended analytically with better system parameters to get more temperature compensation in terms of higher pressure at elevated environmental temperature (85°C). The oil viscosity (μ): 0.543 Pa.sec (viscosity of 1500 cst oil at 85°C) and rotating vane velocity (ω):16.68 rad/sec is taken for the study. The study is done with the different combinations of materials of hydraulic dashpot and moving vane blocks. The results obtained are given in the Table 5.7. Results show that, pressure can be further increased up-to 10.49 bar with brass blocks in the moving vane and rest dashpot material as Invar with Bimetallic strips.

The pressure force which acts on the bimetallic strip in the lateral direction will cause some deflection in the bimetallic strip and hence will result into increased clearance. This effect is studied and it is found that the maximum bimetallic strip deflection in the lateral direction is around 12 microns at the tip and zero at the fixed end. Overall increment in the clearance is negligible, so this effect is neglected.

Table 5.7: Pressure in the hydraulic dashpot with different material combinations

Dashpot material combination	**Coefficient of thermal expansion of block/parent material (10^{-6} m/m K)**	**Pressure in the dashpot (Bar)**
Brass blocks with rest material as SS 17.4 PH	Brass: 16.8	9.52
Brass blocks with rest material as Invar	Invar: 1.5	9.63
Rotating shaft and rotating vane as brass rest as SS 17.4 PH	Brass: 16.8	9.49
Whole solid material as brass	Brass: 16.8	9.48
Whole solid material as SS 17.4 PH	SS 17.4 PH: 12.8	9.47
Brass blocks with rest material as SS 17.4 PH + Bimetallic strips (4 Nos.)	Brass: 16.8	10.41
Brass blocks with rest dashpot material as Invar + Bimetallic strips (4 Nos.)	Invar: 1.5	10.49

Further parametric study has been done by reducing other clearances (side clearances, shaft seal passage and shaft ID clearance) in the hydraulic dashpot. In the present set-up these clearances are 0.3 mm and the clearance near the bimetallic strip is also 0.3 mm. The study shows that if we reduce other clearances then the clearance near the bimetallic strip becomes more effective, hence we get better results in terms of pressure difference with and without bimetallic strip. Table 5.8 and Fig. 5.41 give the results obtained by reducing the other clearances at 85°C, rotating vane velocity (ω): 16.68 rad/sec and oil viscosity (μ): 0.543 Pa.sec. The results show that the difference in pressure obtained with and without bimetallic strip increases with reduction in other clearances. There is a big difference in the pressure values with and without bimetallic strip if other clearances are 0.1 mm. With these clearances (0.1 mm), it is possible to get more temperature compensation with bimetallic strips. By this way, it is possible to make a hydraulic dashpot which will not see any impact up-to 85°C or beyond with bimetallic strip even at low viscosity, which is otherwise not possible.

Table 5.8: Pressure in the hydraulic dashpot by reducing the other clearances

Other clearances (mm)	Dashpot pressure without bimetallic strip (Bar)	Dashpot pressure with bimetallic strip (Bar)
0.3	9.52	10.41
0.2	15.03	22.22
0.1	21.02	35.93

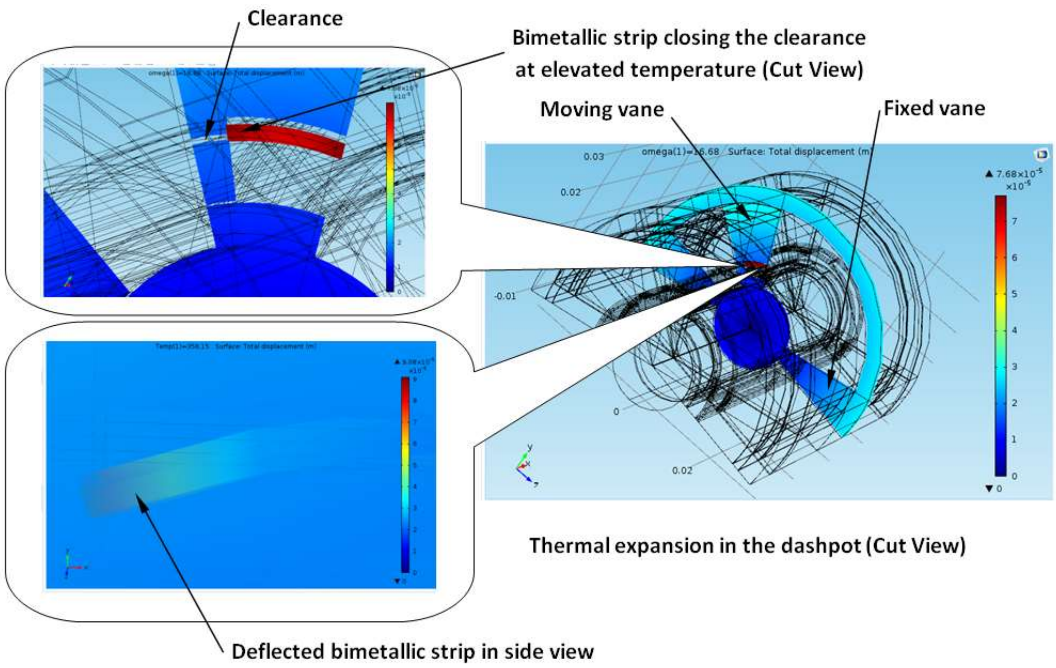

Fig. 5.37 Thermal expansion (y component) of hydraulic dashpot by fluid structure analysis (cut view)

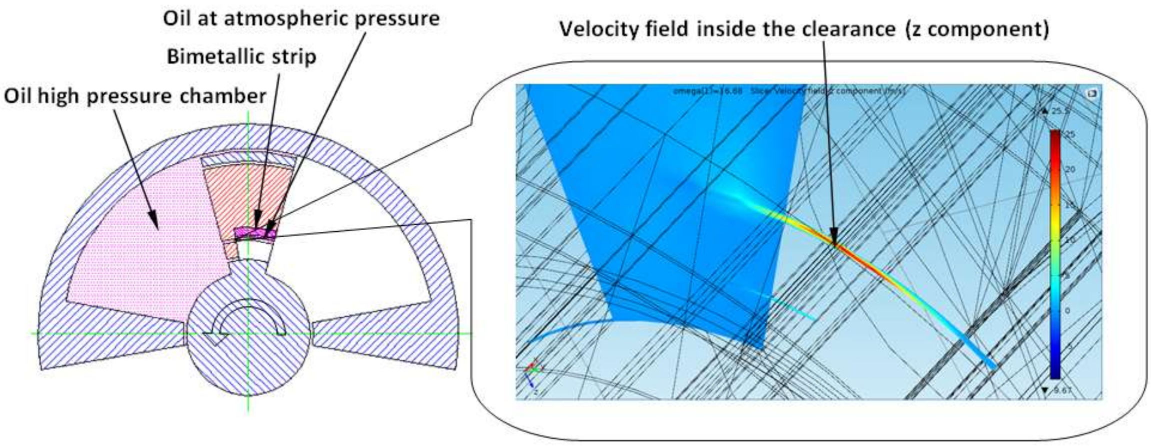

Fig. 5.38 Velocity field in the clearance of hydraulic dashpot by fluid structure analysis (cut view)

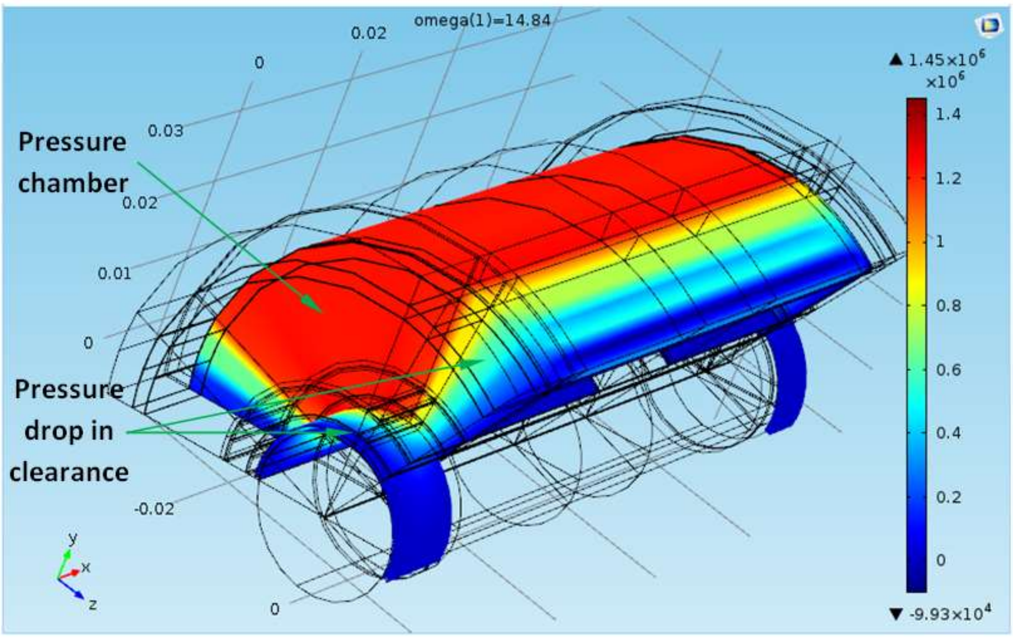

Fig. 5.39 Pressure field in hydraulic dashpot by coupled fluid structure analysis (moving vane at 93% position)

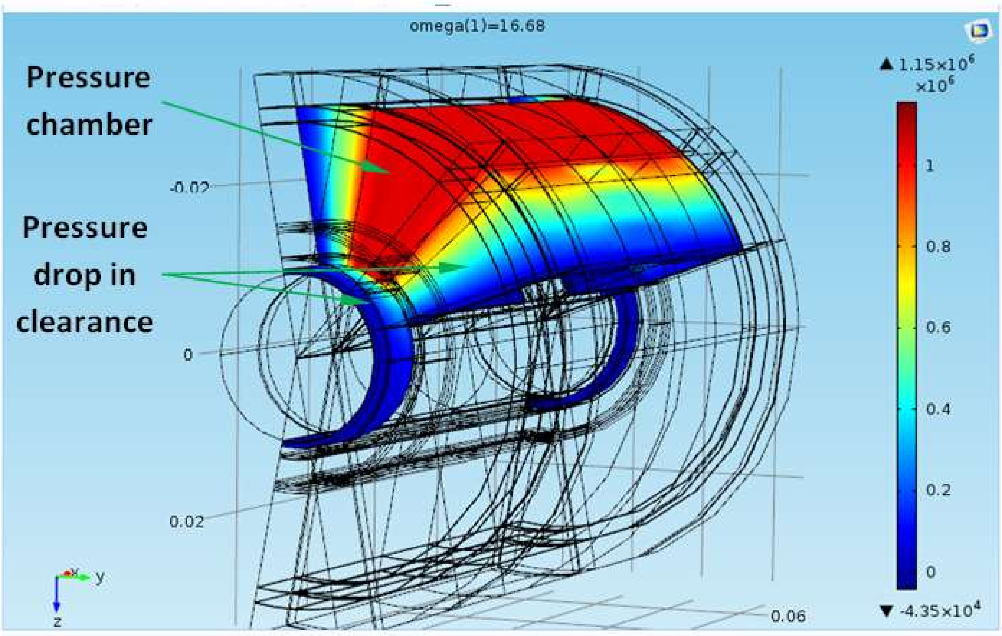

Fig. 5.40 Pressure field in hydraulic dashpot by coupled fluid structure analysis (moving vane at 97% position)

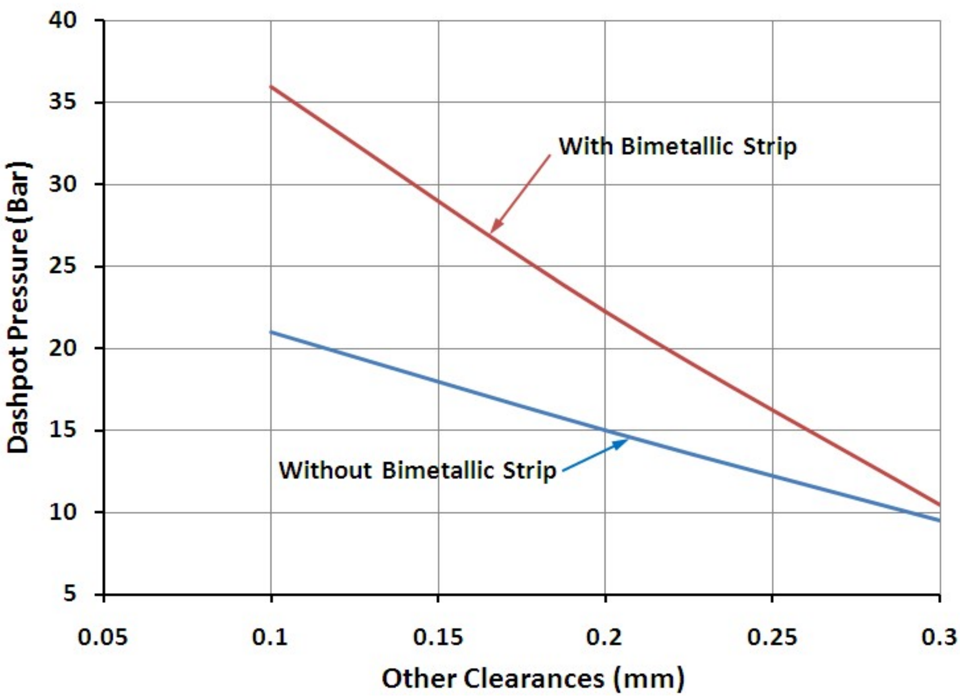

Fig. 5.41 Comparison of dashpot pressure with and without bimetallic strip by changing the other clearances

5.7 Closure

Fluid-structure study of hydraulic dashpot concluded that, the passive temperature compensating hydraulic dashpot design is possible using bimetals. Use of bimetallic strips can effectively reduce the clearances in the hydraulic dashpot at elevated temperature, which can compensate for reduction in the viscosity. Thus, the objective of presenting a novel temperature compensating hydraulic dashpot is achieved.

Chapter VI

CONCLUSIONS, CONTRIBUTIONS AND FUTURE PERSPECTIVE

6.1 Conclusions

Analysis of dashpot parameters shows that the force generated due to differential pressure is the main contributor to the total damping action of the dashpot. Dashpot pressure is highly dependent on its clearance thickness. Apart from clearance thickness, length of clearance is also an important parameter, because of this clearance at OD is least effective. Side clearances are most effective and the pressure becomes negligible with side clearances of more than 1.5 mm. At the elevated temperature when oil viscosity reduces, the dashpot peak pressure doesn't reduce in the same proportion because pressure in the dashpot chamber also depends on chamber volume. Both under-damped and excessively over-damped hydraulic dashpot designs are not suitable for the shut-off rod drive mechanism applications. Presence of 'C' grove in the dashpot shaft flattens the pressure peak and shifts it towards the end of operation, hence improves the design.

Multi-body dynamics model of hydraulic dashpot has resulted into a handy tool to analyze the effects of various parameters on the dashpot performance. Impact hitting velocity increases with increase in environmental temperature of hydraulic dashpot as damping coefficient of dashpot reduces. Initial kinetic energy acquired by the hydraulic dashpot is more at higher temperatures as viscosity of oil goes down. Impact at higher temperatures is more severe because of higher initial kinetic energy and less damping coefficient of hydraulic dashpot. With increase in the moment of inertia, reduction in the constraint angle and increase in the constant applied moment, an over damped dashpot system can become under damped without change in damping and spring coefficients.

Fluid structure analysis for passive temperature compensation shows that; the clearances in the dashpot can be reduced at elevated temperature to compensate for the reduction in oil viscosity. Temperature compensation by only dissimilar material blocks in the dashpot shaft is very limited and doesn't give much improvement in the dashpot performance at the elevated temperature. Use of bimetallic washers and dissimilar materials in 'C' groove also found to be having negligible effects in the dashpot performance. Use of bimetallic strip gives appreciable improvement in the dashpot performance at elevated temperature. At 55°C environmental temperature, the impact was eliminated with the help of bimetallic strip and the severity of impact is reduced at 85°C. Numerically it is found that with better system parameters in terms of clearances, it is possible to have even more temperature compensation effect. It is concluded that a novel temperature compensating hydraulic dashpot design with bimetallic strips is possible.

6.2 Contributions

The main contributions of this research work are:

(i) A novel passive temperature compensating hydraulic dashpot design has been proposed and experimentally verified. This will improve performance of the shut-down device in a nuclear reactor, a very important safety feature.

(ii) Performance improvement of the damping system due to the proposed device is quantified.

6.3 Future Perspective

Future research issues are open on studying the hydraulic dashpot. Further work may include:

(i) Use of shape memory alloys to reduce the clearances at elevated temperature.

(ii) Use of materials having negative coefficient of thermal expansion in hydraulic dashpots to get higher temperature compensating effects.

(iii) Nano fluid-based dampers with increased viscosity at elevated temperature.

REFERENCES

[1] Bajaj S.S., Gore A.R., 'The Indian PHWR'. *Nuclear Engineering and Design*, 236 (2006) 701-722.

[2] Sinha R. K., Kakodkar A., 'Design and development of the AHWR- the Indian thorium fueled innovative nuclear reactor'. *Nuclear Engineering and Design.* 236 (2006) 683-700.

[3] Donis J. M., Goller H., 'A mathematical model of a control rod drop'. *Nuclear Engineering and Design*, 23 (1972) 107-120.

[4] Choi K.S., Yim J. S., Kim I. K. and Kim K. T., 'Development of a computer program for drop time, and impact velocity of the rod cluster control assembly'. *SMiRT-12* / K. Kussmual (Editor) 1993.

[5] Taliyan S.S., Roy D.P., Grover R.B., Singh Manjit, Govindarajan G., 'Dynamics of rod drop in a PHWR'. *Nuclear Engineering and Design*. 147 (1994) 311-319.

[6] Ren M. and Stabel J., 'Analytical Modeling of Control rod drop behavior'. *SMiRT-15*, Seoul, Korea, August 15-20, (1999)

[7] Idelchic, I.E., '*Handbook of Hydraulic Resistance*' (Heme- sphere Publishing Corporation, Washington, 1986a) pp. 64-68 and 151-152.

[8] Hofmann F., Archambeau F., Chaize C., 'Computational fluid dynamics of guide tube in a PWR'. *Nuclear Engineering and Design*, 200 (2000) 117-126.

[9] Wang S. K., Chen Y. N., Chyou Y. P., Yang T. T., 'Identification of damping mechanism of TRR-II reactor control rod during free fall insertion'. *Nuclear Engineering and Design*, 226 (2003) 243-254.

[10] Wenzler C. J., ‘Analysis of dashpot performance for rotating control drums of lithium cooled fast reactor concept’. *NASA technical memorandum*, NASA TM X-67992. (1972)

[11] Lenkei, Andrew, ‘Close clearance orifices’. *Product Eng*, Vol. 36, No. 9, 57-61 (1956)

[12] Hou Chien-Yuan. ‘Fluid dynamics and behavior of nonlinear viscous fluid dampers’. *J. Struct. Eng*., (2008) 134:56-63.

[13] Wang Weining, Yan Weiming, Chen Yanjiang,. ‘Effect of laminar flow to velocity exponent of viscous damper’. *Advanced Material Research*. (2013) Vols. 602-604, 1517-1521.

[14] Jia Jiuhong, Hua Hongxing,. ‘Test verification of a design method for a fluid viscous damper’. *Advanced Material Research.* (2011) Vols. 291-294, 2085-2088.

[15] Black C. J. and Makris Nicos, ‘Viscous heating of fluid dampers under small and large amplitude motions: Experimental studies and parametric modeling’. *Journal of Eng. Mechanics*, (2007) 133:566-577.

[16] Schultz J. C., ‘Rotary hydraulic damper’. *United States Patent* No. 4411341 (1983)

[17] Satoh Y., Takeuchi Y., ‘Motor vehicle suspension with rotary damper’. *United States Patent* No. 5005859 (1991)

[18] Hanawa N., ‘Rotary damper’. *United States Patent* No. 5901821 (1999)

[19] Modi P. N. and Seth S. M., ‘*Text book of hydraulic and fluid mechanics’* (Standard Book House, 1995) pp. 616-638.

[20] Erdogan M. E., Erden Imrak C., 'On the unsteady flows generated by impulsive motion of a boundary'. *Mathematical and Computational Applications.* Vol. 9, No. 2 (2004) pp. 265-274.

[21] Erdogan Emin M., 'On the unsteady unidirectional flows generated by impulsive motion of a boundary or sudden application of a pressure gradient'. *International Journal of Non-linear Mechanics*, 37 (2002) 1091-1106.

[22] Erdogan Emin M., 'On the flows produced by sudden application of a constant pressure gradient or by impulsive motion of a boundary'. *International Journal of Non-linear Mechanics*, 38 (2003) 781-797.

[23] Atta Hazem A., 'Influence of temperature-dependent viscosity on the MHD Coutte flow of dusty fluid with heat transfer'. *Differential Equations and Nonlinear Mechanics*, Vol. 2006, Art. ID 75290, pp. 1-14.

[24] Muzychka Y. S., Yovanovich M. M., 'Unsteady viscous flows and Strokes's first problem'. *International Journal of Thermal Sciences*, 49 (2010) 820-828.

[25] Ogata Hideki, 'Thermodynamic lubrication analysis method pf step bearings'. *IHI Engineers Review*, (2005) Vol. 38, No. 1

[26] Allen P. J., Hameed A. and Goyder, 'Automotive damper model for use in multi-body dynamic simulations'. *Proc. IMechE* Vol. 220 (2006) Part D: J. Automobile Engineering.

[27] Lion A. and Loose S., 'A thermomechanically coupled model for automotive shock absorber; theory, experiment and vehicle simulation on test tracks'. *Veh, Syst. Dynamic*. 37 (2002) 241-261.

[28] Zhong Jingyang, Song Bifeng, Wang Jin, 'Flapping wing multi-body dynamic simulation'. *Procedia Engineering* 99 (2015) 885-890.

[29] Shabana A., 'Viscoelastic analysis of multi-body systems using the finite element method'. *Journal of Sound and Vibration* (1985) 100 (2) 271-284.

[30] Na Kyung-Su, Kim Ji-Hwan, 'Deployment of a multi-link flexible structure'. *Journal of Sound and Vibration* 294 (2006) 298-313.

[31] Cheng C. C., Wang J. Y., 'Free vibration analysis of a resilient impact damper'. *Int. Journal of Mechanical Sciences* 45 (2003) 589-604.

[32] Passlack Katrin, 'Smart Fluids' *University of Oklahoma*, Honors thesis, (2010).

[33] Olabi A.G., Grunwald A., 'Design and application of magneto-rheological fluid'. *Materials and Design*, 28 (2007) 2658-2664.

[34] Wereley Norman M., Linder Jason, Rosenfeld Nicholas and Choi Young-Tai, 'Biviscous damping behavior in electro-rheological shock absorbers'. *Smart Material and Structures* 13 (2004) 743-752

[35] Stanway R., 'Smart fluids: current and future development's. *Material Science and Technology,* August 2004, Vol 20 931.

[36] Shiao Yaojung, and Huang Yao-Kuan, 'Design of a novel damping-controllable damper for suspension systems'. *Advanced Material Research*, Vol 338 (2011) pp 622-625.

[37] Carmignami C., Forte P. and Rustighi E., 'Design of novel magneto-rheological squeeze-film damper'. *Smart Materials and Structures*, 15 (2006) 164-170.

[38] Jennifer Ouellette, 'Smart fluids move into marketplace'. *American institute of physics,* 2004.

[39] Zhu Shixing, Liu Xin, Ding Li, 'Modeling and analysis of magneto-rheological fluid damper under impact load'. *Advanced Material and Research*, Vols 452-453 (2012) pp 1481-1485.

[40] Zhang X. Z., Li W. H. and Gong X. L., 'The rheology of shear thickening fluid (STF) and the dynamic performance of an STF-filled damper'. *Smart Materials and Structures*, 17 (2008) 035027 (7pp).

[41] Song G., Zeng M., 'A thin film magnetorheological fluid damper/lock'. *Smart Materials and Structures* 14 (2005) 369-375.

[42] Samantaray A. K., 'Modeling and analysis of preloaded liquid spring/damper shock absorbers'. *Simulation Modeling Practice and Theory*. (2009) 17, 309-325.

[43] Pan Q., Chongdu C., 'The investigation of a shape memory alloy micro-damper for MEMS applications'. *Sensors* (2007) 7, 1887-1900

[44] Nash J. V., 'Rotary dampers'. *United States Patent* No. 5984057 (1999)

[45] Hlipala E., Arnold S., 'Temperature compensated adjustable damper unit'. *United States Patent* No. 3699369 (1972)

[46] D'Anna F. P., Anthony V. R., 'Rotary viscous damper'. *United States Patent* No. 5400878 (1995)

[47] Molean R. L., 'Temperature compensated viscous damper'. *United States Patent* No. 3107752 (1961)

[48] Rao Venkateswara A., Prasad K. S. V., Avinash M., Nagababu K., Manohar V., Raju P. S. R., Chandra G. R., 'A study of deflection of a bimetallic beam under thermal loading using finite element analysis'. *International Journal of Eng. and Advanced Technology*. (2012) ISSN: 2249-8958, Vol-2, Issue-1.

[49] Zahariea Danut,. 'Structural analysis of helical bimetallic strip thermostat'. *International Journal of Modern Manufacturing Technologies*. (2011) ISSN 2067-3604, Vol. III, No. 1.

[50] Haba Sever Alexandru, Oancea Gheorghe,. 'Thermal expansion analysis of the complex body assemblies'. *Applied Mechanics and Materials*, (2013) Vol. 309, pp 162-169.

[51] Boisseau Sebastien, Despesse Ghislain, Monfray Stephane, Puscasu Onoriu and Thomas Skotnicki,. 'A bimetal and electrets-based converter for thermal energy harvesting'. arxiv:1212.0852 (2012)

[52] Plesca Adrian T., 'Thermal analysis of overload protection relays using finite element method'. *Indian Journal of Science and Technology*, (2013) Vol 6, No. 8.

[53] Martinson E., Delsing J., 'Mechanical thermal expansion correction design for an ultrasonic flow meter'. *FLOMEK (2007),* Sandton, South Africa. RedHook: Curran 2007, pp 96-101.

[54] Kim W., Lee C. M., Hwang Y. K., 'A study on the shirink fits and internal clearance variation for ball bearing of machine tool using FEM'. *Proccedings of the International MultiConference of Engineers and computer Scientists*, (2009), Hon Kong, Vol. II.

[55] Singh H., Shergill H., 'Thermal analysis of disc brake using COMSOL'. *International Journal of Emerging Technologies* (2012) 3(1): 84-88

[56] Antony Jankowski, 'Design of Novel composite pistons for diesel engine'. *Journal of KONES powertrain and Transport*, (2014) Vol. 21 No. 4

[57] Souli M., Ouahsine A., Lewin L., 'ALE formulation for fluid structure interaction problems'. *Comput. Methods Appl. Mech. Engrg*. (2000) 190, 659-675.

[58] Yoon K. H., Kim J. Y., Lee K. H., Lee Y. H., Kim H. K., 'Control rod drop analysis by finite element method using fluid-structure interaction for a pressurized water reactor power plant'. *Nuclear Engineering and Design*, 239 (2009) 1857-1861.

[59] Kuehne Ingo, Linden Ad van der, Seidel Julian, Schreiter Matthias,Fromme Lars and Frey Alexander, 'Fluid-structure interaction modeling for an optimized design of a piezoelectric energy harvesting MEMS generator'. *Excerpt from the proceedings of (2011)* COMSOL conference in Stuttgart.

[60] Czop Piotr, Gasiorek Damian, Gnilka Jacek, Slawik Damian, Wszolek Grzegorz, 'Fluid-structure simulation of a valve system used in hydraulic dampers'. *Modelowanie Inzynierskie. (2012)* Nr 45, t14, ISSN 1896-771X.

[61] Lau C. S., Abdullah M Z., 'Simulation investigations on fluid/structure interaction in the reflow soldering process of board-level BGA'. *International Journal of Computer Theory and Engineering*, (2013) Vol. 5, No. 4.

[62] Braescu L., George T. F., 'Arbitrary Lagrangian-Eularian method for coupled Navier-Strokes and convection-diffusion equations with moving boundaries'. *12th WSEAS Int. Conf. on Applied Mathematics*, Cairo, Egypt. December 29-31, 2007.

[63] Bathe K. J., Ledezma G. A., 'Benchmark problems for incompressible fluid flows with structural interactions'. *Computers and Structures*, 85 (2007) 628-644.

[64] *COMSOL Multiphysics 5.1 Documentation*

[65] COMSOL tutorial: *Fluid damper*. Model library path: CFD_Module / Non-Isothermal_Flow / fluid_damper.

[66] He L., Zheng G.T., 'Effect of viscous heating in fluid damper on the vibration isolation performance'. *Mechanical systems and signal processing*. (2007) 21, 3060-3071.

[67] COMSOL Tutorial: *Tilted pad thrust bearing.* Model library path: CFD_Module / Thin_Film_Flow / tilted_pad_bearing.

[68] Singh Manjit, 'Design and development of drive mechanisms for adjuster rods, control rods & shut-off rods of TAPP-3&4'. *Nu-power: An international journal of nuclear power*. (2002) Vol. 16 No. 1 & 2.

[69] Singh Manjit, Badodkar D. N., Singh N. K., Dalal N. S., Mishra M. K., Veda Vyas, G., Kothari C. B., Rao V. V. S. S. and Saraf R. K.. 'Reliability Assessment of Shut-off Rod Drive Mechanism for TAPP-3&4 and 'Critical Facility' Through Life-Cycle Testing'. *Proceedings of 3rd International Conference on Reliability, Safety and Hazard in Risk-informed Technology* (ICRESH-2005, Mumbai, India), Narosa Publishing House, P 77-82.

[70] Shin-Etsu silicone fluid technical data handbook (2005). *http://www.silicone.jp*

[71] Brookes D. and Kagan M. 'Experimental Uncertainties'. (2011)

[72] COMSOL tutorial: *Stresses and heat generation in landing gear.* Model library path: Multibody_Dynamics_Module/Automotive_and_Aerospace /landing_gear.

[73] Hwa Jin Oh, Young Seok Song, Sung Ho Kim, Seong Yun Kim, Jae Ryoun Youn,. 'Fluid-structure interaction analysis on the film problem of a film insert molded part'. *Polymer Engineering and Science*. (2011) 812-818.

[74] Gao Feng, Hiroshi Ueda, Gang Li, Hiroshi Okada, 'Fluid structure interaction simulation in three-layered aortic aneurysm model under pulsatile flow: Comparison of wrapping and stenting'. *Journal of Biomechanics*. (2013) 46, 1335-1342.